3D wave transmission around permeable submerged breakwater with the use of ANNs

Master of Science Thesis

Nicholas Socrates Tavouktsoglou
10/7/2013

Delft University of Technology

Faculty of Civil Engineering and Geosciences

DELFT UNIVERSITY OF TECHNOLOGY
FACULTY OF
Civil Engineering and Geosciences
Department of Hydraulic Engineering

Graduation committee:

Prof.dr.ir. M.J.F. Stive
        Delft, University of Technology
        Hydraulic Engineering, Coastal Engineering
Prof. R.R. Simons
        University College of London (UCL)
        Fluid Mechanics, Coastal Engineering
Dr.ir. P.J. Visser
        Delft, University of Technology
        Hydraulic Engineering, Rivers, Ports & Waterways and Dredging Engineering
Ir. H.J. Verhagen
        Delft, University of Technology
        Hydraulic Engineering, Coastal Engineering

Submitted in partial fulfillment of the requirements for the degree of Master of Science in
Civil Engineering at Delft University of Technology

Preface

This report contains the study conducted on the field of 3D wave transmission of permeable breakwaters using ANN modeling, which is my Master of Science Thesis for the department of Coastal Engineering at Delft University of Technology (TUD).

This research has been carried out at the University College of London (UCL). For this reason I would like to express gratitude and acknowledgment to Professor Richard Simons at UCL for giving me the possibility of conducting this study with the necessary supervision. I would also like to thank Amir Ahmadian for his valuable help and guidance during my study.

I would also like to thank my supervisors at TUD for their support during this study. I would also like to thank my fellow researchers at UCL for supporting me and making my stay at UCL as pleasant as possible. Finally, I would like to thank my parents and friends for their support during my MSc studies.

The author,

Nicholas Tavouktsoglou

London-Delft, 7/10/2013

Abstract

Wave transmission is a very important design parameter for submerged porous breakwater design, as it defines the dimensions of the breakwater as well as the cost and construction process. The spatial distribution of the wave transmission parameter influences the current pattern on the lee of the breakwater and therefore the sediment transport process. For this reason it is important to create a design tool capable of predicting the variation in wave height around detached submerged breakwaters.

This study has been conducted as an extension of the work completed by Amir Ahmadian for his PhD project the University College of London under the supervision of Professor Richard Simons. During his research a large number of experiments were conducted in order to create an extensive database on wave transmission around semi-infinite impermeable breakwaters. The results of these experiments where then used to create an ANN model capable of predicting the 3D wave transmission coefficients around submerged breakwaters.

This thesis therefore aims to create an ANN model capable of predicting the 3D wave field around permeable submerged breakwaters, by using the algorithm architecture proposed by Ahmadian. To the author's knowledge there are a limited number of experimental studies on the field of 3D wave transmission of permeable breakwaters and therefore creating an ANN model based on physical measurements is impossible. For this reason a large number of 3D experiments where performed using MIKE21 BW in order to create a database that will then could be used to train and test the ANN model. Important evidence of the significance of diffraction and breakwater permeability on the wave transmission phenomenon for submerged porous breakwaters where obtained. In addition the results of the simulations where then cross validated against the empirical formula provided by Vicinanza et al (2009). This analysis showed that the quality of the data was very good and could be used for training a Neural Network. During this process it was proposed that the empirical prediction formula of Vicinanza could be improved by introducing a correlation factor, as the numerical simulations showed strong evidence that the diffraction and wave transmission over and through the breakwater have a negative correlation. With regards to ANN modeling the algorithm showed that it has an excellent capability to predict the test dataset (obtained from MIKE21 BW simulation). The analysis of the ANN model revealed that the model predictions are in very good agreement with the prediction method of Vicinanza. Finally the sensitivity analysis of implemented showed that the permeability factor introduced to account for the effects of permeability has the most important contribution to the models performance.

Concluding this thesis suggests that the proposed model has the potential to become a valuable design tool for engineering purposes in the field of submerged breakwater design.

Contents

List of Figures

List of Tables

List of Symbols/Acronyms

Symbol	Definition	Units
ANN	Artificial Neural Network	
B	Crest Width	[m]
C	Chezy coefficient	[-]
d	Water depth	[m]
D50/d50	Nominal stone diameter of breakwater elements	[m]
g	Gravitational acceleration	[m/s^2]
Hi	Incoming wave height	[m]
Hm0i	Incoming significant wave height based on wave energy spectrum	[m]
hs	Submergence depth of the crest of the breakwater	[m]
Kd	Diffraction coefficient	[-]
Kdissipation	Wave dissipation coefficient	[-]
Kr	Wave reflection coefficient	[-]
Kt	Wave transmission coefficient	[-]
L0p	Wave length corresponding to peak period	[m]
Lo	Wave length at deep water	[m]
MLP	Multilayer Perception network	
n	Porosity	[-]
P	Flux density in x direction	[m^3/m/s]
Q	Flux density in y direction	[m^3/m/s]
R	Correlation coefficient	[-]
R*	Dimensionless run-up coefficient	[-]
RBF	Radial Basis Function network	
Rc	Freeboard of breakwater's crest	[m]
s/Som	Wave steepness (Ho/Lo)	[-]
T	Significant wave period	[s]
t	time	[s]
Tp	Spectral peak period	[s]
Vt	Total volume	[m^3]
Vv	Volume of voids	[m^3]
α	Side slope angle of breakwater	[o]
γf	Roughness factor for the structure	[-]
ξ	Irabarren number, Surf-similarity index	[-]
Ψ1/Ψ2	Dispersive Boussinesq terms	[-]

1   Introduction

1.1   Background to the Research

Wave action in the surf zone is responsible for many phenomena that influence the morphology of the coastline. The driving force for these morphological changes is sediment transport which results in the accretion or erosion along various parts of the coast. The need to protect coasts has increased dramatically over the last years as the result of the population growth and urbanization. Half of the world's population lives in coastal regions, many of them exposed to the dangers of wave action as a result of the sea level rise. For that reason the need to protect the water boundaries of these areas has increased. Over the past decades numerous shoreline protection schemes have been proposed designed and implemented such as: dikes, revetments, groynes, nourishments, and detached submerged and emerged breakwaters. Over the past 30 years considerable amount of research has been conducted in the field of breakwater design and wave-structure interaction. In recent years there has been a shift of preferences in coastal structures from structures that completely prevent wave transmission to submerged structures that only allow a restricted amount of energy to pass over them and allow waves to break at some distance from the shore. There are several reasons that contributed to this shift such as:

- Low construction costs compared to other hard structures that completely block waves.
- Aesthetics, submerged structures do not disturb the line of site (especially in regions where the tide variation is negligible, such as the Mediterranean and the Persian Gulf).
- Environmental, SS's allow create a mild wave environment on the lee side which provides a friendly environment for marine fauna and flora
- Recreational, enhancing surfing conditions as in the artificial reef in the Golden Coast, Australia.
- Effectiveness in trapping sediment and consequently protecting the shore from erosion.

Despite the research that has been conducted many questions have still not been answered with respect to the hydrodynamic phenomena that occur on the lee side of SS's. There is a lack of information regarding information about the wave steepness, spectral shape, wave period, current patterns, sediment transport etc. In order to find an answer, there is a need of developing a prediction tool that is capable of not only to predict average values of wave transmission but also the special distribution of the wave heights in the lee side of the structure. Very few studies have examined the 3D effects around detached breakwaters and even less the combined effects overtopping diffraction and permeability. The main reason behind this is that scaling both seepage and wave structure interactions are contradicting processes (Froude Number versus Weber number). Only a small number of studies can be found on the topic of near shore wave transmission at submerged breakwaters. This was the main stimulus and driving force behind the present report.

Artificial Neural Networks (hereafter ANN's) which are data-driven algorithms have been used in the past to solve complicated nonlinear problems. A number of studies have implemented them in the area of coastal engineering (Mase et al. 1995, van Gent and van den Boogard 1998, Medina 1999, van der Meer et al. 2005, van Gent et al. 2007, Panizzo and Briganti 2007, Sharifahmanian 2013).

The PhD project of Amir Sharif Ahmadian under the supervision of professor Richard Simons at the University College of London (UCL) developed a design tool using an ANN that is intended to improve 3D wave prediction behind breakwaters (Sharif Ahmadian and Simons, 2012). The model includes both diffraction and overtopping effects. Unfortunately the model did not include permeability effects. This tool may allow the more successful prediction of sediment and current patterns on the lee side of breakwaters.

The study described in this report has the purpose of examining the effects of permeability on wave transmission at submerged breakwaters and to create a forecasting tool capable of predicting the spatial variation of the wave transmission coefficient behind submerged permeable breakwaters.

1.2 Objectives

This report has two main objectives which can be defined in the form of two questions and are presented below:

1. Does the permeability of submerged breakwaters influence the wave transmission process?
2. Is it possible to predict more accurately the wave field behind submerged breakwaters by incorporating permeability in an ANN program which is trained using data from a well calibrated 2DH Boussinsesq wave model?

In the process required to answer the above questions several other problems arise. These are as follows:

1. How can permeability be incorporated in an ANN model and how can we optimize the models predicting capabilities?
2. Can data obtained from a wave model (e.g. MIKE 21 2DH Boussinsesq) be used in the training of an ANN algorithm without introducing a considerable error?
3. Are the results obtained by the updated ANN model more accurate than the results produced by the ANN model developed by Sharifahmanian?

1.3 Aim of this report

The aim of this study is to develop a new design tool that will effectively predict the spatial distribution of the wave transmission coefficient by taking into account the combined effects of diffraction overtopping and permeability of submerged breakwaters. Until now it was believed that the governing phenomenon driving wave transmission in permeable

submerged breakwaters was overtopping. This report aims to provide proof that permeability has an effect on the wave transmission behind rubble mound breakwaters.

It is known that the physical phenomena governing wave transmission are:

- Wave overtopping
- Diffraction
- Permeability

It is therefore important to develop a design tool that will take into account all three driving forces responsible for the phenomenon of wave transmission. This will allow predicting accurately the spatial distribution of the transmitted wave field. This in turn will allow describing more accurately the flow circulation and sediment transport around the breakwater.

1.4   Methodology

The purpose of this report is to update an existing ANN algorithm capable of predicting the spatial wave height distribution around submerged breakwaters (Sharif Ahmadian and Simons, 2012) by including effects of permeability.

 The wave field around submerged breakwaters is attributed to the following phenomena:

- Overtopping
- Diffraction
- Permeability
- Sub-harmonic generation due to non-linear interaction within the breakwater itself

The latter has a negligible effect on the wave heights but contributes more to the shift of energy to higher/lower frequencies.

The original model includes the effects of overtopping and diffraction. In this study the possibility of including the effects of permeability in the ANN model, by training it with pseudo-data obtained from MIKE21BW will be examined. It is therefore essential for this study to calibrate and validate the wave model as well as possible.

Database description

It is not possible to obtain three dimensional data for permeable breakwaters within the short period of this study therefore an indirect way of obtaining training and testing data for the ANN is applied. Available two dimensional data are obtained from the DELOS project, which includes datasets for permeable/impermeable, smooth/rough, emerged and submerged breakwaters. 2D and 3D measurements for impermeable and smooth submerged breakwaters are available from Sharif Ahmadian and Simons, 2012. The following table demonstrates a summary of the available data:

		Dataset Name	
		DELOS	UCL
Main Characteristics of data	2D	included	included
	3D	not included	included
	Impermeable	included	included
	Permeable	included	not included
	Smooth	included	included
	Rough	included	included

Table 1.1: Summary of most important characteristics of datasets included in this study

Approach to the study

Initially a number of datasets will be collected from various sources. The next phase of the study includes a filtering process where all unnecessary information will be discarded. Additionally a preliminary analysis based on curve fitting was conducted in order to determine which parameters from the datasets could potentially help describing the phenomenon of wave transmission; particular focus was given on finding a new dimensionless parameter that could account for permeability effects. Following this, the wave model (MIKE21 BW) was calibrated for the scenarios where the breakwater heads are not included (2-D) using the DELOS database. Based on the equations that MIKE21 BW uses, it can be safely assumed that if the calibrated model can reproduce correctly the wave field behind the breakwater for the scenario where diffraction is excluded, then it can be applied to a scenario where diffraction is included (3-D), giving realistic output. The outputs of the 3-D model are then tested against the 3-D theory developed by Vicinanza et al. (2009) in order to verify the above mentioned assumption. Following that a new dataset will be created, using the wave model in order to train and validate the ANN. The next step will be to test the accuracy of the ANN model using several statistical measures and examine its sensitivity to several parameters. Finally the layout of future physical experiments that will allow training the ANN with a dataset that includes physical variability is proposed.
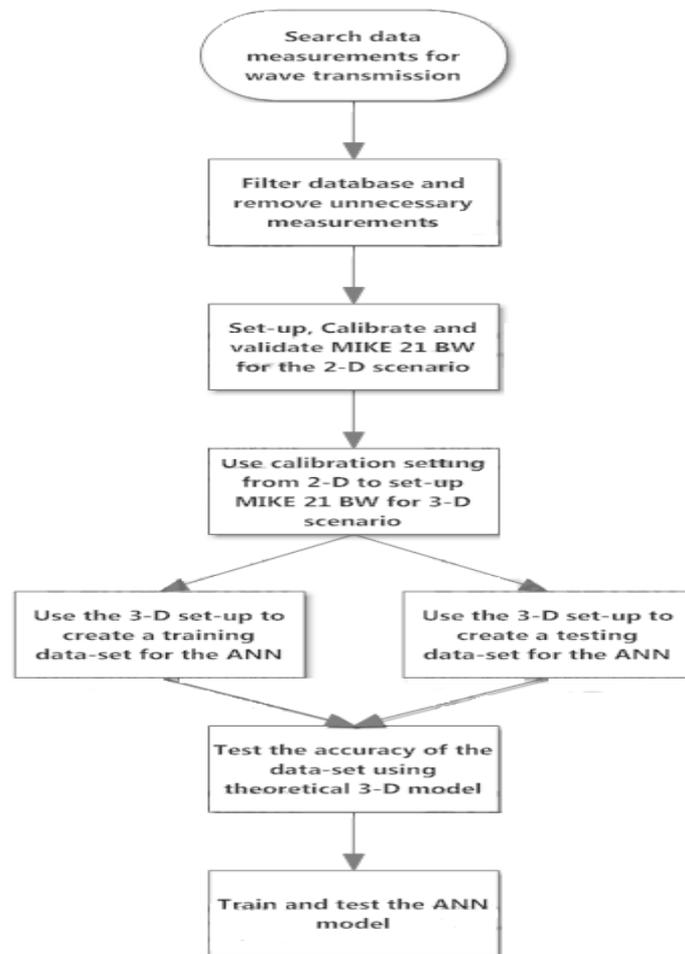
Figure 1.1: Flow chart presenting the methodology followed in this report

1.5   Layout of Report

As described in the previous section this thesis deals with the numerical modelling of wave fields around submerged breakwaters in two ways, first with the numerical a hydrodynamic model used to create an extensive database that includes information of the spatial distribution of the wave field around submerged porous breakwaters and then with the an ANN algorithm capable of predicting the 3D wave transmission around breakwaters. The structure of this thesis is as follows.

Chapter 1 gives an outline of the structure of the report and provides an introduction to the main objectives and aims of this study. It also provides a description of the methodology that was used in order to complete this research.

Chapter 2 provides an introduction to the wave transmission phenomenon followed by an extensive literature review of previous publications relevant to this study which include prediction formulation and numerical studies. This chapter concludes with an outline of the most relevant parameters to the wave transmission process based on previous studies.

Chapter 3 presents all the theory relevant to this study. First the key equations and theory used by the numerical wave model (MIKE21 BW) will be presented, followed by an introduction to ANN modelling in general and finally an overview of several diffraction theories and the 3D wave transmission theory used for verifying the results of this study will be presented.

Chapter 4 provides the procedure followed in order to obtain the data used for validation of MIKE21 BW and the ANN model training. In addition it presents the key finding of the 2D and 3D wave transmission modelling.

Chapter 5 contains the results of the validation process of the 2D and 3D experiments. The validation of the 3D experiments has been performed with the use of the traditional and modified empirical method proposed by Vicinanza et al. (2008).

Chapter 6 presents the process followed to create the ANN model. In addition the results of two different sensitivity analyses and the validation process are also presented.

Finally chapters 7 and 8 will provide an outline of the conclusions of this project along with the recommendations for improving the results and knowledge on this subject.

2   Literature review

2.1   The Wave Transmission phenomenon

Detached breakwaters, reef breakwaters and spurs are all shore parallel structures constructed to reduce the wave climate on the lee side of the breakwater or to obstruct the sediment transport along the coast. This report will focus on submerged breakwaters which are a special subcategory of the shore-parallel structures, where the crest is located below the water surface. Within this category two main structure types are distinguished, namely the reef type and the detached type. Reef type breakwaters are wide crested rubble mounds consisting of large rocks; they are designed in order to deform and to adjust to the local wave climate. Detached submerged breakwaters are structures of similar nature to the reef type, with their main difference located to the fact that they are usually constructed out of prefabricated material and are not allowed to deform.

As stated above the primary purpose of breakwaters is to reduce the transmitted wave energy on the lee side. "Wave transmission" refers to the wave energy that is allowed to travel over and past the breakwater. The three governing mechanisms transporting this energy are seepage, overtopping and diffraction. The wave energy that is attenuated is either dissipated by the structure through friction, turbulence, wave breaking and armor unit movement or reflected back creating a weak standing wave pattern in front of the breakwater.

Submerged breakwaters have been proven to be a popular tool against coastal erosion, especially in areas with low tidal range. The main advantages of these structures are the low construction cost and the negligible impact they have on the landscape. Also in some cases reef type breakwaters have been designed in order to improve the local wild life by providing corals and fish with favorable conditions for reproduction.

This chapter will present the most relevant studies associated with this thesis. Literature related to submerged breakwaters and the associated wave transmission around them will be presented in two main groups:

- Literature related to wave transmission prediction formulae, which cover the physical processes of seepage (permeability) and overtopping.
- Literature related to numerical models designed for treating wave transmission problems.

Finally an overview of the main parameters influencing wave transmission will be presented.

2.2 Prediction Formulas

This section will present an extensive literature review on empirical formulations.

Goda et al. (1967) conducted a series of experiments on vertical and composite breakwaters in a wave flume. They found that the wave transmission was most dependent on the submergence ratio ($\frac{h_s}{H_i}$) and proposed the following wave formula:

$$K_t = \frac{1}{2}\left(1 - \sin\left(\left(\frac{\pi}{2\alpha}\right)\beta - \frac{h_s}{H_i}\right)\right)$$

Eq. 2.1

Where α and β are dimensionless coefficients that depend on the structure type and ranging from 2 to 2.2 and 0.1 to 0.5 respectively.

Under Allsop's (1983) study LCS's were tested in order to determine the influence of wave overtopping to the wave transmission phenomenon. Allsop recommended that a dimensionless overtopping parameter should be introduced to the formula developed by Goda. The modified formula was now:

$$K_t - \frac{1}{2} = \frac{1}{2}\left(1 - \sin\left(\left(\frac{\pi}{2\alpha}\right)\beta - R^*\right)\right) \text{ with } R^* = \frac{h_s}{H_i}\left(\frac{s}{2\pi}\right)^{0.5}$$

Eq. 2.2

Ahrens (1987) conducted an extensive number of experiments in order to examine the stability of reef type breakwaters. During his research he derived the following formula for wave transmission using regression analysis:

$$K_t = \frac{1}{1 + \left(\frac{H_i A_t}{L_p d_{50}^2}\right)^{0.592}} \text{ for } \frac{h_s}{H_i} < -1$$

Eq. 2.3

$$Kt = \frac{1}{1 + \left(\frac{d}{h}\right)^{c_1}\left(\frac{A_t}{hL_p}\right)^{c_2} e^{\left(c_3\left(\frac{h_s}{H_i}\right) + c_4\left(\frac{A_t^{\frac{3}{2}}}{L_p d_{50}^2}\right)\right)}} \text{ for } \frac{h_s}{H_i} > -1$$

Eq. 2.4

In the above $c_1, c_2, c_3 \text{ and } c_4$ are dimensionless constants with values of 1.188, 0.2611, -0.592 and 0.00551 respectively. Also A_t (m^2) is the breakwater cross sectional area, L_p (m) the peak wave length, d_{50} (m) nominal stone diameter of the breakwater, d (m) is the height of the breakwater measured from the bed, h (m) is the still water level and h_s (m) the submergence depth of the breakwater measured. It should also be mentioned that Ahrens was the first researcher who understood that porosity could potentially influence the wave transmission process and for that reason measured it in his experiments. In his experiment the porosity (n) was determined to be 0.40.

Van der Meer (1991) collected data from previous studies on wave transmission and developed a wave transmission formula in which the wave transmission coefficient is determined based on their submergence to incoming wave height ratio:

$$K_t = 0.8 \; for \; 2 > \frac{h_s}{H_i} > 1.13$$

$$K_t = 0.46 + 0.3 * \frac{h_s}{H_i} \; for \; 1.13 > \frac{h_s}{H_i} > 0.2 \hspace{4cm} \text{Eq. 2.5}$$

$$K_t = 0.1 \; for - 0.2 < \frac{h_s}{H_i} < -1.2$$

In 1994 Daemen and Van der Meer proposed a new relationship for the determination of the wave transmission coefficient. They observed that the ratio $\frac{h_s}{d_{50}}$ gave the best fit to the measured data up to that period and proposed the following formula:

$$K_t = a + \left(-\frac{h_s}{d_{50}}\right) - b \hspace{4cm} \text{Eq. 2.6}$$

with:

$$a = 0.031 \left(-\frac{h_s}{d_{50}}\right) - 0.24 \hspace{4cm} \text{Eq. 2.7}$$

$$b = -5.42 \left(\frac{H_i}{L_0}\right) + 0.0323 \left(\frac{H_i}{d_{50}}\right) - 0.0017 \left(\frac{B}{d_{50}}\right)^{1.84} + 0.51 \; for \; reg. \, breakwaters$$

$$\text{Eq. 2.8}$$

$$b = -2.6 * \left(\frac{H_i}{L_0}\right) - 0.05 \left(\frac{H_i}{d_{50}}\right) + 0.85 \; for \; reef \; type \; breakwaters \hspace{1cm} \text{Eq. 2.9}$$

The validity of the above formula is restricted to the range of the following dimensional parameters:

$1 < \frac{H_i}{d_{50}} < 6, 0.01 < \frac{H_i}{L_0} < 0.05$. Rivero et al. (1997) showed that both equations proposed by Van der Meer under-predicted the wave transmission coefficient.

D' Angremond et al. (1996) reanalyzed the experimental results collected by Van der Meer and proposed an new empirical formula, which proved to give very accurate results for non-breaking waves (information for extremely steep waves were discarded). The new empirical formula was:

$$K_t = \frac{0.4 h_s}{H_i} + \left(\frac{B}{H_i}\right)^{-0.31} a\left(1 - e^{-0.5\xi}\right) \hspace{3cm} \text{Eq. 2.10}$$

Where a is a dimensionless coefficient that equals 0.64 for rubble mound breakwaters and 0.8 for impermeable breakwaters.

Seabrook and Hall (1998) performed a large number of two and three dimensional experiments. Their work was focused strictly on submerged breakwater and they concluded that the width of the structure is the governing parameter determining the wave transmission coefficient. Their new formula proved to be capable of predicting accurately the wave transmission coefficient and particularly in the case where the breakwaters had a relatively wide crest:

$$K_t = 1 - (e^{-0.56\left(\frac{h_s}{H_i}\right)-1.09\left(\frac{H_i}{B}\right)} + 0.047\left(\frac{Bh_s}{L_0 d_{50}}\right) - 0.067(\frac{h_s H_i}{B d_{50}}) \qquad \text{Eq. 2.11}$$

This function is valid for the following ranges: $0 \leq \frac{Bh_s}{L_0 d_{50}} \leq 7.08$ and

$0 \leq \frac{h_s H_i}{B d_{50}} \leq 2.14$. Additionally their work showed that the equation given by Ahrens (1987) and Van der Meer (1991) did not predict accurately K_t for structures with wide crests. The findings also showed evidence of energy shift to higher harmonics for waves passing over breakwaters, based on their work the parameter determining the extent of this energy shift was the crest width.

Gironella and Sanchez-Arcilla (1999) reanalyzed several experimental data and found that the dimensionless parameter that best described the wave transmission coefficient was $\frac{h_s}{L_0}$. The new empirical formula gave a very high accuracy of $R^2 = 0.98$. The domain in which the proposed formula is valid is: $3.2 \leq \xi \leq 5.5$, $0 \leq \frac{h_s}{L_0} \leq 0.04$ and $\frac{H_i}{L_0}$. Finally the new equation reads as:

$$K_t = 6.43\left(\xi \frac{h_s}{L_0}\right) + 14.63\frac{h_s}{L_0} + 0.52 \qquad \text{Eq. 2.12}$$

Bleck and Oumeraci (2001) conducted a series of experiments on submerged rectangular breakwaters. During their analysis they found that the dimensionless submergence ratio $\left(\frac{h_s}{H_i}\right)$ was the most influential parameter. This finding agreed with the findings of Van der Meer (1990) and Goda (1967). The formula reads as follows:

$$K_t = 1 - 0.83e^{-\frac{0.72h_s}{H_i}} \qquad \text{Eq. 2.13}$$

Calabrese et al. (2002) proposed a formula based on information obtained from large scale experiments.

$$K_t = \frac{(-0.562e^{-0.0507\xi})h_s}{B} + ((\frac{0.6957H_i}{h} - 0.7021)e^{\frac{0.2568B}{H_i}})e^{-\frac{0.0845B}{H_i}} \qquad \text{Eq. 2.14}$$

The range of validity is as follows: $-0.3 \leq \frac{h_s}{B} \leq 0.4$, $1.06 \leq \frac{B}{H_i} \leq 8.13$, $0.31 \leq \frac{H_i}{h} \leq 0.61$, $3 \leq \xi \leq 5.2$.

Briganti et al. (2004) recalibrated the formula for rubble mound breakwaters proposed by d' Angremond et al. (1996). They recommended that the equation should remain the same for the range of $\frac{B}{H_i} < 10$ and for the range of $\frac{B}{H_i} > 10$ should become:

$$K_t = \frac{0.35h_s}{H_i} + \left(\frac{B}{H_i}\right)^{-0.31} 0.51\left(1 - e^{-0.5\xi}\right)$$

Eq. 2.14

Also a new upper limit of the equation was proposed improving the accuracy in the region of high K_t; the new limit was:

$$K_{t_{upper}} = -0.006\frac{B}{H_i} + 0.93$$

Eq. 2.15

In the same study the equation for smooth impermeable structures was recalibrated as well but it is out of the scope of this report and therefore will not be demonstrated.

Buccino and Calabrese (2007) in their paper presented a semi empirical model capable of predicting the wave transmission coefficient very accurately. The method used is based on a crude schematization of the physical processes that they believed governs wave transmission. In their work they treated emerged and submerged breakwaters separately. Unfortunately one of their main assumptions for submerged breakwaters is that seepage is not a phenomenon that influences wave transmission significantly. As emerged barriers do not fall within the scope of this study only the equation for submerged structures will be presented:

$$K_t = \left(0.75 - \frac{0.25B}{\sqrt{H_{moi}L_{0p}}}\right)^2 e^{\left(-\frac{11R_C}{H_{moi}}*\frac{1}{\gamma_f}*\sqrt{\frac{S_{0m}}{2\pi}}\right)}$$

Eq. 2.16

Goda and Ahrens (2008) developed a new prediction formula that treats separately emerged and submerged breakwaters. Their study was based on field measurements in observation sites around Japan. In their formulation wave transmission due to seepage and overtopping is calculated separately. Based on this the proposed prediction formula reads as:

$$K_t = min\left\{1.0, \sqrt{K_{t_{over}}^2 + K_h^2 K_{t_{thru}}^2}\right\}$$

Eq. 2.17

where:

$$K_{t_{over}} = max\left\{0, 1 - \exp\left(0.248\,exp\left(-0.384\,ln\left(\frac{B_{eff}}{L_0}\right)\right)\frac{h_c}{H_i} - F_0\right)\right\}$$

Eq. 2.18

With $K_{t_{over}}$ denoting the wave transmission coefficient passing over the breakwater, $B_{eff} = \frac{4(B + bottom\ width)}{5}$ the effective width of submerged breakwater and $F_0 = max\left\{0.5, min\left(1.0, \frac{H_i}{D_{n_{50}}}\right)\right\}$ which is a dimensionless measure of the run-up limit.

$$K_{t_{thru}} = \frac{1}{\left(1 + 1.135\left(\frac{B}{D_{n_{50}}}\right)^{0.65}\sqrt{\frac{H_i}{L_0}}\right)^2}$$

Eq. 2.19

$K_{t_{thru}}$, for the transmission coefficient of wave passing through the breakwater

$K_h = 1$, for submerged breakwaters and represents a proportionality factor.

The formula presented above has the advantage that it is designed specifically for submerged porous breakwaters, in contrast with the majority of the others presented above. Again its disadvantage is that it is not capable of predicting the 3D effects of wave transmission behind semi-infinite breakwaters.

In order to get a feel of how the functions above behave at different conditions two different plots of the most widely used formulas have been created.
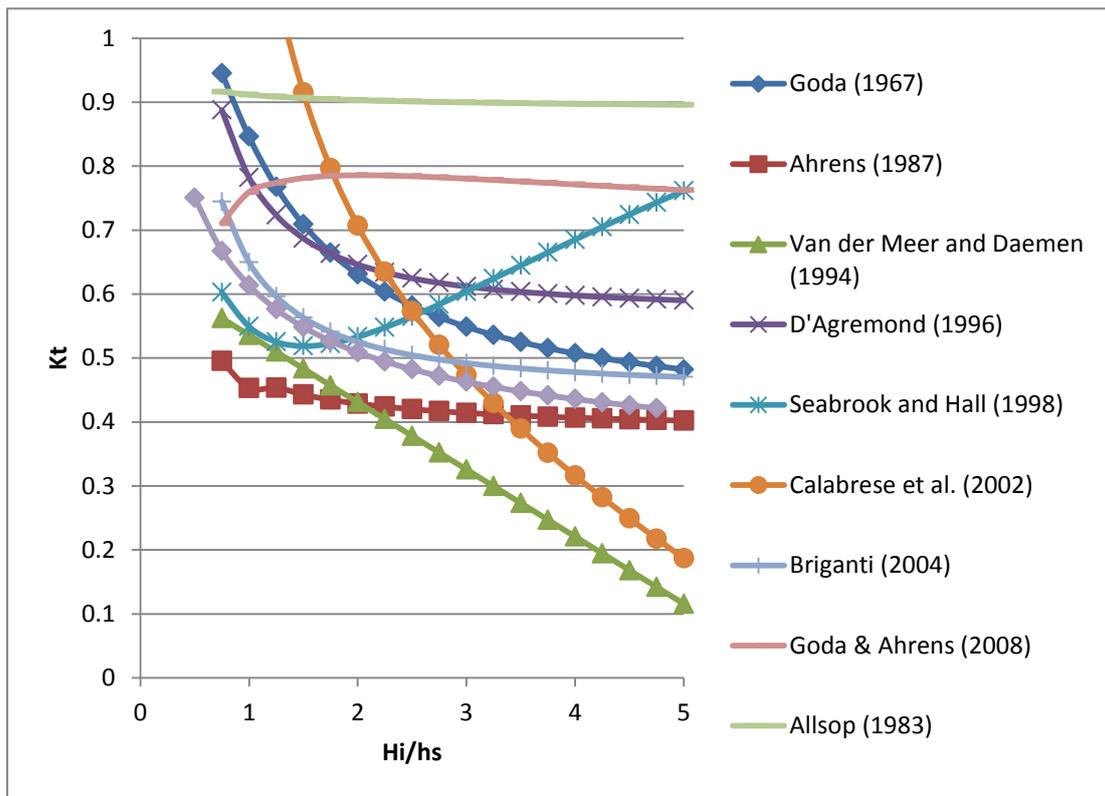
Figure 2.1: Kt versus dimensionless incoming wave height for different prediction formulae
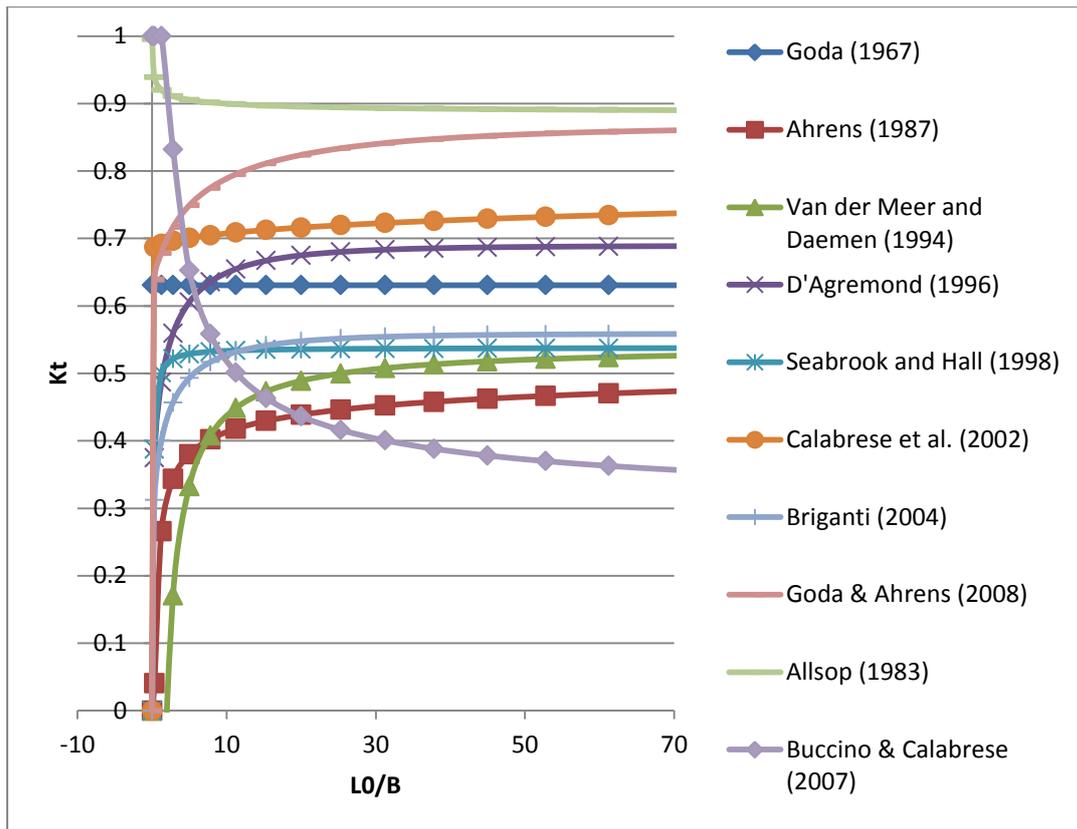
Figure 2.2: Kt versus Dimensionless wave length for different prediction formulae

From the graphs above it can be seen that all formulae follow a different path and are influenced differently by each parameter. In figure 2.1 the equation of Seabrook and Hall (1998) follows a completely different path as the others as is the case for the Buccino and Calabrese (2007), and Alsop (1983) equations in figure 2.2. These evident discrepancies may be attributed to the different ranges of validity that each formula has. Therefore when designing, one should always be aware under what conditions each formula has been calibrated in order to have reliable results. In addition two important conclusions may be drawn from the figures presented above. Firstly the dimensionless parameter $\frac{H_i}{h_s}$ has a very strong influence an all prediction formulae except in the one proposed by Allsop (1983). Secondly, that the dimensionless wave length has a strong influence on the wave transmission coefficient when the width of the structure is in the same order of magnitude as the wave length. For this reason it is sensitive to examine in some more detail the physical processes governing wave transmission though permeable breakwaters.

2.3   Numerical Studies

Massel's (1980) analysis was undertaken in order to extend a previous simplified theory for the determination of transmission and reflected characteristics of porous breakwaters subjected to the action of the wind - induced waves. The key points of his study were:

- The original nonlinear equation of motion into porous structure was linearized using statistical linearization techniques.
- The computed output consists of the spectral density functions for the reflected and transmitted waves.
- The statistical transmission and reflection coefficients are introduced in terms of the standard deviations and the wave spectra.

Even though this model gave good results in 2D, it was not capable of predicting 3D wave transmission. Nevertheless this model was the first of its kind and opened the road for developing more sophisticated programs that eventually could be used to predict three dimensional wave transmission phenomena.

Kobayashi and Warjanto (1989) developed a numerical model based on the nonlinear shallow water equations under the hypothesis of hydrostatic conditions by integrating the Navier-Stokes equations in the vertical column. This method presents a main limitation as it cannot be applied in shallow waters and produces poor results when dealing with high frequencies. The semi-empirical formulation for wave breaking and porous flow introduces an additional source of error and makes the model less reliable for determining wave transmission coefficients.

Rojanakamthorn (1990) developed a mathematical model capable of predicting wave transformation over submerged permeable breakwaters. The model relies on the equations for waves on a porous layer which were derived under the mild-slope assumption. The model equation is given as a two-dimensional elliptic. Wave breaking over the barrier is modeled via the modified mild-slope equation. Finally the numerical model is validated using experiments for trapezoidal breakwaters. The method yielded excellent prediction capacity. Unfortunately as for all previous models this was developed only for 2D scenarios, as the computation capacity of computers was limited.

Battjes (1994) developed a numerical model based on a one-dimensional time domain Boussinesq model with improved dispersion characteristics. The model was designed to simulate long, unidirectional waves propagating over submerged barriers. The model had the capability to mimic relatively well the phenomena of harmonic generation and wave decomposition. The model was validated against experimental data for non-breaking waves and showed good agreement.

Van Gent (1994) designed a PC-model named ODIFLOCS capable of predicting the wave conditions behind several types of structures. The model had the ability to deal with several types of structures such as:

- Dikes
- Revetments
- Submerged and emerged breakwaters
- Permeable and impermeable breakwaters

The model was capable of simulating two dimensional external and internal flows. Also the model was able to take into account several one dimensional phenomena such as: reflection, permeability, infiltration, seepage, overtopping, varying roughness along the slope, linear and non-linear porous friction (Darcy and turbulent friction), added mass, internal set-up and the disconnection of the free surface and the phreatic surface. Again the model was not capable of predicting the spatial variation of the wave heights behind the breakwater.

Lossada (1995) developed a model that successfully predicted the transformation and interaction of regular wave trains with submerged permeable barriers. Special attention was given to the influence of wave characteristics including oblique incidence, structure geometry and porous material properties on the hydrodynamics outside and inside the breakwater. The model had two modes:

- 3-D mode, which was based on eigenfunction expansions.
- 2-D mode, based on a mild-slope equation for porous media to account for breakwater slope.

Lin and Liu (1998) developed COBRA (Cornell Breaking and Structures). COBRA is a RANS (Reynolds Average Navier-Stokes) model based on a previous developed model by Kothe et al. (1991) called RIPPLE. This model is an extensively validated model capable of simulating breaking waves and wave-structure interactions. In addition it has been the most tested model of its kind and one of the most reliable tools for examining the wave-structure interactions of porous elements as it takes into account the turbulent generation and dissipation mechanisms within the structure itself. This method as well requires considerable computation time.

Lynett et al. (2000) introduced a new model in which the shallow limit problem encountered by solving the nonlinear shallow water equations was solved by using the modified Boussinesq equations. The results presented had a high level of accuracy. Despite the encouraging findings of Lynett et al. the computational time required to solve the modified Boussinesq equations made it very difficult to use in real life applications.

Dalrymple et al. (2001) developed a new Smoothed Particle Hydrodynamics (S.P.H.) model for free surface flows. It is based on the grid-less Langrangian method which is capable of tracking deformations of free surface flows. As the Boussinesq equations the S.P.H. method requires high computation times and makes it an unfavorable choice for researchers.

Additionally this model requires high numbers of particles as well as fixed particle spacing which makes the model very hard to validate.

Van Oosten and Peixo (2005) developed a neural network based on the concept of a homogeneous database that was capable of predicting 2D wave transmission behind a large number of LCS's, based on the DELOS database. The method proved to be more successful than any previous established prediction formula. The shortcoming of this model was it was not designed to predict the 3D spatial variation of the wave field.

The last relevant study was by Panizzo and Briganti (2007). As Van Oosten and Peixo (2005) they developed a new ANN model capable of forecasting the wave transmission behind breakwaters. The project successfully developed a more accurate and robust method for predicting the wave transmission coefficient for two dimensional situations.

Summarizing, even though several models were developed over the fifty years, literature lacks a comprehensive model capable of predicting the three dimensional effects related to wave structure interaction. The literature review shows that only 2D effects have been studied with high detail. The accuracy of these models is high and allows them to be used for simple engineering applications and desk studies, in order to obtain a first order understanding of the transmitted wave height. On the other side 3D effects have not been studied due to their complexity and high computational demand. Producing a model capable of predicting 3D wave transmission seems to be difficult and computationally expensive. For this reason in this thesis an attempt will be made to produce a tool capable of predicting the wave field behind the breakwater that could be used as a simple design tool. The model will have the capability to give a first feel about the wave pattern behind the breakwater without the need to use a time consuming hydrodynamic model.

3 Theoretical Background Relevant to the Study

3.1 Introduction

In this chapter all relevant theories that are related to this study will be presented. The purpose of this section is to provide the reader with all the background knowledge associated with this study that is required in order to understand the analysis to be followed. As stated before only a little research related to three dimensional wave transmission by breakwaters has been conducted and even fewer on permeable breakwaters. For that reason obtaining reliable data that could be used for training an ANN model accurately is impossible. The way to overcome this obstacle is to create "artificial" data using a computer model capable of reproducing accurately the wave field around the breakwater, such as MIKE 21 BW. It is therefore very important for the precision of the A.N.N. model to create a training database that is as accurate as possible. Thus a large part of this report will be spent analysing the dataset created by MIKE 21 BW. The accuracy analysis of the training data set will be accomplished by the following two methods:

- First a qualitative comparison with the 3 dimensional tests conducted by Sharif Ahmadian (2012) will be conducted in order to ensure that the overall behaviour of the model coincides with the actual physical measurements.
- Secondly a direct comparison of the training dataset with the three dimensional prediction model proposed by Vicinanza et al. (2009) in combination with empirical formulations for the prediction of the wave transmission and wave diffraction.

This chapter will first present the equations used by MIKE21 BW, following by a description of ANN models in general and will conclude with the diffraction theory and the 3D-prediction method proposed by Vicinanza et al (2009).

3.2   Important wave transmission parameters

For the sake of consistency this section will provide a description of the most important parameters for the wave transmission process along with the notation that will be used in this study.
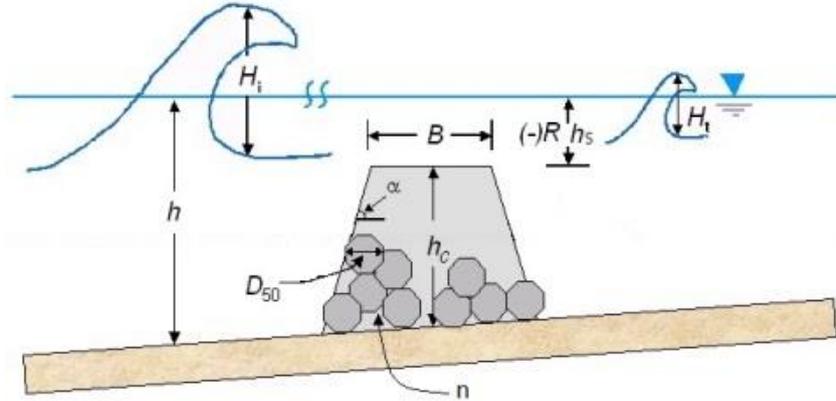
Figure 3.1:Physical parameters influencing the wave transmission process

Incident wave height (H_i)

The wave height is defined as the vertical distance between the highest (crest) and the lowest (trough) part of the wave. The incident wave height is measured at the front toe of the breakwater. This parameter can be characterized as the most important of the entire dataset as it will be used to make dimensionless various other parameters. This will be demonstrated in the following chapters.

Wave Period and Peak Wave Period (T_0 and T_p)

The incident wave period is defined as the time interval between the start and the end of the wave (i.e. the interval between two zero crossings upward or downward). Wave period is connected with the wave length with the following relation, according to linear wave theory:

$$L = L_0 \tanh\left(\frac{2\pi d}{L}\right) \qquad\qquad \text{Eq. 2.20}$$

where:

$$L_0 = \frac{gT^2}{2\pi} \qquad\qquad \text{Eq. 2.21}$$

The wave period influences the wave transmission process significantly as it has been observed that longer waves result in a higher wave height on the lee side of the structure. This can be explained in two ways:

- Longer waves have the capability to move through the breakwater without losing much energy due to turbulent losses.
- If the breakwater is located in relatively deep water longer incident waves have a higher probability of not breaking.

Furthermore it has been found the peak wave period describes better spectral waves. The relation between peak wave period and zero moment wave period is given by:

$$T_0 = 0.95 T_p \qquad\qquad\qquad \text{Eq. 2.22}$$

Submergence Depth (h_s)

The submergence depth is defined as the vertical distance between the structur's crest and the water surface. In the case of LCS's the variable is defined as the crest freeboard (R) which is positive in the case of emerged breakwaters and negative in the case of submerged. This is one of the most contributing variables for the wave transmission process. A large submergence depth relative to the incoming wave height results in high wave transmission coefficients K_t and vice versa.

Crest Width (B)

Crest width is defined as the distance between the sea side edge of the crest and the lee side edge. The width of the structure is of significance as longer structures result in more wave energy dissipation due to turbulent losses and a higher probability of wave breaking.

Slope of the structure (α)

The slope of the structure contributes to the overall wave transmission process in more than one ways. The slope angle influences significantly the Iribarren number (ξ) which is a measure of the relative wave steepness over the structure, defined as:

$$\xi = \frac{\tan(\alpha)}{\sqrt{\frac{H_i}{T}}} \qquad\qquad\qquad \text{Eq. 2.23}$$

A low value of ξ means that the slopes of the structure are gentle compared to the wave which results in a longer distance where energy is dissipated and therefore to a lower K_t. On the other hand a larger Iribarren number means that the slope is steep compared to the wave which then would result in more violent wave breaking that would finally create a larger disturbance on the lee side. Finally larger ξ values are associated with larger partial reflection coefficients (K_r) of waves, which results in a lower transmission coefficient as $K_t = \sqrt{1 - K_{dissipation} - K_r}$. As can be understood these are contradicting phenomena and the influence of ξ on the transmission coefficient is very complex.

Nominal Stone Diameter ($D_{n_{50}}$)

The nominal stone diameter is defined as the mean value of the diameter of the stone comprising the breakwater core. This value influences the energy dissipation due to turbulence. It is expected that larger stones allow more energy to flow through the structure and therefore result is less energy dissipation, at the same time larger voids volumes are associated with larger eddies inside the breakwater which result is higher energy dissipation. The influence of the stone diameter in numerical modelling depends strongly on the turbulence theory applied for simulating the Non-Darcy friction losses.

Porosity (n)

The definition of porosity *n* is given by the ratio of the volume of voids to the total volume of the structure $\left(\frac{V_v}{V_T}\right)$. It can be perceived as a measure of the degree of grading of the rock, as more wide grading will result in more small pores and therefore less voids vice versa. This parameter is also of importance as together with the nominal stone diameter it can describe successfully the degree of energy dissipation that is expected from the breakwater.

3.3 MIKE 21 BW

MIKE 21 BW is a numerical modelling tool devoted to the study and analysis of wave disturbance in coastal areas. Its accuracy and wide range of applicability makes it a very powerful tool for analysing any coastal wave problems. MIKE 21 BW is capable of reproducing the combined effect of the most important wave processes that are important for the study of coastal engineering problems such as:

- shoaling
- refraction
- diffraction
- wave breaking
- bottom dissipation
- partial reflection
- wave transmission
- non-linear wave-wave interactions

This model works by solving numerically the time domain Boussinesq equations based on the approximations of Madsen et al (1991, 1992, 1997a, b), Sørensen and Sørensen (2001) and Sørensen et al (2004). The enhanced Boussinesq equations make it possible to simulate the propagation of non-linear directional waves from deep to shallow water and also to reproduce accurately the combined effect of seepage and diffraction which are of significant importance for this study.

MIKE 21 BW solves the enhanced Boussinesq equations expressed in two horizontal dimensions in terms of the free surface elevation, ξ, and the depth-integrated velocity-components, P and Q. Using the Boussinesq dispersion coefficient B
The Boussinesq equations are:

- Continuity:

$$n\frac{\partial}{\partial t} + \frac{\partial P}{\partial t} + \frac{\partial Q}{\partial t} = 0 \qquad\qquad \text{Eq. 3.1}$$

- X-momentum:

$$n\frac{\partial P}{\partial t} + \frac{\partial}{\partial x}\left(\frac{P^2}{h}\right) + \frac{\partial}{\partial y}\left(\frac{PQ}{h}\right) + \frac{\partial R_{xx}}{\partial x} + \frac{\partial R_{xy}}{\partial x} + n^2gh\frac{\partial}{\partial x} + n^2P\left(\alpha + \beta\frac{\sqrt{Q^2+P^2}}{h}\right) + gP\frac{\sqrt{P^2+Q^2}}{h^2C^2} +$$
$$n\Psi_1 = 0 \qquad\qquad \text{Eq. 3.2}$$

- Y-momentum:

$$n\frac{\partial P}{\partial t} + \frac{\partial}{\partial y}\left(\frac{Q^2}{h}\right) + \frac{\partial}{\partial x}\left(\frac{PQ}{h}\right) + \frac{\partial R_{xx}}{\partial x} + \frac{\partial R_{xy}}{\partial x} + n^2gh\frac{\partial}{\partial y} + n^2Q\left(\alpha + \beta\frac{\sqrt{Q^2+P^2}}{h}\right) + gQ\frac{\sqrt{P^2+Q^2}}{h^2C^2} +$$
$$n\Psi_2 = 0 \qquad\qquad \text{Eq. 3.3}$$

with:

$$\Psi_1 \equiv -\left(B + \frac{1}{3}\right)d^2(P_{xxt} + Q_{xyt}) - nBgd^3(\xi_{xxx} + \xi_{xyy}) - dd_x\left(\frac{1}{3}P_{xt} + \frac{1}{6}Q_{yt} +\right.$$
$$\left. nBgd(2\xi_{xx} + \xi_{yy})\right) - dd_y\left(\frac{1}{6}Q_{xt} + nBgd(\xi_{xy})\right) \qquad\qquad \text{Eq. 3.4}$$

and

$$\Psi_2 \equiv -\left(B + \frac{1}{3}\right)d^2(Q_{yyt} + P_{xyt}) - nBgd^3(\xi_{yyy} + \xi_{xxy}) - dd_y\left(\frac{1}{3}Q_{yt} + \frac{1}{6}P_{xt} +\right.$$
$$\left. nBgd(2\xi_{yy} + \xi_{xx})\right) - dd_x\left(\frac{1}{6}P_{yt} + nBgd(\xi_{xy})\right) \qquad\qquad \text{Eq. 3.5}$$

here:
d is the still water depth
h is the total water depth (d+ξ)
α resistance coefficient of laminar flow through porous media
β resistance coefficient of turbulent flow through porous media

The simulation of wave breaking in the model is incorporated using the concept of surface rollers. R_{xx}, R_{yy} and R_{xy}, which describe the excess momentum generated by the non-uniform velocity distribution due to the roller. The above parameters are defined as follows:

$$R_{xx} = \frac{\delta}{1-\frac{\delta}{h}}\left(c_x - \frac{P}{h}\right)^2 \qquad\qquad \text{Eq. 3.6}$$

$$R_{xy} = \frac{\delta}{1-\frac{\delta}{h}}\left(c_x - \frac{P}{h}\right)\left(c_y - \frac{Q}{h}\right) \qquad\qquad \text{Eq. 3.7}$$

$$R_{yy} = \frac{\delta}{1-\frac{\delta}{h}}\left(c_y - \frac{Q}{h}\right)^2 \qquad\qquad \text{Eq. 3.8}$$

where:
δ is the thickness of the surface roller
c_x and c_y are the components of the roller celerity

This model will be used in order to construct the database in order to train the ANN model. 1080 virtual experiments (with combinations of different structural and wave conditions) will be conducted in an environment mimicking that of the physical experiments described by Sharif Ahmadian (2012). The final database will include 10800 measurements corresponding to 10 different points in the virtual wave flume.

3.4   Artificial Neural Networks

Artificial Neural Networks are mathematical models inspired by biological neural networks. An ANN consists of an interconnected group of artificial neurons. It uses a method where interconnections are used in order to process information. Neural Networks are usually an adaptive system changing their structure during a learning phase. Neural networks have been used extensively for modeling complex relationships between inputs and outputs or to find patterns in data. Models such as the above have been successfully used to solve coastal engineering problems in the past, such as:

- Prediction of near shore morphology (Bazartseren, 2005)
- Study the stability of rubble mound breakwaters (Mase et al., 1995)
- Study of run-up and overtopping (Medina 1999,2002 and Verhaeghe, 2005)
- Tidal prediction (Mandal et al. 2001)
- Prediction of surge (Lee, 2006)
- Two dimensional wave transmission over low crested structures (Panizzo and Briganti, 2007; Van Oosten and Peixo, 2005)

3.4.1   The framework of ANN's

Neural networks are comprised of a group of simple processing units (see figure 3.2). These elements are interconnected allowing them to communicate which enables them to send information to each other over a large number of weighted interconnections. According to McClelland and Rumelhart (1986) the most important features of a parallel distributed neural network are:

- A set of processing units called the "neurons";
- A state of activation (y_k) for every unit, corresponding to the output of each unit;
- The connections between the units. In general each connection is described by a weight factor (w_{jk}) that determines the influence that unit j has on k;
- A propagation rule that describes the effective input (s_k) of a unit's external inputs;
- The activation function (F_k) which determines the new level of activation based on the effective input (s_k) and current activation (y_k);
- An external input (bias, error or offset) (θ_k) for every unit.
- A "learning rule"
- An environment in which the model can operate which may include input signals and error signals
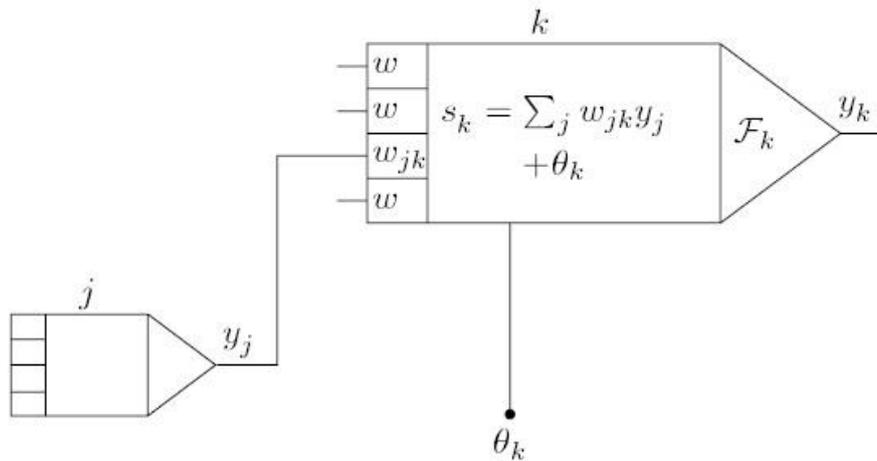
Figure 3.2: The basic components of an A.N.N (source: Liebovitch *et al.*)

Processing Units

In a neural network each unit receives information from its neighbours or from external sources and computes an output signal which in turn is propagated to the next unit and so on. At the same time the corresponding weight factors are adjusted as well. During operation, units can be updated at the same time (synchronously) or each unit can have a fixed probability of updating its activation at a time (asynchronously).

Connections between units

The most common connection between units assumes that each unit provides an additive contribution to the input of the unit with which it is connected; this propagation rule is named the "sigma rule". The total input to the net unit (k) is then defined as:

$$s_k(t) = \sum_j w_{jk}(t)y_j(t) + \theta_k(t)$$ Eq. 3.9

In addition to the above rule a second rule of propagation is popular among the field of ANN algorithms. It is called the sigma pi rule and it is described by the following relationship:

$$s_k(t) = \sum_j w_{jk}(t) \prod_m y_{j_m}(t) + \theta_k(t)$$ Eq. 3.10

In this rule y_{j_m} is usually weighted before the multiplication.

Activation and output rules

It is also important to create a function that gives the effect of the total input of the activation of the unit. This function takes the total input (s_k) and the current activation (y_k) and yields a new activation value for the unit k.

$$y_k(t+1) = F_k[y_k(t), s_k(t)]$$ Eq. 3.11

It is common practice to use non-decreasing functions to do the procedure described above. The activation function is usually a non-decreasing function of the total input of the unit:

$$y_k(t+1) = F_k[s_k(t)] = F_k\left(\sum_j w_{jk}(t)y_j(t) + \theta_k(t)\right)$$

Eq. 3.12

In general, some kind of limiting function is used. Examples of such are (see fig. 3.3):

- A hard limiting function;
- A linear or semi-linear limiting threshold function;
- A smooth limiting function such as a sigmoid;
- Or the neuron input determines the probability p that a neuron will get a high activation value: $\quad p(y_k \leftarrow) = \dfrac{1}{1+e^{-\frac{s_k}{T}}}$
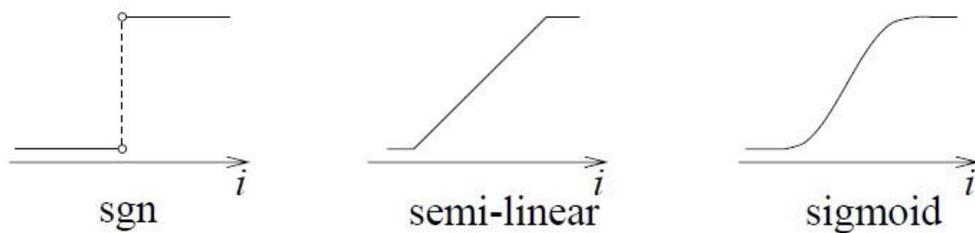
Figure 3.3: Examples of activation functions

3.4.2 Network Topologies

There are two main types of topologies in artificial neural networks (i.e. patterns of connection between units). These are:

i. The feed-forward networks at which information moves only in the forward direction. In this scheme the processing of data can extend over numerous units but no feedback is allowed, meaning that there is no loop at which outputs from one unit can be used as inputs in units of the previous layers (see fig. 3.4).
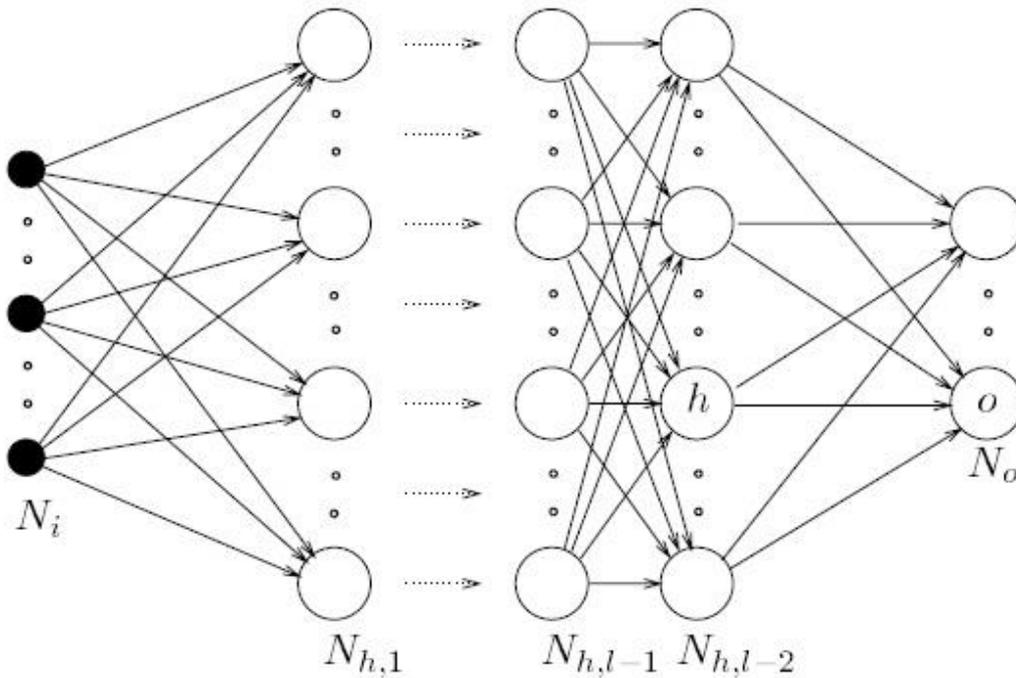
Figure 3.4: Feed-forward network (source: Liebovitch *et al.*)

ii.   Recurrent networks. These networks have feedback connections. In these types of topologies the activation values usually experience a relaxation process which allows the total network to converge to a stable state at which the activation values stop changing (see fig 3.5).
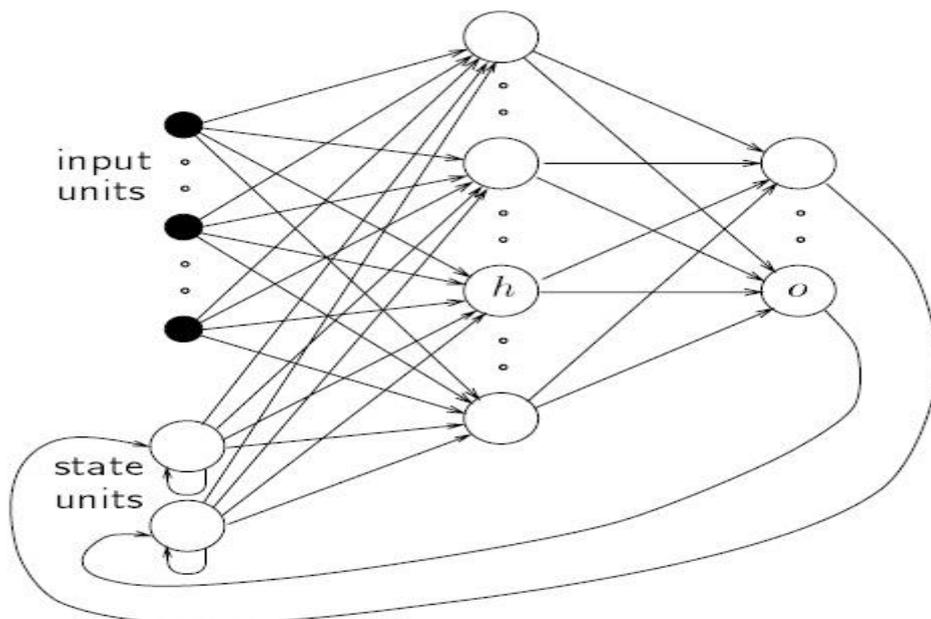
Figure 3.5: Recurrent network (source: Liebovitch *et al.*)

3.4.3 Training of artificial neural networks

There are numerous ways an ANN can be organized in order to produce the desired set of outcomes. There are two main learning methods:

i.   Supervised learning, in which a neural network is trained by providing it with a set of inputs and outputs pairs. These data can be provided externally or internally from the system (self-supervised networks).

ii. Unsupervised learning, in which an output unit is trained to respond to groups of patterns originating from the inputs. The network is able to create its own way of representing the input information.

The learning methods above describe certain ways in which the weights of the connections can be changed. This modification of the weights is defined by a rule. The most common rules for this procedure are:

i.   The Hebbian learning rule which basically states that the interconnection between two units must be reinforced by:

$$\Delta w_{jk} = \gamma y_i y_k$$ <div style="text-align:right">Eq. 3.13</div>

With γ corresponding to a predefined constant of proportionality describing the learning rate

ii. The second rule uses the difference between the actual and desired activation, in order to re-adjust the weights. This method is called the Widrow-Hoff rule or the Delta rule and is commonly applied to supervised learning networks:

$$\Delta w_{jk} = \gamma y_i (d_k - y_k)$$ <div style="text-align:right">Eq. 3.14</div>

Here d_k is the desired level of activation provided externally by the user. A very popular variant of this rule is the Mean Squared Error (MSE)

$$MSE = \sum_{i=1}^{N} \frac{(y_i - \bar{y}_i)^2}{N}$$ <div style="text-align:right">Eq. 3.15</div>

3.4.4 Networks used in this study

This study will focus its attention on feed-forward supervised neural networks. The two most popular networks of this kind are:

i.   Multilayer perceptions networks (MLP) are nonlinear models which are very general and can represent almost anything. They are composed of an arbitrary number of neurons named perceptrons. The perceptron has the ability to compute a single output from multiple inputs by forming a linear combination according to its input weights and then possibly putting the output through some nonlinear activation function (Rosenblatt, 1958). The activation method is a sigmoid function which allows MLP's to approximate very accurately linear and nonlinear sets of data.
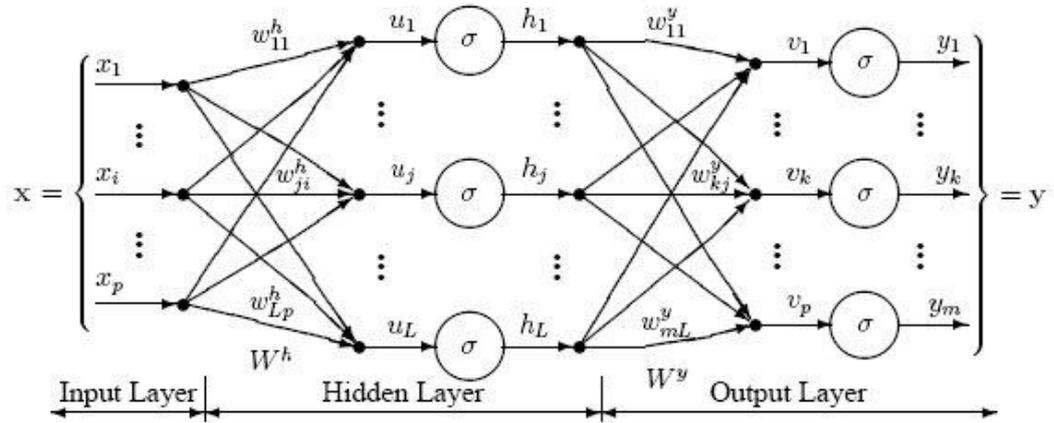
Figure 3.6: MLP network (source: _K. Suzuki 2013)_

ii.   Radial basis function network (RBF) is a network which has universal approximation properties. RBF's notion is derived from the theory of function approximation. They are two-layer feed-forward networks with hidden layers which implement a set of Gaussian functions (i.e. radial basis functions) with one output layer that uses a linear summation function as in an MLP network. The network training consists of two stages:

- The hidden layer which undergoes unsupervised learning
- The output layer which is trained using supervised learning

The main advantages of this networks are that they are highly computational efficient and very efficient in interpolating.
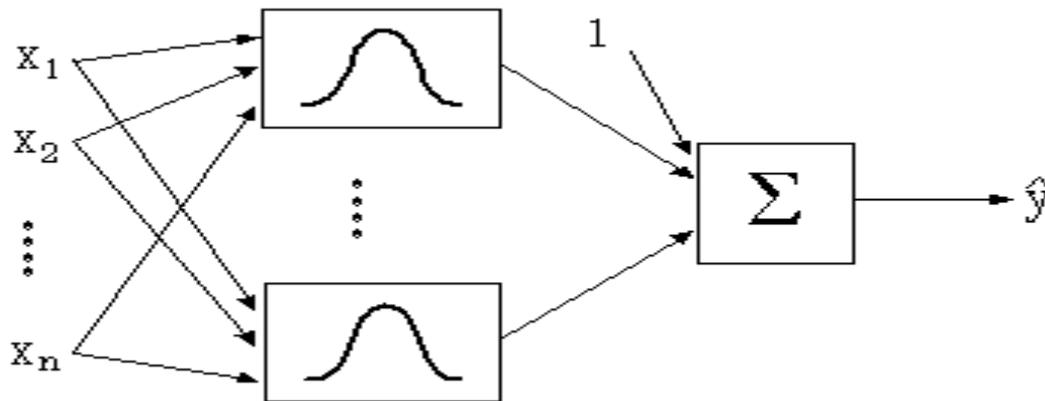
Figure 3.7: RBF network (source: _K. Suzuki, 2013_)

3.5 Combined Diffraction and Overtopping Methods

The hydrodynamics of a submerged breakwater are contributed by several processes with the most important ones being overtopping, seepage and diffraction. The two first phenomena constitute the two dimensional phenomena associated with the wave transmission and the latter is the sole contributor to the three dimensional effect. The EU funded project DELOS brought together engineers and scientists from across Europe in order to develop a methodology for designing environmentally friendly low crested structures. Unfortunately even though a considerable amount of research was conducted during the DELOS project none of it focused on diffraction.

This section serves as an introduction to the key theories that will be used in order to examine the accuracy of the data created by MIKE 21 BW which will eventually be used in order to train the A.N.N. model. The first part will explain the diffraction theory that will be used and the second part will demonstrate the theory developed by Vicinanza et al. (2009) that will allow uniting two dimensional wave transmission with the diffraction theory. This theory is based on the simple idea of summing the energies corresponding to wave transmission and diffraction. The aforementioned model will allow validating the data coming from the wave model.

3.5.1 Wave diffraction

Wave diffraction is a phenomenon which occurs when semi-infinite or finite structures interact with waves. Wave diffraction is the phenomenon in which wave energy is bent around the head of the breakwater into the "shadow zone". The diffracted wave height depends on several parameters, with the most important being:

- Porosity of the breakwater

- Incident wave conditions

- Submergence depth (in the case of submerged breakwaters)
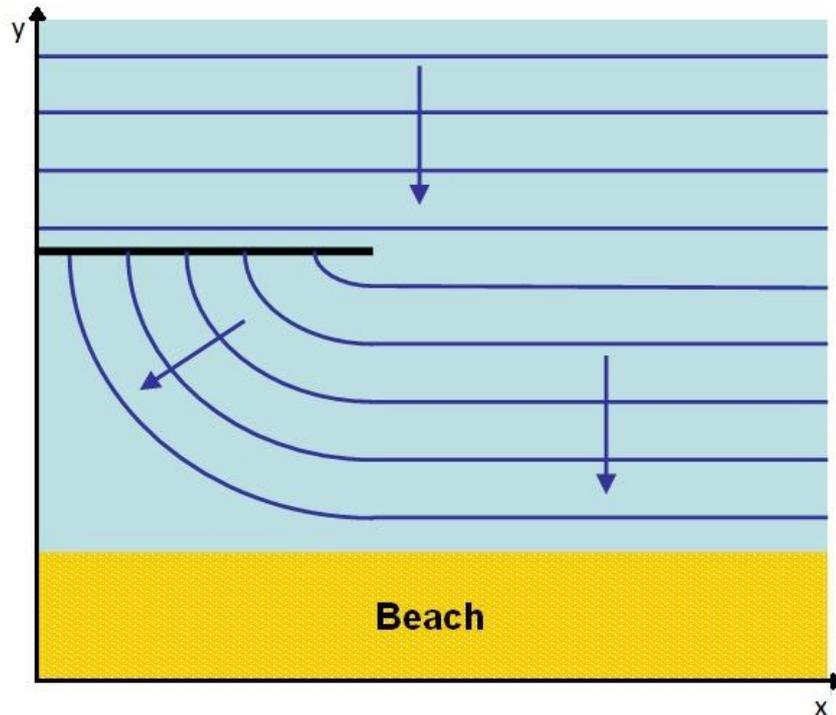
Figure 3.8: Diffraction of water waves behind semi-infinite breakwater (source: cronodon.com)

Wave diffraction has a significant role in the three dimensional wave transmission process and for that reason the most important wave diffraction theories will be discussed briefly in this section.

Penny and Price (1952) applied the diffraction theory for optical developed by Somerfield (1896) which is based on the Fresnel–Kirchhoff diffraction formula, to ocean wave diffraction. This theory makes use of the velocity potential theory. The results found have good agreement with experimental measurements in the "shadow zone" but tend to underestimate the diffraction coefficient (K_d) outside of it.

Dalrymple and Martin (1990) developed a similar approach to that developed by Penny and Price. They make use of an eigenvalue - expansion approach and variational methods that provided accurate approximations of the wavelength regardless of the breakwater gab width. This method gives accurate predictions for problems where the gap size is one order of magnitude larger than the incoming wave lengths. On the contrary for smaller gap sizes this method tends to give non-reliable results.

Williams et al. (1993) used the Green's function approach in order to solve the diffraction problem for segmented breakwaters. By implementing this function the problem reduces to a singular integral equation for the potential difference across a single screen element. The integral is then solved using the Chebyshev polynomials. This method produces very accurate results as well, but has the same disadvantage as the previous methods which is it cannot predict accurately the diffraction coefficient for absorbing breakwaters.

McCornmick and Kreamer (2001) proposed a new approximation to the Fresnel integrals used by Penny and Price which were used to solve the wave diffraction problem and semi-

infinite and finite breakwaters problem. This method allows calculating the diffraction coefficient for compliant and rigid breakwaters. The approximation over the entire range of arguments gives an error of 0.2% which allows one to characterize it as an excellent estimation tool.

The Penny and Price (1952) theory gives a very good approximation of the diffraction coefficient (at a semi-infinite breakwater) when the peak period, Tp, is used instead of the regular one, T. In short-crested seas the agreement is reasonable only in a zone that extends behind the structure for about three times the peak wave length; shoreward, underestimations can reach 50% (Boccotti, 2000). As the wave conditions examined in this study are characterized as long crested waves the approximation given by McCornmick and Kreamer (2001) will be used in order to calculate the diffraction coefficient for every point for a number of different wave conditions. For the purpose of this study the approximation for compliant breakwaters will be presented as it will be the one used later on in this study

The diffraction potential for the real part of the solution reads as:

$$F_r = \frac{1}{2}\{[C(\sigma) - C(\sigma') + S(\sigma) - S(\sigma')]\cos(ky) + [C(\sigma) + C(\sigma') - S(\sigma) - S(\sigma')]\sin(ky)\}$$

Eq. 3.16

And the imaginary part is:

$$F_i = \frac{1}{2}\{[C(\sigma) - C(\sigma') - S(\sigma) + S(\sigma')]\cos(ky) - [2 + C(\sigma) + C(\sigma') + S(\sigma) + S(\sigma')]\sin(ky)\}$$

Eq. 3.17

where:

- $\sigma = \pm 2\sqrt{\frac{r-y}{\lambda}}$ and $\sigma' = \pm 2\sqrt{\frac{r+y}{\lambda}}$

- r is the radial coordinate.

- λ and k the wave length which is the uniform in the entire domain and the wave number respectively.

- y is the distance of the point from the head of the breakwater along the vertical axis.

- $C(\sigma) \approx \frac{1}{2} + \frac{(1+0.926\sigma)\sin\left(\frac{\pi}{2}\sigma^2\right)}{2+1.792\sigma+3.104\sigma^2} - \frac{\cos\left(\frac{\pi}{2}\sigma^2\right)}{2+4.142\sigma+3.492\sigma^2+3.104\sigma^3} + \epsilon(\sigma)$ Eq. 3.18

and

- $S(\sigma) \approx \frac{1}{2} - \frac{(1+0.926\sigma)\cos\left(\frac{\pi}{2}\sigma^2\right)}{2+1.792\sigma+3.104\sigma^2} - \frac{\sin\left(\frac{\pi}{2}\sigma^2\right)}{2+4.142\sigma+3.492\sigma^2+3.104\sigma^3} + \epsilon(\sigma)$ Eq. 3.19

The sine of σ depends on the quadrant at which the point to be calculated is located.

Finally the diffraction coefficient can be calculated using the following formula:

$$K_d = \frac{H_d}{H_i} = |F(x;y)| = \sqrt{F_r^2 + F_i^2}$$ Eq. 3.20

3.5.2 Method for predicting the three dimensional wave field

Calabrese et al. (2005) suggests that predictive equations have the tendency to underestimate wave heights on the lee side of the breakwaters in the three dimensional scenario; this fact is also supported by other authors such as Seabrook and Hall (1998) and Adams and Sonu (1987).

Based on these findings Vicinanza et al. (2009) proposed the following simple predictive formula that allows incorporating diffraction with existing wave transmission formulae. They assume that there is no statistical correlation between the diffraction coefficient and the wave transmission coefficient (R=0). This statement seems to be a reasonable assumption since the two processes are completely different. This allows summing the two energies which yields the global wave transmission coefficient:

$$K_{D,t} = \sqrt{K_D{}^2 + K_t{}^2}$$ Eq. 3.21

where:

- K_D is the wave diffraction coefficient calculated for each point in the domain of interest, which is calculated using the approximation given in the previous section.
- K_t is the wave transmission coefficient calculated by any empirical formulae that suits better the breakwater layout. For the purpose of this study four different wave transmission formulae will be used. The criterion by which they were selected was their suitability to incorporate the structural properties of the breakwater considered in this study.
  - D'Angremond (1998)
  - Buccino Calabrese (2007)
  - Seabrook and Hall (1998)
  - Goda and Ahrens (2008)

By the above it is noticeable that the influence of the diffraction coefficient should decrease with increasing wave overtopping or seepage. It is also obvious that the influence of K_D decrease as the point of interest shifts deeper into the "shadow zone". Finally this study shows evidence via numerical simulations that by assuming a negative correlation between the two phenomena the agreement of the results gets improved significantly. For this reason two individual analyses under the assumption of negative and no correlation will be conducted in chapter 5

4   Data Compilation

This chapter will discuss the data obtained from the "virtual" experiments. A series of experiments were conducted in order to obtain the data required to train and test the ANN model. All experiments have been conducted using regular waves. The advantage of using regular waves in the analysis is that it gives a more clear understanding of the physical processes involved in 2D and 3D wave transmission (as opposed to random waves). These experiments can be divided into two groups:

- 2D experiments. These experiments were commenced in order to create a small data set that would allow validating MIKE 21 BW and examining its robustness. This step is important as a 3D model based on a robust 2D model will also be reliable, as the only additional phenomenon that would be simulated in the latter would be diffraction. In this way the only source of error for the 3D wave model would be the combined effects of diffraction with the other 2D effects.
- 3-D experiments. A large number of experiments using MIKE 21 BW were conducted. The data obtained from this process are aimed to train and test the ANN model. It is important to test the reliability of these data sets in order to ensure that the ANN is trained using data that correspond to actual physical circumstances.

4.1   Calibration of the 2-D Model

All tests are carried out in a 30m by 2.5m by 1.3m wave flume resembling the exact dimensions of the experiments conducted by Sharif Ahmadian (2012). The dimensions of the flume are representative of the dimensions of most of the flumes were wave transmission experiments have been conducted. For this reason it was decided that the numerical simulations should be conducted at flume with these dimensions.

Scale:

10:0.4m
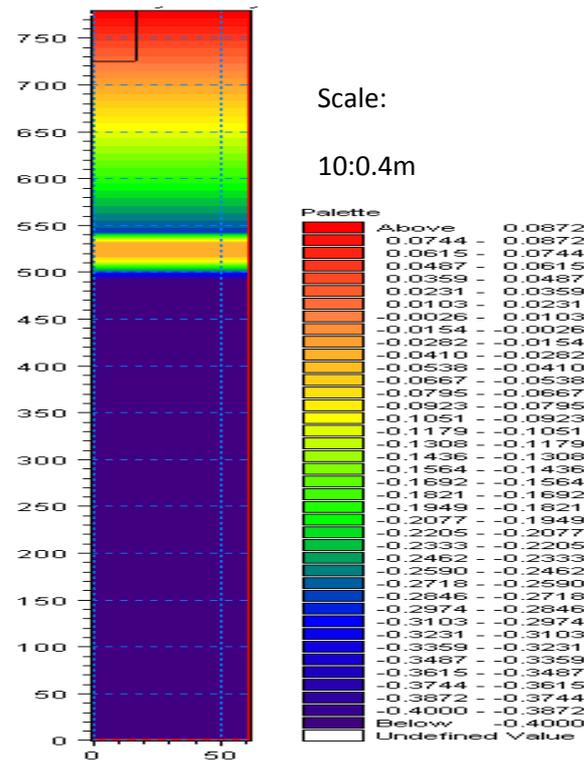
Figure 4.1: Bathymetry of the 2-D numerical wave flume

Extra caution should be given when setting up a numerical model such as MIKE 21 BW, especially when the purpose of the simulations is to create a reliable data set. In this section the setup of the numerical model will be discussed. It is important to calibrate the model in such a way that it is able to resemble the actual physical conditions that are observed in the wave flume. This procedure is time consuming, involving an iterative process, where key parameters are adjusted until the model functions properly. A flow chart of the procedure is presented in figure 4.2. A detailed description of all the parameters that were required will be presented in the next section.
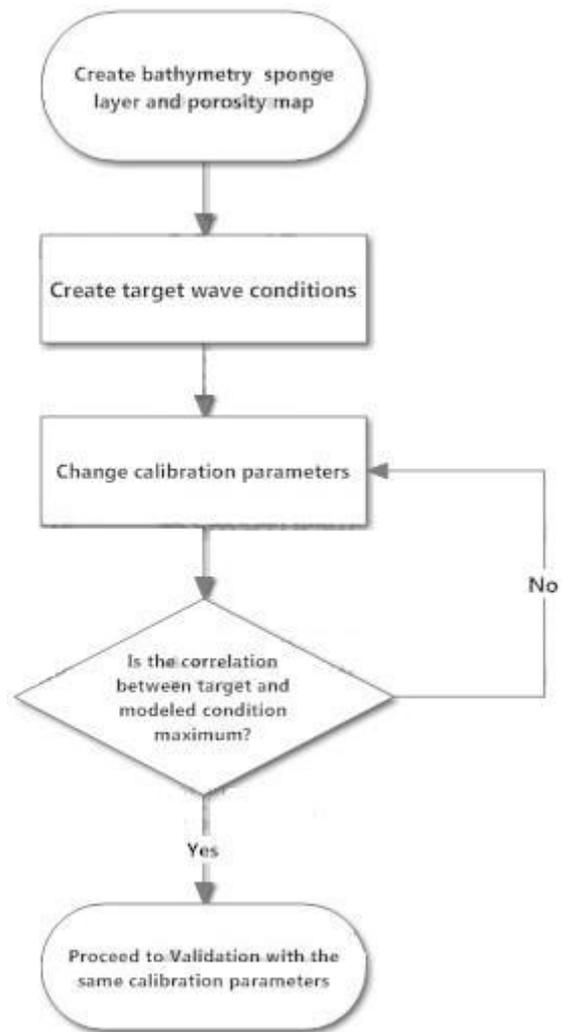
Figure 4.2: Flow chart of the calibration process

4.1.1 Basic Parameters

Wave Module

MIKE 21 BW has two options:

- 2DH Boussinesq wave module
- 1DH Boussinesq wave module

In this report the 2DH was selected as it has an excellent capability of predicting wave fields of short and long waves in shallow and deep water. This module solves the enhanced Boussinesq equations in the horizontal space (x-y coordinates) using implicit finite difference techniques.

Bathymetry

As mentioned above a two dimensional matrix describing the topology of the wave flume as was used in the physical experiments of Sharif Ahmadian (2012) (see figure 4.2). Artificial land values coupled with sponge layers were subscribed on the north end south end of the flume in order to reduce the computation time. Two regions with different spatial resolutions were selected in order to make the model as computational efficient as possible. In the regions of no wave breaking the grid spacing was approximately 10 nodes per lowest wave length (0.026m). At the surf and swash zone where more energetic waves are found a dense resolution was selected corresponding to 40 nodes for the minimum wave length (0.014m). The denser grid is required as the enhanced Boussinesq equations models wave breaking based on the notion of surface roller which requires a very fine resolution in order to produce accurate results. The following grid spacing mesh results in a Courant number ($C_r = 0.497$) that fulfils the CFL criterion ($C_r \leq 1$).

where:

$$C_r = c \frac{\Delta t}{\Delta x}$$
Eq. 4.1

Equation Type

In order to produce a large range of wave conditions the deep water terms of the Boussinesq equations were included. This allowed to extend the application range of the model to situations were $\frac{h_{max}}{L_0} = 0.5$.

Discretization Technique

MIKE 21 offers 4 discretization techniques:

- Central differencing with side feeding
- Central differencing with simple upwinding at steep gradients and near land
- Quadratic differencing with simple upwinding at steep gradients and near land
- Simple upwinding differencing

For the purpose of this research the central differencing with simple upwinding at steep gradients and near land technique was used with a time extrapolation factor of 1. This method is the most stable with the least numerical dissipation and therefore produces the most accurate results. It should be mentioned that the other methods introduce a lower time – extrapolation factor that produces more stable results by introducing more numerical dumping at the expense of accuracy.

Simulation period

The total simulation time is given by the following formula:

$$Sim.Time = \Delta t * No. of\ time\ steps \qquad\qquad Eq.\ 4.2$$

The total simulation time was selected to be 1400 sec. This period allows waves to reach all parts of the domain and continues the computation for more than 20 min which enables the model to produce statistically accurate results of the significant wave height. Additionally the time step (Δt) should fulfil the CFL requirements. For that reason it was selected to be 0.005 resulting in 1000000 time steps.

4.1.2   Calibration Parameters

Bathymetric Parameters

The main bathymetric parameters included in MIKE 21 BW are the land value and the reference water level. The land value is the minimum value of the bathymetry which is considered as land and is excluded from the calculations in order to reduce the computation time. The reference water level is the main reference level for the Boussinesq wave simulation; changing this parameter allows to simulate different water levels without changing the bathymetry file.

In this study the land value was selected to be 1m. The land value was assigned to all side walls of the numerical flume. Additionally it should be mentioned that the reference water level was shifted accordingly in order to simulate different breakwater submergence depths.

Boundary conditions

Two types of boundaries exist:

- Open boundaries are usually represented by time series of water elevation or flux densities, in the situation where no boundaries are present (open boundaries)
- Closed boundaries which represent fully reflective vertical surfaces.

Fully closed boundaries were applied to all walls of the numerical wave flume. This means that no flow is allowed to cross the boundaries. For this reason sponge layers are introduced at all walls which effectively absorb all the wave energy. An absorbing sponge layers in front of closed boundaries allows wave energy to pass out of the model area without allowing energy to reflect back in to the model domain (the construction of sponge layers will be elaborated further in the next sections).

Internal wave generation

The internal wave generation represents the wave maker in an ordinary wave flume. It is represented by a line equal to the width of the numerical wave flume. It creates waves by adding the discharge of the specified incident wave field along the line. In order to avoid resonance phenomena a sponge layer just behind the generation line was introduced. For the simulations produced in this study the internal wave generation line was defined along the line y = 201.

Bottom friction

Bottom friction can successfully be modeled in MIKE 21 BW using the bed friction rule derived by Chezy. This rule states that the bed shear stress equals to:

$$\tau_b = \frac{\rho g U |U|}{C^2}$$

Eq. 4.3

Where C is the Chezy number given by:

$$C = \frac{U}{U_b}\sqrt{\frac{2g}{f_w}}$$

Eq. 4.4

And U_b is the velocity at the bed and f_w is wave friction factor which for short waves reads as:

$$f_w = e^{-5.977+5.213\left(\frac{a_b}{k_n}\right)^{-0.194}}$$

Eq. 4.5

In these simulations it was assumed that there is no damping due to bed friction as all surfaces in the flume are constructed with frictionless materials (glass and aluminum).

Eddy viscosity

Eddy viscosity is introduced in the model for the purpose of modeling wave current interaction and mixing processes. The adoption of the concept of eddy viscosity allows us to simulate the turbulent fluctuations which lead to the corresponding stress terms in the governing equations. Therefore the momentum equations contain both turbulent and laminar stresses.

The eddy viscosity can be calculated using the formulations by means of the eddy coefficient or by the Smagorinsky coefficient. As neither wave current interaction nor mixing will be treated in this report eddy viscosity will be excluded.

Wave breaking

The incorporation of wave breaking in MIKE 21 BW is achieved using the concept of the surface roller. Wave breaking is assumed to start when the wave exceeds a predefined value. The surface roller is assumed to be an isolated bulk of water travelling at the wave speed (c). The influence of the roller is then taken into account by the momentum equation using an additional convective term. Based on this concept:

- The roller thickness is determined as the water thickness above the tangent of the wave slope multiplied by a shape factor (roller form factor) and has a value of 1.5.
- The roller celerity is proportional to the linear shallow water celerity and its value is 1.3 (-).
- Breaking is assumed to start when the slope of the surface wave exceeds an angle of 20⁰
- The critical angle at which the initial wave breaking shifts to "bore-line" breaking (final breaking) is 10⁰.
- The half-time for the cut-off roller defines the transmission between the two breaker types and has a value of 0.39(s)
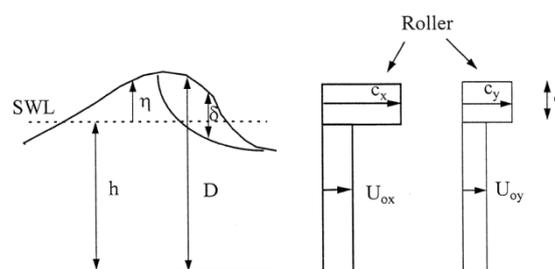
Figure 4.3: Surface roller schematization (source: MIKE21 BW user manual)

The values of the above parameters were determined on a trial and error basis, during the calibration process and are summarized in the following table.

	Roller form factor	Roller celerity factor	Initial breaking angle (º)	Final breaking angle (º)	Half-time for cut off roller
Value	1.5	1.3	20	10	0.39

Table 4.1: Calibrated wave breaking parameters

Porosity

By including porosity layers in MIKE 21 BW the model is allowed to simulate non-Darcy (turbulent) flows through the structure. This enables the model to predict wave seepage and partial reflection at coastal structures. The effects of porosity are introduced by the inclusion of additional laminar and turbulent friction terms. It should be stressed that in large scale simulations the laminar friction losses are negligible whereas in small scale simulations laminar and turbulent losses are also present. The flow resistance term inside the porous structure is calculated based on the following term:

$$(\alpha + \beta|U|)U$$
Eq. 4.6

α and β are empirical values determined by the following expressions (Engelund, 1953):

$$\alpha = \alpha_0 \frac{(1-n)^3}{n^2} \frac{\nu}{d^2}$$
Eq. 4.7

$$\beta = \frac{\beta_0(1-n)}{n^3}$$
Eq. 4.8

where:

α_0 is the laminar particle form resistance coefficient

β_0 is the turbulent particle form resistance coefficient

n is the porosity of the structure

d is the nominal diameter of the particles comprising the structure

ν is the kinematic viscosity of water

For small scale breakwaters the expected porosity is usually 0.4 (Ahrens, 1980). Based on this notion several values of α_0 and β_0 were applied until the wave conditions in front and behind the breakwater matched the target conditions of the calibration process. The final values of the turbulent and laminar friction coefficient were determined as 0.3 and 1000 correspondingly which agree with van Gent's experimental findings for oscillatory flow (1990, 1994). Finally the porosity map of the model is presented. A porosity of 0.4 throughout the entire area of the breakwater ins applied.
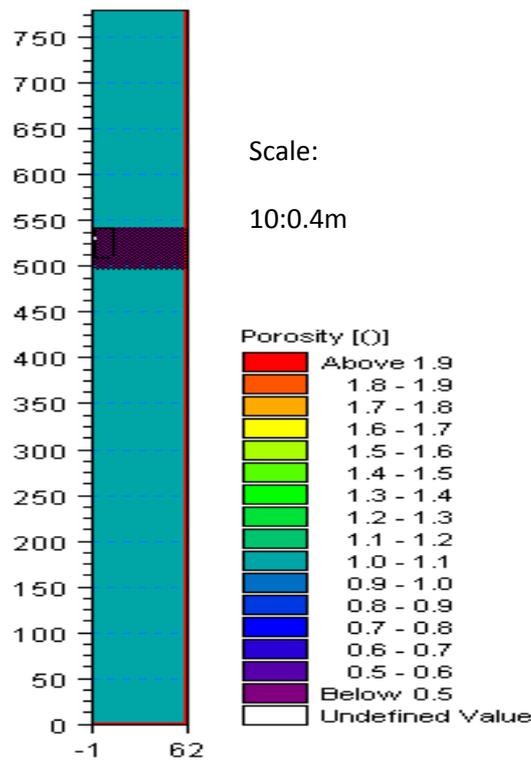
Figure 4.4: Porosity map of numerical wave flume

Sponge layer

Sponge layers are a type of wave absorber for numerical simulations in MIKE 21 BW. As mentioned in the previous paragraphs when a sponge layer is backed up by land values it can produce radiating boundary conditions which may allow partial reflection or complete absorption. For the purpose of this study a fully absorbing layer has been implemented in the south boundary of the model in order to reduce wave reflection and resonance phenomena due to the presence of the internal wave generator. A sponge layer has also been installed at the north boundary in order to absorb the remaining wave energy on the lee side of the breakwater. During the calibration process it was determined that a sponge layer in the North of the flume should have 100 nodes and the South sponge layer 200 nodes in order to produce accurate results with no "noise" (see figure 4.4).
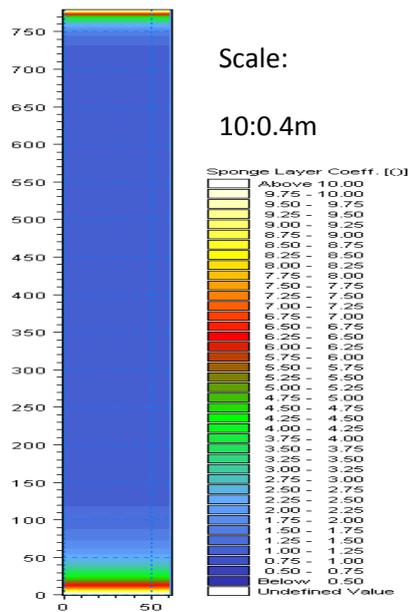
Figure 4.5: Sponge layer map of the numerical flume

4.2 Results of 2D Experiments

4.2.1 Introduction

The purpose of creating a dataset is for two purposes:

- Validate the MIKE 21 BW model. 12 different experiments with different wave conditions and submergence depths were selected from the DELOS dataset and simulated using the previously defined numerical model. This will allow a comparison of physical experimental results and the numerical model and evaluation of the predictability of the model for 2D effected which include the combined effects of overtopping and permeability.
- Create a dataset that serves as a base scenario that will be used in order to examine the effect of permeability on diffraction. Namely different incoming wave conditions will be simulated in order to determine variation of the H_t along the y-axis.

4.2.2 Test Conditions

31 tests were conducted in the numerical model described earlier. These can be divided into two specific subcategories:

i.   Results for validation (hereafter Class A). In these experiments the exact wave and structural conditions as in the DELOS database were replicated with the exception of slope angle. These conditions are incident wave height, periods, spectral shapes and submergence depth. The slope angle has been proven to have minor influence in the wave transmission process for normally incident waves (Van der Meer, 2004) and therefore was kept constant at 1:1. This statement is only valid for large slope

angles. As the slope angle decreases significantly the effect of the angle becomes more important. As dissipation effects become more dominant.

ii.   Results for comparisons and analysis (hereafter Class B). This class of experiments includes a small dataset (15 experiments) where different wave conditions were tested against different structural permeability parameter (porosity and stone diameter). Slope angle and submergence depth have been kept constant.

The following tables show the exact structural and wave conditions used in both Class A and B experiments.

Test No	Name of experiment	H_i (m)	T (s)	h_s (m)	$D_{n_{50}}$ (m)	B (m)
1	Daemen	0.135	1.988	-0.040	0.028	0.340
2	Daemen	0.067	1.549	-0.040	0.028	0.340
3	Daemrich	0.062	1.000	-0.025	0.042	0.200
4	TUDELFT	0.121	1.593	0.000	0.034	0.205
5	Ahrens	0.134	2.230	-2.770	0.019	0.300
6	Powell	0.112	1.640	-0.045	0.076	0.204
7	Seebrook & Hall	0.128	1.280	-0.050	0.017	0.350
8	Daemrich	0.114	1.633	-0.056	0.024	0.280
9	Daemrich	0.127	2.280	-0.056	0.024	0.280
10	Seebrook &Hall	0.069	1.138	-0.031	0.024	0.120
11	Seebrook &Hall	0.084	2.328	-0.031	0.024	0.405
12	Seebrook &Hall	0.066	2.297	-0.031	0.024	0.405
13	Daemen	0.114	1.859	-0.040	0.028	0.340
14	Delft Hydraulics	0.163	1.739	-0.050	0.011	0.200
15	Seebrook &Hall	0.129	1.164	-0.050	0.017	0.600
16	Seebrook &Hall	0.090	1.178	-0.031	0.024	0.450
17	Seebrook &Hall	0.115	1.687	-0.031	0.024	0.450

Table 4.2: Class A data set (source: Van Oosten and Peixó, 2005)

Test No.	H_i (m)	T (m)	$D_{n_{50}}$ (m)	n (-)	h_s (m)	B (m)
1	0.1	1.5	0.02	0.4	-0.04	0.308
2	0.1	1.5	0.04	0.4	-0.04	0.308
3	0.1	1.5	0.07	0.4	-0.04	0.308
4	0.1	1.5	0.02	0.3	-0.04	0.308
5	0.1	1.5	0.02	0.4	-0.04	0.308
6	0.1	1.5	0.02	0.5	-0.04	0.308
7	0.1	1.5	0.02	0.6	-0.04	0.308
8	0.01	1.5	0.04	0.4	-0.04	0.308
9	0.05	1.5	0.04	0.4	-0.04	0.308
10	0.1	1.5	0.04	0.4	-0.04	0.308
11	0.15	1.5	0.04	0.4	-0.04	0.308
12	0.1	0.8	0.04	0.4	-0.04	0.308
13	0.1	1.1	0.04	0.4	-0.04	0.308
14	0.1	1.4	0.04	0.4	-0.04	0.308
15	0.1	1.7	0.04	0.4	-0.04	0.308

Table 4.3: Class B data set

4.2.3   Key findings of 2D experiments.

The incident wave height in the experiments described above was assumed to be the average significant wave height between nodes 400-450 and the transmitted wave height was assumed to be the average wave height between nodes 540-570.

Table 4.4 presents the computed wave transmission coefficients for the class A experiments. Following this, a two dimensional plot of the transmitted wave height variation along the y-axis for different permeability parameters is presented.

No	Name of experiment	$K_{t_{calc}}$
1	Daemen	0.534
2	Daemen	0.568
3	Daemrich	0.439
4	TUDELFT	0.703
5	Ahrens	0.534
6	Powell	0.619
7	Seebrook & Hall	0.540
8	Daemrich	0.548
9	Daemrich	0.617
10	Seebrook &Hall	0.532
11	Seebrook &Hall	0.419
12	Seebrook &Hall	0.418
13	Daemen	0.530
14	Delft Hydraulics	0.590
15	Seebrook &Hall	0.350
16	Seebrook &Hall	0.361

Table 4.4: Calculated Kt for class A experiments
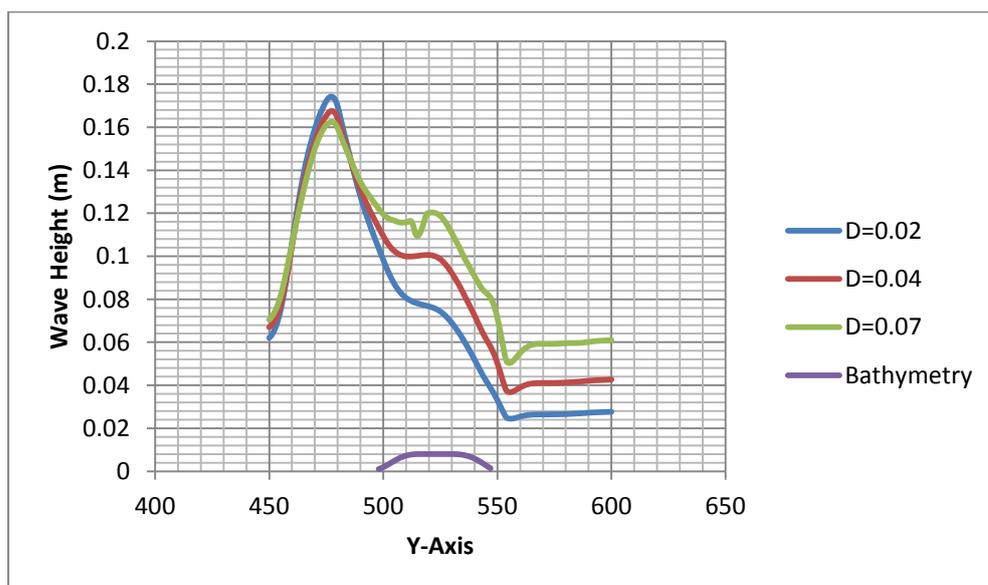
Figure 4.6: Variation of H along y-axis for varying and Dn50 and Hi=0.1m, T=1s and n=0.4.
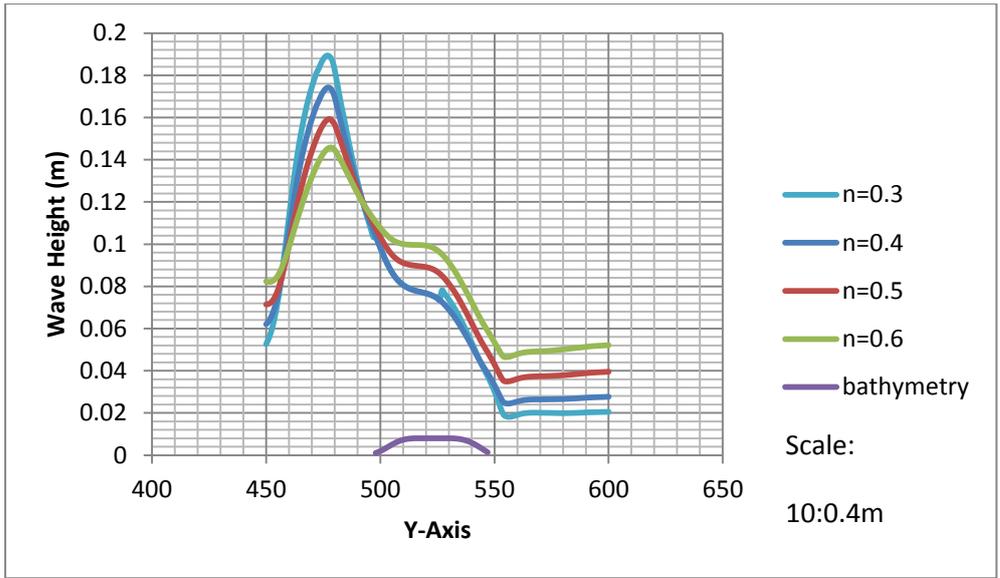
Figure 4.7: Variation of H along y-axis for varying and n and Hi=0.1m, T=1.5s and Dn50=0.02m.
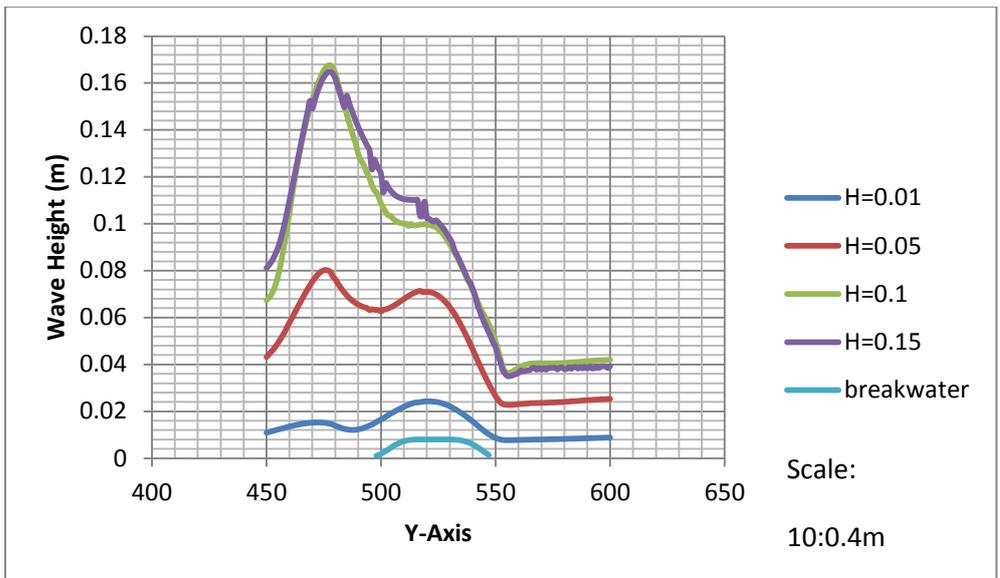
Figure 4.8: Variation of H along y-axis for varying and H_i and n=0.4, T=1. 5s and Dn50=0.02m.
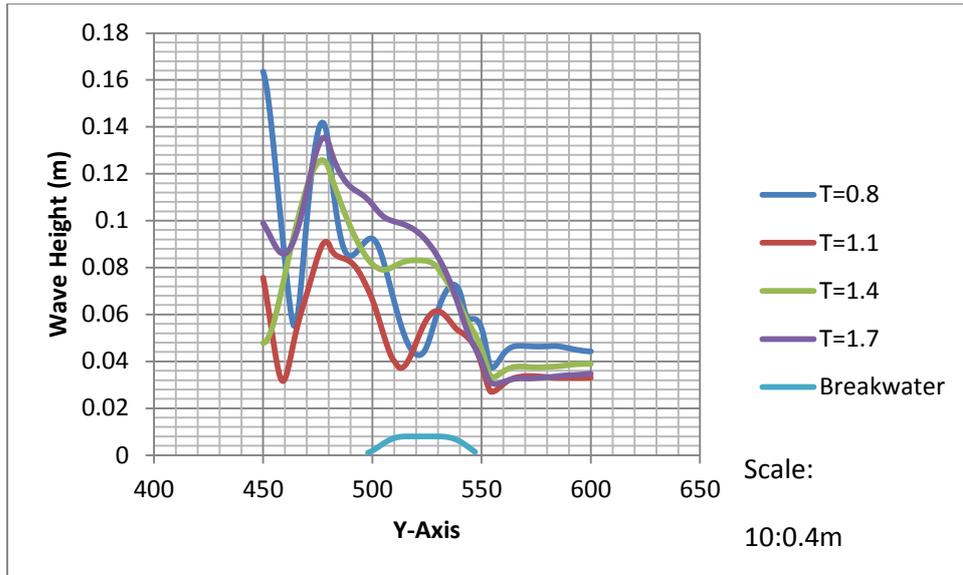
Figure 4.9: Variation of H along y-axis for varying and T and n=0.4, Hi=0.1m and Dn50= 0.02m.

From the figures 4.6 to 4.9 several interesting results are found with respect to the effects that structural permeability has on 2D wave transformation over submerged permeable breakwaters. The results show that the transmitted wave height increases as the porosity increases. Larger values of n mean that the grading of the elements comprising the breakwater is narrow which effectively means that the pore volumes within the structure are also large. This decreases the effects that capillary forces have within the breakwater and therefore more energy is allowed to travel through the structure. There is also an increase of the wave height in front of the breakwater which is partially contributed by the partial reflection of the incoming wave energy and the shoaling due to the breakwater. For small incoming wave heights the wave amplitude above the breakwater increases as n or $D_{n_{50}}$ decreases. Small structural porosities mean that more water mass is forced to travel above the breakwater forcing the wave to increase in amplitude. As the incoming wave height increases the additional mass forced to travel over the breakwater forces the wave to break and therefore results in smaller wave heights above the breakwater. From the above one can understand that an optimum porosity value exists, for which a minimum wave transmission can be achieved. For the scenarios described in the above figures this optimum value lied between 0.3 and 0.4 for a nominal stone diameter equal to 0.02. It can also be concluded that by decreasing or increasing simultaneously n and $D_{n_{50}}$ the above mentioned effects are magnified. Finally it can be seen that the specific geometry reduces the transmitted wave height for an increasing wave period. It can also be observed that smaller period waves are forced to break before they reach the breakwater and shoal again over it.

4.3   Results of 3D experiments

4.3.1   Introduction

These experiments serve two main reasons:

- Produce a large number (1080) of experiments for combinations of different structural permeability and wave conditions. This dataset will then be divided into two different groups, a training and testing dataset that will be used in order to create an ANN model that will be capable of predicting the spatial variation of the wave transmission coefficient behind porous submerge breakwaters.
- Create a dataset that will be compared with the base scenarios produced in the previous section that will allow detecting the influence of diffraction on the wave transmission process. For this reason different structural permeability conditions will be compared for 2D and 3D conditions.

For the purpose of these experiments the breakwater that extended throughout the entire width of the flume was substituted with a breakwater with a breakwater head. As in the previous breakwater both slopes have a value of 1H: 1V (see figure 4.10).
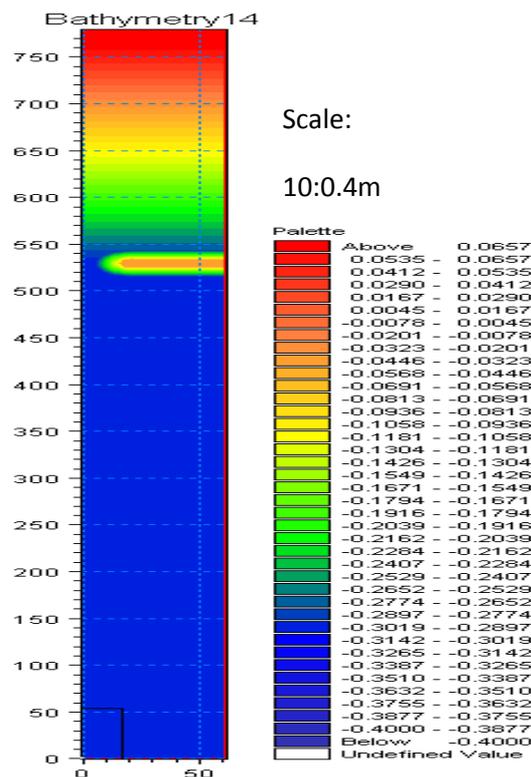
Figure 4.10: Wave flume layout for the 3D experiments

25 wave probes were installed in the locations shown in the following table. They were implemented in order to obtain wave height data that will be used for training the ANN model.

Wave probe coordinates				
12,470	24,470	36,470	48,470	60,470
12,492	24,492	36,492	48,492	60,492
12,523	24,523	36,523	48,523	60,523
12,550	24,550	36,550	48,550	60,550
12,570	24,570	36,570	48,570	60,570
12,600	24,600	36,600	48,600	60,600

Table 4.5: Wave gauge positions, as nodes in computational domain

As mentioned earlier different wave conditions were examined for combinations of different structural parameters. Namely 180 different wave conditions were applied to 6 different combinations of structural permeability conditions, summing to a total of 1080 experiments. The summary of the wave conditions is shown in table 4.6:

Wave Conditions	
Incoming Wave Height, H_i (m)	0.01, 0.03, 0.05, 0.07, 0.09, 0.11, 0.13, 0.15, 0.17, 0.19
Wave Period, T (s)	0.8, 0.88, 0.96, 1.04, 1.12, 1.20, 1.28, 1.36, 1.44, 1.52, 1.60, 1.68, 1.76, 1.84, 1.92, 2.00, 2.08, 2.16
Structural Permeability Conditions	
Nominal Stone Diameter, $D_{n_{50}}$ (m)	0.02, 0.04, 0.06
Porosity, n (-)	0.4, 0.5
Other Structural Parameters	
Submergence Depth, d_s (m)	0.04
Breakwater Width, B (m)	0.308
Water Depth, d (m)	0.4

Table 4.6: Summary of experimental conditions

4.3.2   Key Findings

In this section a discussion of the finding of the 3D experiments will be provided. The discussion will be divided into two categories dimensional results and non-dimensional. Wave transmission behind semi-infinite breakwaters is a complex phenomenon which includes wave breaking, generation of higher harmonics seepage and diffraction. For this reason an attempt to better understand the influence of porosity and diffraction will be made as well.

For the purpose of training the ANN model the phase averaged transmitted wave height was calculated at each probe using the average root mean squared wave height ($H_{t_{rms}}$) based on the following formula:

$$H_{t_{rms}} = \frac{2\sqrt{2}\sum_{i=1}^{n}\sigma_i}{n}$$

Eq. 4.2

4.3.2.1   Dimensional Results

Influence of wave period

In order to determine the influence of the wave period on the wave transmission process three 2D plots were composed for an incoming wave height of 0.1m and wave periods of 0.8s, 1.1s and 1.7s seconds correspondingly, the porosity was 0.4 and the nominal stone diameter 0.04m. For the sake of clarity it was decided to focus on the area close to the breakwater therefore the origin of the graphs (0, 0) corresponds to point (0,400) in the numerical flume (figure 4.11) and the centre of the breakwater is located along the line y=123. From the graphs bellow is can be deduced that for an increasing wave steepness less wave energy is allowed to pass on the lee side of the breakwater. The influence of the wave period is of significance for one more reason. As the plots in figure 4.11 shows, the effect of diffraction decreases as the wave length increases, resulting in more straight lines on the lee side of the structure. A possible explanation for this phenomenon is that longer waves have the ability to travel through the breakwater, therefore contributing more to transmitted wave height, reducing the contribution of diffraction to the lee side wave field. Also an interesting result is that the area of low wave energy moves from the head of the breakwater towards the sheltered zone behind the breakwater as the wave length increases. It is also observed that wave breaking is shifted towards the offshore direction as the wave period increases, which is a consequence of the larger wavelength that is partially reflected. In addition it can be observed that for smaller wave periods and therefore higher Iribarren number the partial reflection is higher which results in high spatial variation of the wave height in front of the breakwater.
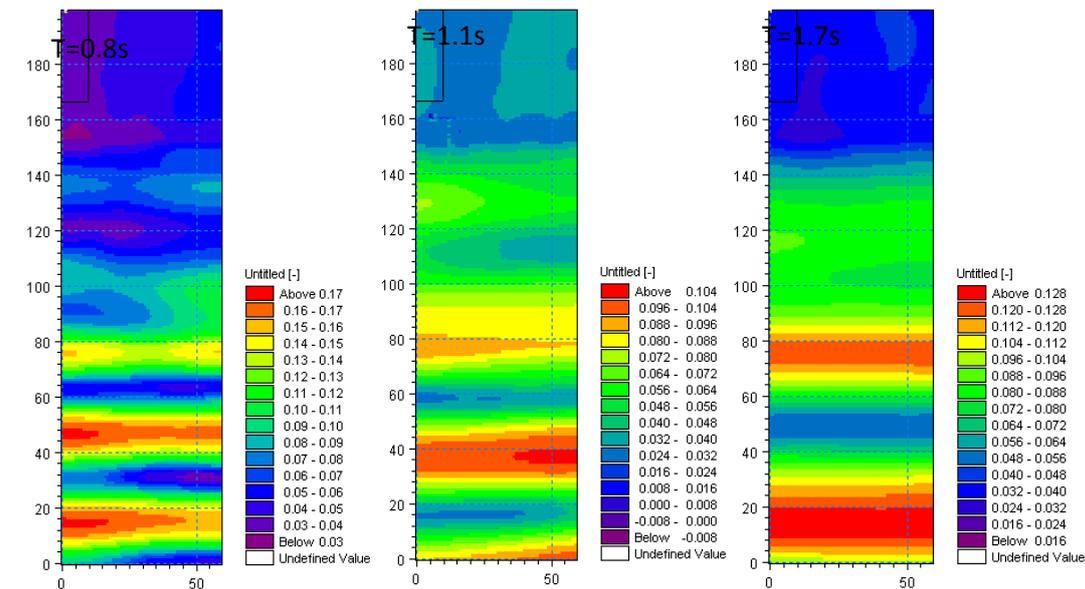
Figure 4.11: 2D plot of significant wave height around the breakwater for n=0.4, Dn50=0.04m, Hi=0.1m for periods of 0.8, 1.1 and 1.7 seconds (scale 10:0.4m)

Influence of wave height

Examining the influence of the wave height is also important. For that reason four 2D plots of the significant wave height were created for constant n=0.4, $D_{n_{50}} = 0.04m$, T=0.9s and varying H_i of 0.01m, 0.05m 0.09m and 0.13m. The figures depict the same "zoomed" in area of the wave flume as in figure 4.12 and the breakwater is located at the same position. From the figures it is observed that the location of the area of low wave energy is not influenced by H_i, although there is dependence between the incoming wave height and the magnitude and extent of the area of low wave energy. Namely an increased incident wave height results in a broader area with lower wave heights. The area of high wave energy is mainly determined by the location of the beach behind the breakwater which forces the waves passing through the gap to shoal. With respect to the wave field in front of the breakwater the figures suggest that for small wave heights the partial wave reflection is negligible therefore the area of high wave energy is located close to the breakwater. As the incident wave height increases more, more energy is reflected shifting the area of higher wave height towards the offshore direction.
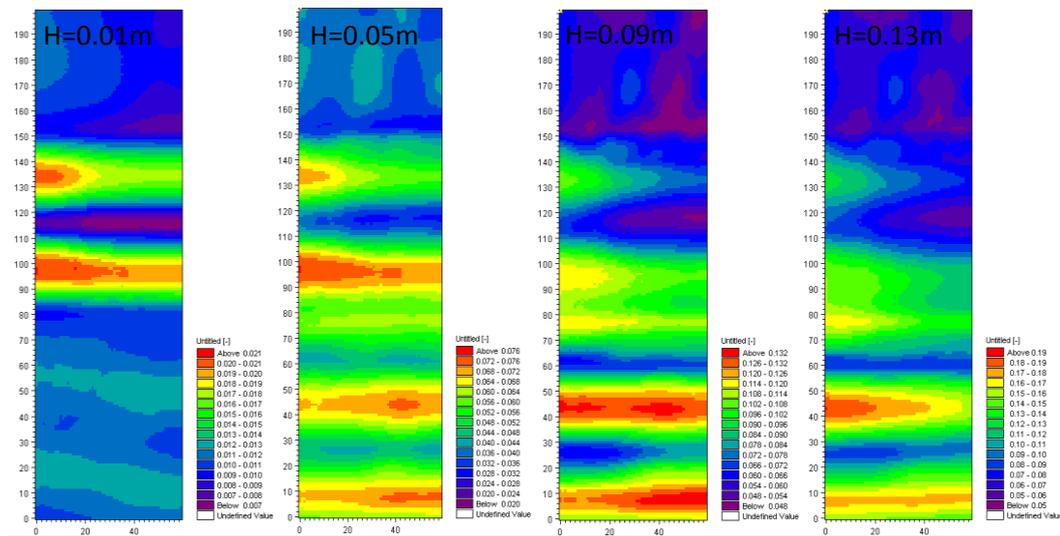
Figure 4.12: 2D plot of significant wave height around the breakwater for n=0.4,Dn50=0.04m, T=0.9s for incident wave height of 0.01, 0.05 and 0.09 and 0.13 meters (scale 10:0.4m)

Influence of structural permeability

It is important to answer the question of "is structural permeability a parameter that affects the wave field behind porous submerged breakwaters"? In this section the results of the wave flume experiments will be presented. Figure 4.13 depict the spatial variation of the wave field around the breakwater in which the centerline is located at y=123. As in the case of increasing wave period the wave field becomes more homogeneous and the influence of diffraction is lessened. This is a result of the reduced energy dissipation inside the breakwater. As porosity increases the mass of the water follows the path of least resistance which in this case is through the breakwater. It is also observed that with increasing porosity the overall wave energy behind the breakwater also increases. Finally the area of least wave

energy shrinks and shifts towards the shadow zone as the porosity of the breakwater increases. It should be mentioned that with an increase in stone diameter the same trends are observed but at a smaller magnitude.
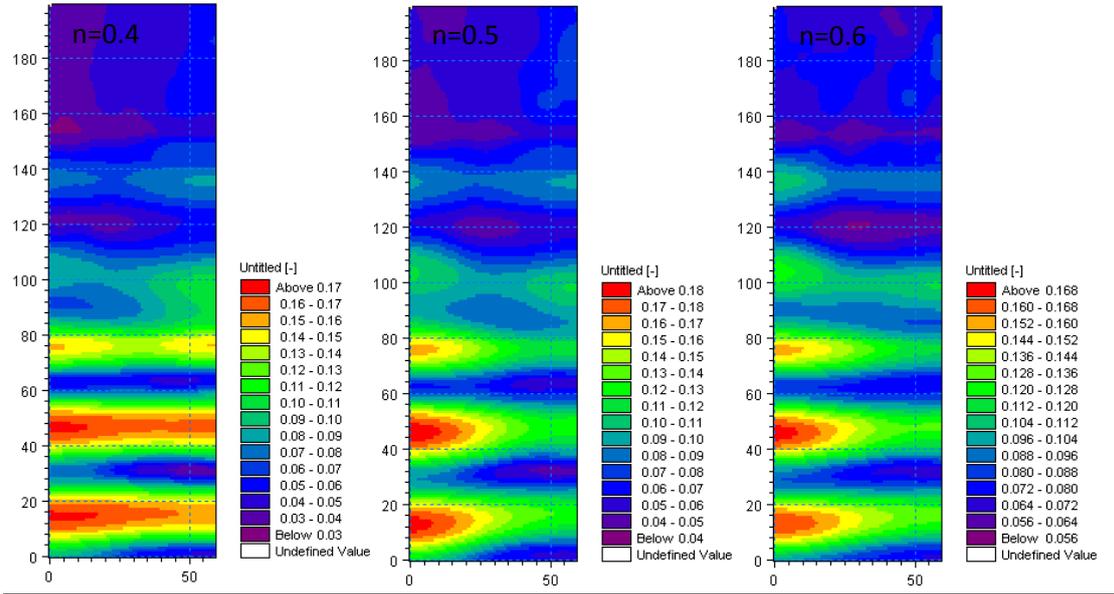
Figure 4.13: 2D plot of significant wave height around the breakwater for T=0.90s, Dn50=0.04m, Hi=0.10m for porosity values of 0.4, 0.5 and 0.6 (scale 10:0.4m)

Influence of diffraction on wave transmission process

Another interesting aspect that was treated in this study is the assessment of the difference between 2D and 3D wave fields in front and behind permeable submerged breakwaters. Numerous studies have been performed examining the diffraction effect behind breakwaters. Unfortunately all of them were carried under the assumption that the breakwaters are infinitely high and impermeable therefore not allowing any overtopping or seepage (i.e. Penny and Price (1952), Goda et al. (1978)). Only recently Vicinanza et al. (2009) proposed a theory for determining the wave height behind submerged breakwaters using a combination of diffraction and transmission theories. This section provides a direct comparison of the wave energies associated with 2D (no diffraction effects included) and 3D (diffraction effects included) wave fields, using the ratio:

$$K_{d,t,s} = \frac{H_{m0_{3D}}^2}{H_{m0_{2D}}^2}$$
Eq. 4.3

where:

$H_{m0_{3D}}$ = The significant wave height of the scenario where all phenomena are present (i.e. diffraction overtopping and seepage)

$H_{m0_{2D}}$ = The significant wave height of the scenario where diffraction is excluded

Figure 4.14 shows the spatial variation of $K_{d,t,s}$ for porosity values of 0.4, 0.5 and 0.6 respectively, nominal stone diameter of 0.04m wave height of 0.1m and wave period of 0.9s. As can be seen the 3D wave field has a significant spatial variation around the breakwater when compared to the 2D scenario. A general trend observed is that $K_{d,t,s}$ in front of the breakwater has lower wave energy compared to the wave field offshore of the gap. With respect to the wave field behind the breakwater it is observed that the area of high $K_{d,t,s}$

63

depends on the porosity. It is noticed that as n increases the 3D wave field behind the breakwater becomes more homogeneous and resembles that of the 2D scenario with the exception of the gap, where higher wave heights are detected. Also the region of high wave energy directly in front of the gap of the breakwater increases in area and magnitude for an increasing porosity. Based on the results presented above it can be concluded that the wave field behind submerged permeable breakwaters is strongly influenced by the porosity and the 2D and 3D wave field have a significant difference.
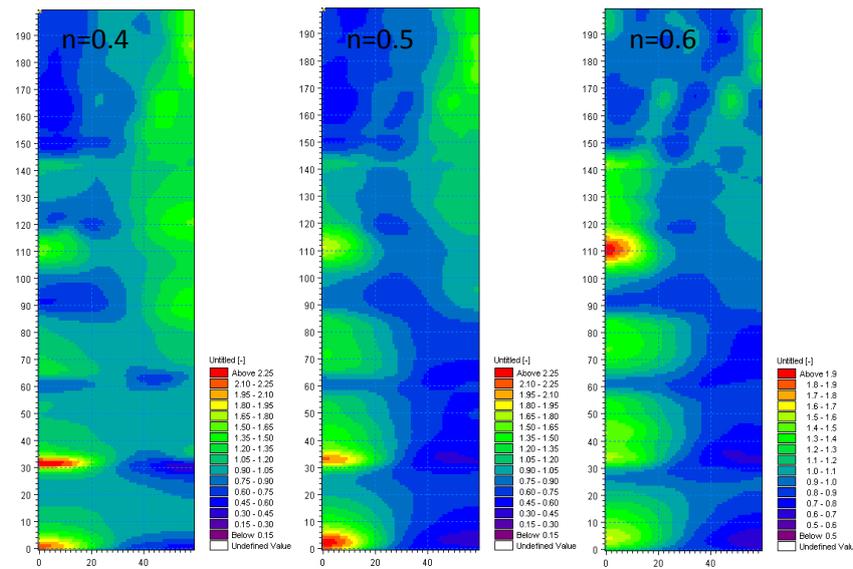
Figure 4.14: 2D plot of the ratio Kd,t,s around the breakwater for T=0.9s, Dn50=0.04m, Hi=0.10m for porosity values of 0.4, 0.5 and 0.6 (scale 10:0.4m)

4.3.2.2   *Dimensionless Results*

A dimensionless analysis of the results is required for the sake of understanding in depth the behavior of the data with respect to wave transmission. It is essential to create a method that makes the results transferable and comparable to other test conditions. This can be accomplished in two ways:

- By scaling each parameter to the corresponding situation using Froude's number.
- By creating non-dimensional parameters that are capable of describing accurately the situation examined.

The first method is tedious and has caused confusion when implimented. The second has been used extensively by other authors for analyzing trends and results (Seeling, 1980; Ahrens, 1987; van der Meer, 1991; Seabrook and Hall, 1998 etc); the latter has proven to give a productive correlation between the involved parameters and serves as a good tool for engineering design purposes. For these reasons this report will focus on presenting the results of the experiments in a non-dimensional manner. Figures 4.15 through 4.18 show the correlation between various dimensionless parameters with the transmission coefficient for different position behind the breakwater.
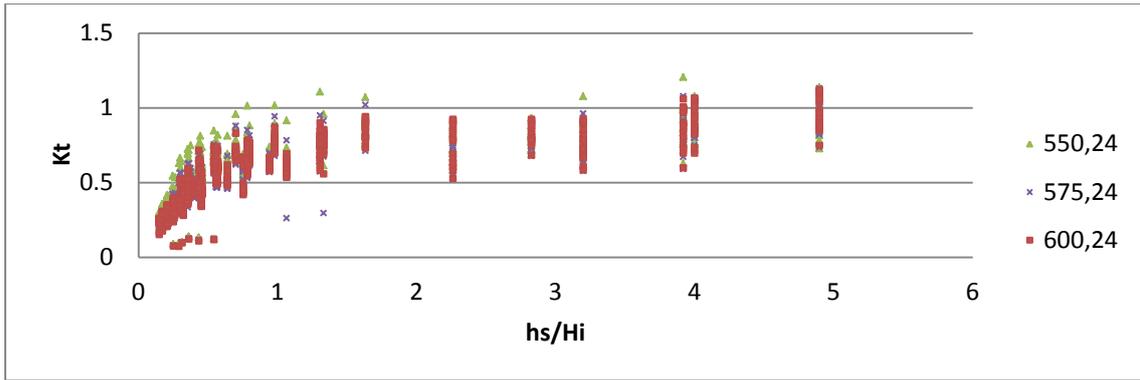
Figure 4.15: Correlation of Kt with hs/Hi for 3 locations behind the breakwater
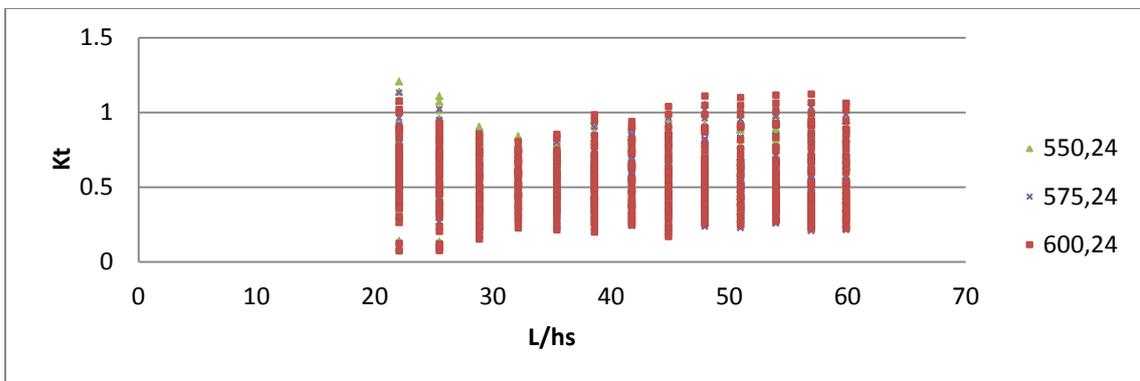
Figure 4.16: Correlation of Kt with L/hs for 3 locations behind the breakwater
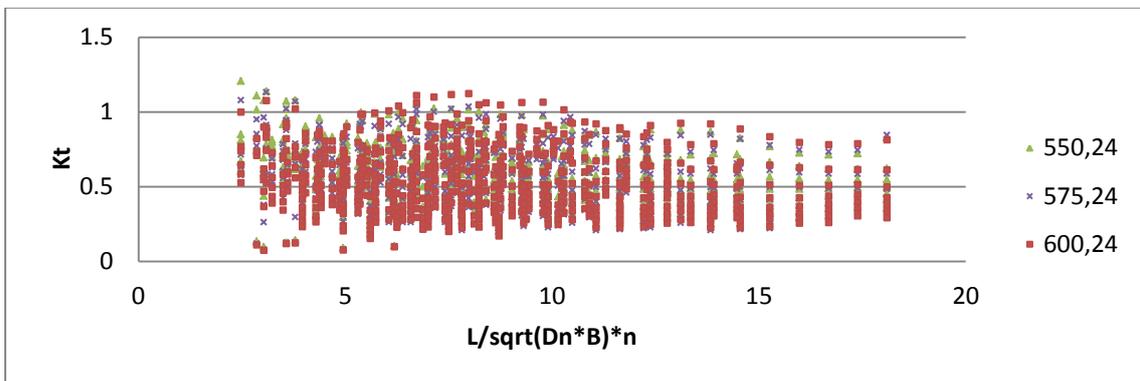
Figure 4.17: Correlation of Kt with L/sqrt(Dn*B)*n for 3 location behind the breakwater
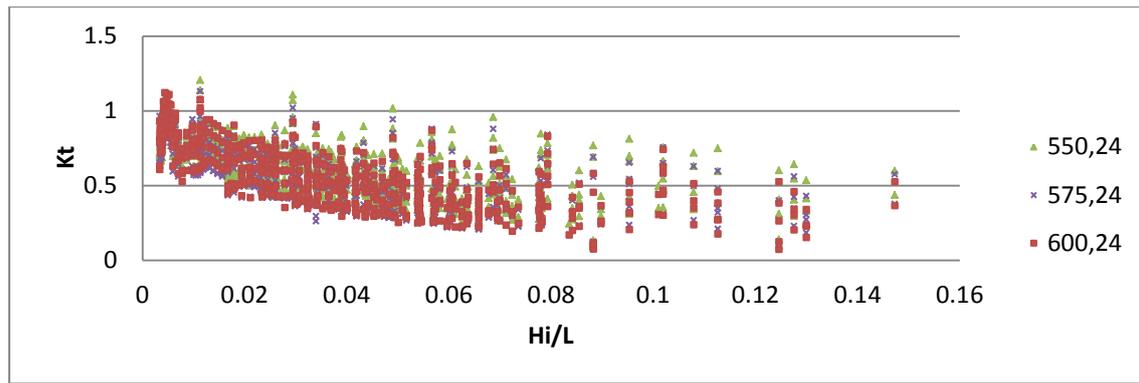
Figure 4.18: Correlation of Kt with wave steepness for 3 locations behind the breakwater

As can be seen from the figures above the transmission coefficient shows a strong dependence with hs/Hi. As the submergence depth relative to the incoming wave height increases, larger wave transmission coefficients are observed. K_t also shows a spatial variation behind the breakwater, as it increases when moving further inshore due to shoaling. Regarding the incoming wave length sinusoidal envelopes enclosing the K_t values for varying L/hs are observed (as can be seen in figure 4.16). This can be explained by the influence of diffraction and permeability. Namely, at small values of L the effects of diffraction are strongest therefore resulting in high wave transmission coefficients; as L increases further diffraction effects lessen but permeability effects start to contribute more and therefore increase again the wave height behind the breakwater. It is also worth noting that in the third plot which includes the influence of stone diameters and porosity the same trend as in figure 4.17 can be observed but with a visible dampening of the effect of permeability at high values of $\frac{L_0}{\sqrt{D_{n_{50}}B}} n$. Finally, the fourth plot shows that for increasing wave steepness the wave transmission coefficient reduces. The physical explanation for this trend is found in the higher wave reflection associated with high wave steepness which reduces the amount of energy left to be transmitted over the barrier.

It is also important to examine the distribution of the data that will be used for training the ANN model. It is known that ANN models are capable of producing very accurate results in the regions where a sufficient amount of data is available. For this reason the absolute distribution of the all input parameters and measured K_t is presented (figure 4.19). This maps the regions of high and low expected accuracy of ANN model.
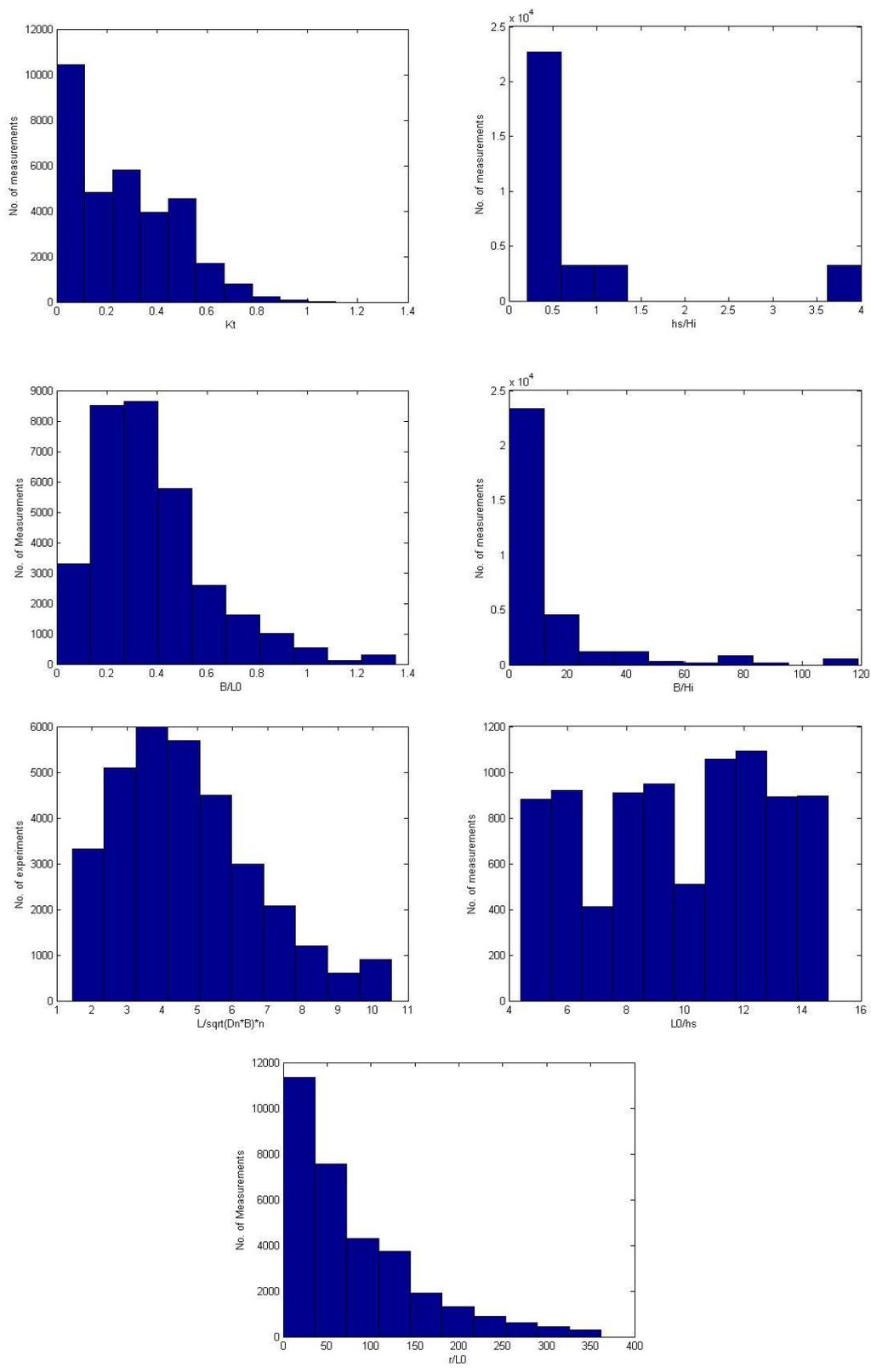
Figure 4.19: Absolute distribution plots for various non-dimensional parameters

It is concluded from the distribution plots in figure 4.18 that the overall data have a sufficiently wide distribution. The wave transmission coefficient follows a gamma distribution associated with the small number of extreme wave conditions. $\frac{H_i}{h_s}$ has a discontinuous distribution which is associated with the extremely low incoming wave height of 0.01m which produces a class of data that is located far away from the rest, the ANN is not expected to perform well between the values of 1.5 and 4 but these are values that are unrealistic for real world situation and therefore will not cause any significant problem regarding the outputs of the model. ξ and $\frac{B}{H_i}$ also have a wide gamma distribution as a result of the same extreme wave conditions mentioned earlier. $\frac{L_0}{\sqrt{D_{n_{50}}B}}n$ and $\frac{B}{L_0}$ follow a slightly skewed normal distribution which is a good indicator of variability. Finally the distribution of $\frac{L_0}{h_s}$ and $\frac{r}{L_0}$ behave as homogeneous and gamma distribution correspondingly.

Concluding, based on the above mentioned findings the wave steepness and the relative submergence ratio along with the relative permeability coefficient $\left(\frac{L_0}{\sqrt{D_{n_{50}}B}}n\right)$ are the most influential parameters influencing the wave transmission process. $\frac{r}{L_0}$ and ϑ are also of great importance for the wave transmission process as they introduce the spatial variation of the wave transmission coefficient in polar coordinates. It is also deducted that the distribution of the dimensionless parameters is satisfactory for training the ANN model.

4.3.3 Discarded data for ANN modeling

For the purpose of producing a homogeneous data set it was required to discard several data subsets.

Data obtained from the wave probes foreshore of the breakwater were all discarded, as the main focus of this report is the transmission coefficient. Including data measurements from the front of the breakwater would introduce a large error when used to train the ANN model. This is because the data trends influencing wave transmission and reflection are completely different. Another source of error might come from reflected waves off the sidewall. These waves could influence the accuracy of the measurements. For this reason a numerical a filter capable of isolating the reflected wave heights was installed. Nevertheless it was decided to discard data coming from these gages to assure a high level of accuracy. The location probes used for training and testing the ANN model are listed below.

Coordinates of probes used for ANN training			
24,550	36,550	48,550	60,550
24,570	36,570	48,570	60,570
24,600	36,600	48,600	60,600

Table 4.7: Coordinates of probes used for training and testing the ANN model, as nodes in computational domain

5 Accuracy analysis of 2D and 3D Data

As discussed in the previous chapter a large number of experiments were performed in order to create a large database that would train the ANN model. For that reason it was essential to assure the accuracy of the results. This chapter will provide the accuracy analysis for the 2D and 3D experiments. The 2D experiments are compared to the 2D experiment of the DELOS database and the accuracy of the 3D experiments is compared with the 3D wave disturbance model proposed by Vicinanza et al (2009).

5.1 Validation of 2D data

The numerical modelling of the 2D wave field at submerged porous breakwaters was performed using MIKE 21 BW. This section will provide an analysis of the capability of the numerical model to predict the wave transmission coefficient. The validation of the wave model is conducted by comparing the results of the wave transmission coefficient for the calibrated model (Class A experiments) against the corresponding coefficients found during the compilation of the homogeneous wave transmission database during the DELOS project. In order to assure high level of accuracy, each numerical simulation resembled the exact structural and wave parameters (see section 4.2.2 for details) as in the original experiments with the exception of porosity (no porosity measurements were performed during the DELOS experiments). For that reason the porosity value was assumed to be 0.38 which is a typical value for small scale experiments. The transmitted wave height values from the wave model were calculated using the mean value of the significant wave height for ten consecutive grid points on the lee side of the breakwater; namely for points (30,561) to (30,571). Finally K_t was calculated by taking the ratio of the transmitted wave height over the incoming wave height.

Figure 5.1 shows a Quantile - Quantile plot of the calculated wave transmission coefficient found in chapter 4 versus the K_t measured during the DELOS experiments. The agreement between the measured wave transmission coefficients and the calculated is excellent as can be seen in figure 5.1. The model is able to simulate successfully the quasi-standing wave pattern in front of the breakwater that is due to partial wave reflection. The reason for this is that van Oosten and Peixo (2006) used the value of the incoming wave height at the toe of the structure for the calculation of K_t (which by definition captures the quasi-standing wave pattern in front of the breakwater), which matches that of the simulation conducted in this study. Also the increase in wave steepness due to wave reflection and shoaling in front of the breakwater is simulated realistically.
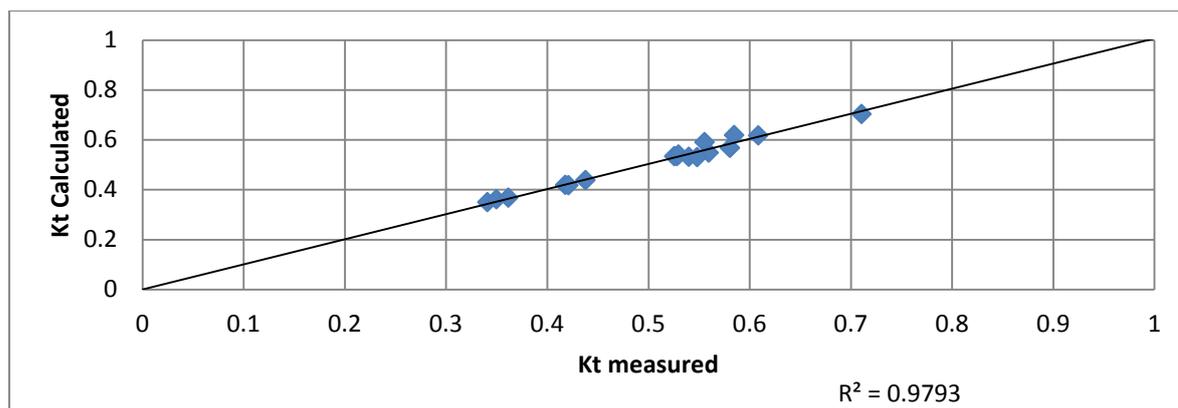
Figure 5.1: Validation result for experiment excluding wave diffraction

In order to examine more closely the robustness of the model, 5 different types of statistical parameters were calculated. The analysis reveals that the wave model has an excellent predictive skill (Brier Skill score of 0.98), also all computed errors are considerably low which allows us to conclude that the wave model can be used to simulate realistically and with very high precision wave transformation phenomena near submerged porous breakwaters.

Index	Bias	M.A.E.	M.S.E.	R.M.S.E.	Error	B.S.S.
Value	0.0039	0.01122	0.0002	0.0146	0.0205	0.9793

Table 5.1: Statistical evaluation of Wave Model

Concluding the MIKE 21 BW can be used to successfully predict wave transmission coefficients behind infinitely long submerged porous breakwaters (2D wave transmission). Therefore it can be deducted that when MIKE21 BW is used to model 3D wave transmission effects the only source of error can be diffraction. The next section will treat the accuracy of 3D wave transmission in detail.

5.2   Validation of 3D data

As the 2D modelling of wave transmission, the 3D modelling using MIKE 21 BW was performed in order to determine the spatial wave distribution around submerged breakwaters under the influence of diffraction. To the knowledge of the author only a limited number of experiments have been performed examining the three dimensional behaviour of the wave field around submerged breakwaters and even fewer on permeable submerged breakwaters. As a result it was not possible to obtain physical wave measurement data for 3D wave transmission for the validation of the dataset. For that reason it was decided to use prediction method proposed by Vicinanza et al. (2009) (elaborated in Chapter 3). A wide number of different wave and structural conditions from the dataset covering the entire range of data were tested against this method. The data

tested had different combinations of nominal stone diameter and porosity as well as different values of incoming wave heights and periods. A table that summarizes the conditions tested is presented below.

Test Number	H_i (m)	T (s)	$D_{n_{50}}$ (m)	n	h_s (m)	H (m)	B (m)
572	0.03	1.04	0.04	0.4	0.04	0.4	0.3388
575	0.09	1.04	0.04	0.4	0.04	0.4	0.3388
576	0.11	1.04	0.04	0.4	0.04	0.4	0.3388
32	0.03	1.04	0.04	0.5	0.04	0.4	0.3388
35	0.09	1.04	0.04	0.5	0.04	0.4	0.3388
36	0.11	1.04	0.04	0.5	0.04	0.4	0.3388
992	0.03	1.52	0.06	0.4	0.04	0.4	0.3388
995	0.09	1.52	0.06	0.4	0.04	0.4	0.3388
996	0.11	1.52	0.06	0.4	0.04	0.4	0.3388
752	0.03	1.04	0.02	0.4	0.04	0.4	0.3388
755	0.9	1.04	0.02	0.4	0.04	0.4	0.3388

Table 5.2: Summary of test conditions for 3D validation

The prediction method proposed by Vicinanza et al. (2009) was developed for low crested structures with $R_c \geq 0$ and impermeable cores under the hypothesis that wave transmission over and through the breakwater are independent of the diffraction effects (correlation of 0). As showed in the findings of the numerical simulations there is strong evidence that the two processes, 2D transmission and diffraction are negatively correlated as an increase in the transmitted wave height results in a reduction of the overall transmitted wave height. For this reason the following sections will present a comparison between the calculated data and the Vicinanza method for the cases where:

- Correlation factor is zero (R=0)
- Correlation factor is negative ($R < 0$)

5.2.1   Comparison under the hypothesis of zero correlation
As mentioned in chapter 3 the method adopted for this analysis makes use of prediction formulas for 2D transmission and then combines them with a diffraction theory in order to calculate the combined effect, using Eq. 3.21.

For the calculation of the diffraction coefficient the method proposed by Penny and Price (1952) is implemented using the McCormick and Kraemer (2002) approximation. This method has been proven to produce very reliable results for long crested waves, which is the case in this study. Also four different prediction formulae for 2D wave transmission have been selected in order to detect the sensitivity of the MIKE 21 BW results to different formulations. The prediction formulae used at are:

- D'Angremond (1998)
- Buccino and Calabrese (2007)
- Seabrook and Hall (1998)
- Goda and Ahrens (2008)

The first formula was selected as it is the most extensively tested formula for low crested structures throughout the literature and it has been proven to give accurate results. The formula was based on the successful method propose by D'Angremond and adjusted for permeable structures. The Buccino and Calabrese formula has been designed for submerged and impermeable breakwaters. And the latter two formulations have been designed for submerged porous breakwaters, which is the exact same classification as the structures examined in this report. By comparing the results of the wave model with these formulations, valuable information will also be obtained regarding the importance of treating separately submerged permeable structures from LSC's in engineering problems.

Figure 5.2 shows the relation of transmission coefficient (Seabrook) for submerged porous breakwaters and the overall wave transmission coefficient measured in the wave model ($K_{D,t}$). According to this we can conclude there is a significant difference between 2D and 3D wave transmission.
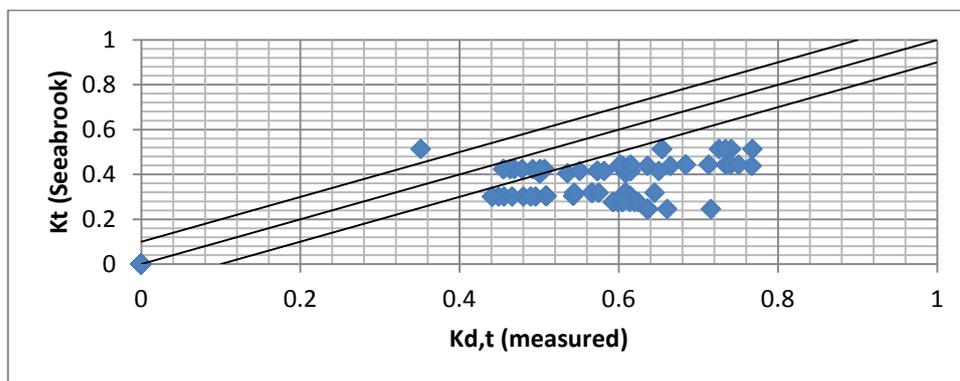
Figure 5.2: Kt (Seabrook) versus $K_{D,t}$ (measured)

For this reason the following graphs where developed. They show the agreement between the measured wave transmission coefficient and the calculated. Figure 5.3 shows that a reasonable agreement exists between the results. The D'Angremond formula seems to over predict the wave height behind the breakwater at very high and low measured $K_{D,t}$. A possible explanation is that the specific wave transmission formula is developed for treating a variety of different structure types (mainly emerged); this formulation also does not

incorporate the effects of permeability which have the potential to reduce the wave climate on the lee side of the breakwater. As the D'Angremond formula the method proposed by Buccino and Calabrese tends to overestimate $K_{D,t}$ values at the lower tail of the data (see figure 5.4). As was the case in the previous graph this method fails to predict the dissipation effects due to filtration. The latter two figures (figure 5.5 and 5.6) depict the agreement between MIKE21 BW results and the methods of "Seabrook and Hall" and "Goda and Ahrens". R^2, representing the agreement between the prediction method and the actual data is 0.82 and 0.77 respectively, indicating a good agreement. Most of the data points lie between the 10% confidence lines. Therefore we can conclude that the wave model used to create the dataset for the training of the ANN is reliable. The increased accuracy compared to the two first formulations also indicates that permeability has a significant influence in the wave transmission over submerged porous breakwaters.
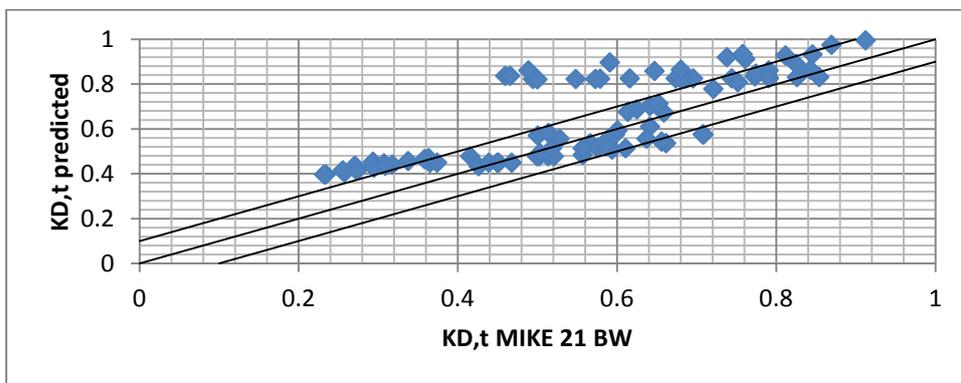
Figure 5.3: KD,t (D'Angremond) Vs KD,t (MIKE 21 BW)
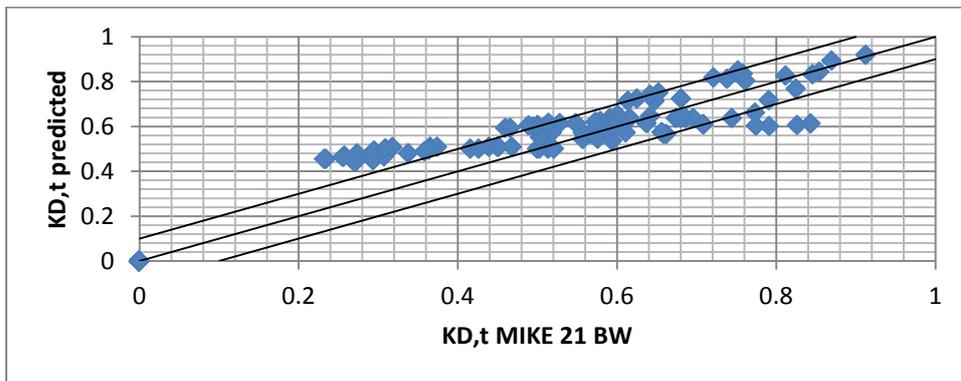
Figure 5.4 KD,t (Buccino and Calabrese) Vs KD,t (MIKE 21 BW)
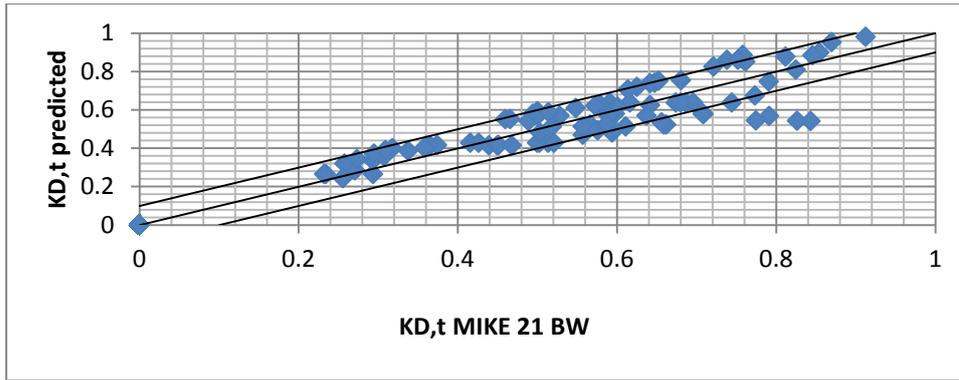
Figure 5.5: KD,t (Seabrook) Vs KD,t (MIKE 21 BW)
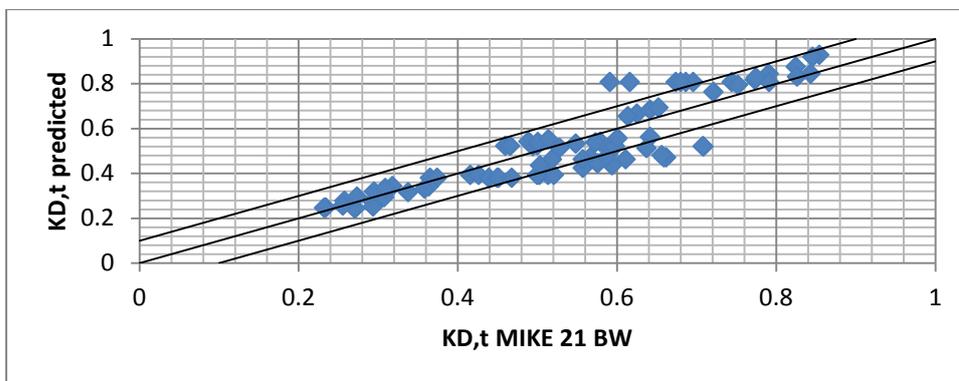
Figure 5.6: KD,t (Goda and Ahrens) Vs KD,t (MIKE 21 BW)

For the purpose of understanding in more depth the behaviour of the model data we can also examine the spatial distribution of the error behind the breakwater. For this reason error contour maps of several combinations of different structural permeability and wave conditions were produced for each prediction formula. All plots depict the "shadow" area behind the breakwater. The line y=0 corresponds to the centreline of the breakwater and the axis origin in the figures corresponds to point (24,523) in the numerical models domain (the head of the breakwater)

The figures bellow present the error contours for a nominal stone diameter of 0.04m, permeability of 0.4 incoming wave height of 0.11 and wave period of 1.04s. The plots suggest that the point of higher error in all formulation lies near the breakwater. The source of this error comes from the nature of the diffraction theory used. All diffraction theories are developed for vertical barriers with no slopes on either side of the structure. Due to this, the empirical model has the tendency to produce error at these locations. It is also found that the agreement also becomes better further onshore in all situations. As suggested in the Q-Q plots above, the best agreement is found for the methods of "Seabrook and Hall" and the "Goda and Ahrens", these methods incorporate all the physical processes relevant to this study and therefore it seems reasonable to have the best agreement. Overall all the methods show that the data have good agreement as the absolute error in the largest part of the domain is below 10%, with the exception of the method of D'Angremond.
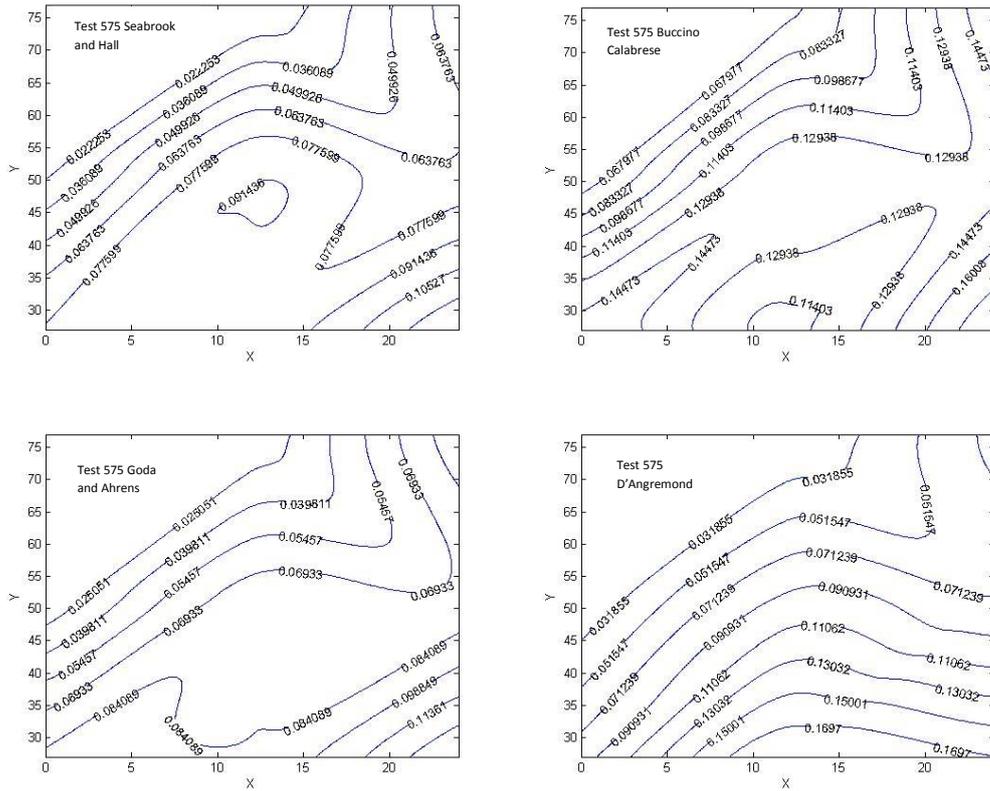
Figure 5.7: Error contours of test 575 for different prediction methods (scale 10:0.4m)

The next set of figures demonstrate the spatial distribution of error for the different methods for the conditions of test 35, where a high porosity value was used (n=0.5). This set of data shows a large disagreement throughout the entire domain. This deviation is explained as all methods fail to account for the effect of porosity. The formulas used in this analysis were calibrated under average porosity conditions which lie in the range of 0.3 to 0.4 and therefore under-predict the actual wave height. Nevertheless the same trends as in the previous figures are observed, where high discrepancies are observed near the breakwater. Finally, it is also observed that the highest error area increases in size as n increased.
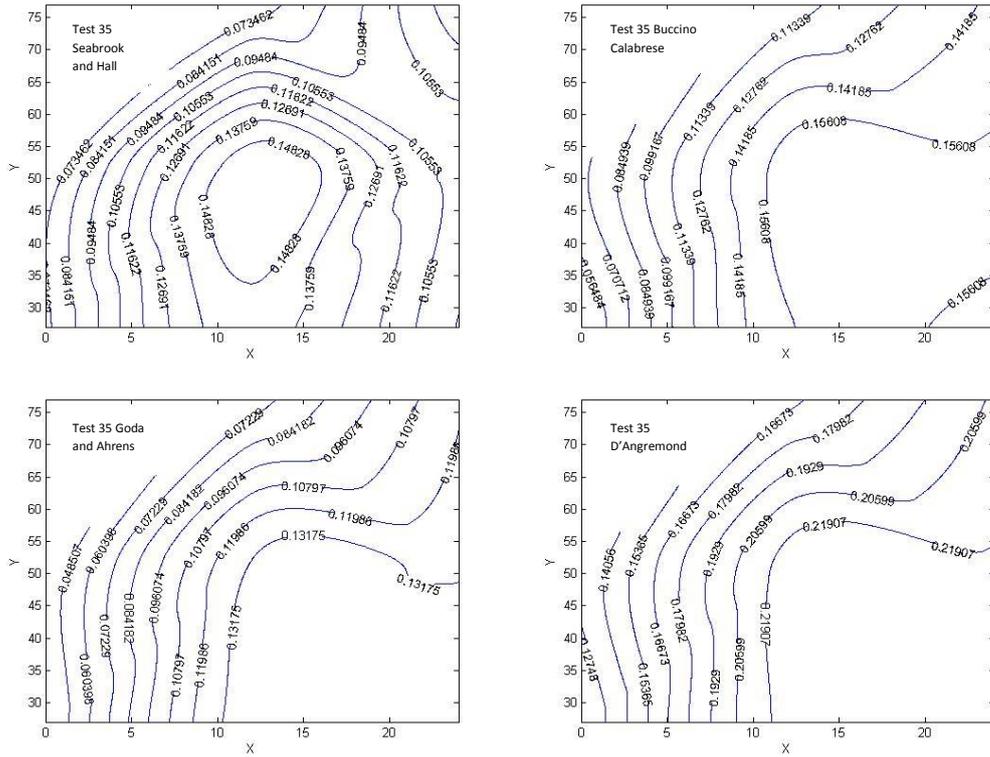
Figure 5.8: Error contours of test 35 for different prediction methods (scale 10:0.4m)

Also figure 5.9 illustrates the error contour-maps for the test conditions of test 996. Again the largest error between the prediction method and the data of MIKE 21BW is located near the crest of the breakwater. In this scenario though, the error throughout the entire domain is reduced significantly. Again the methods of "Seabrook and Hall" and "Goda and Ahrens" show the best agreement. Also the gradient of the error $\left(\frac{d\varepsilon}{ds}\right)$ is significantly reduced; this gradient can be interpreted as the deviation of error with respect to the coordinate system which indicates that the agreement is improved.
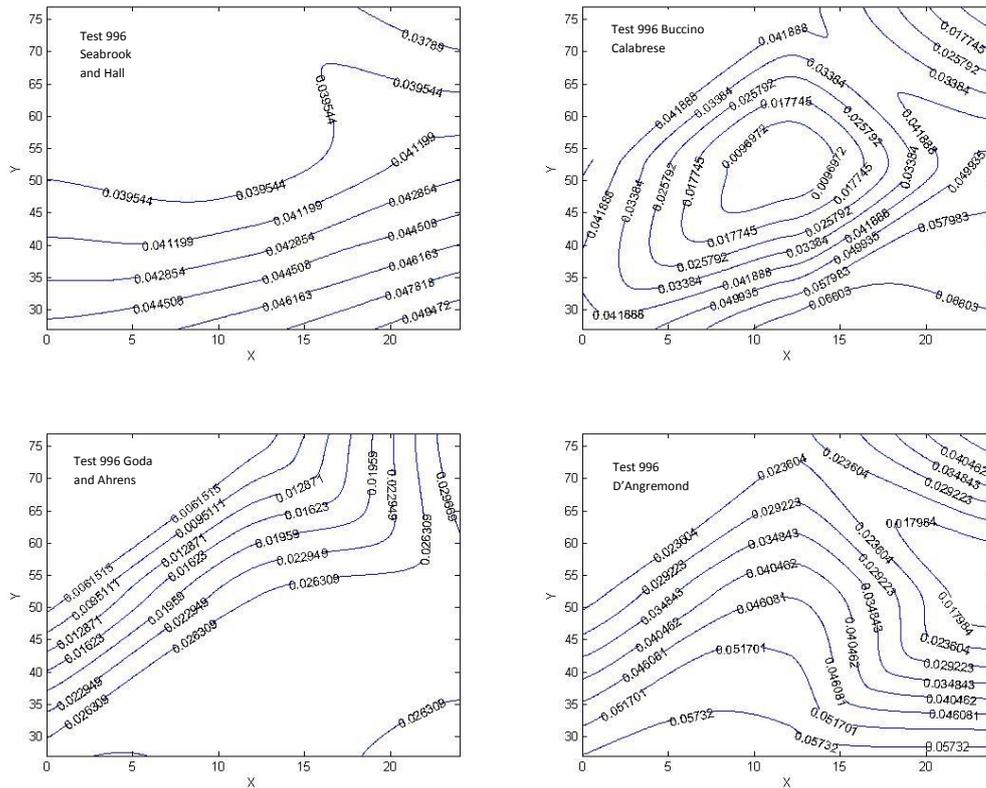
Figure 5.9: Error contours of test 996 for different prediction methods (scale 10:0.4m)

Concluding, the information above suggests that the data generated by MIKE 21 BW have a good level of accuracy. The high error levels in figure 5.8 are mainly a result of the incapability of the adopted prediction method to account for the effects of porosity. Additionally because the methods of "Goda and Ahrens" and "Seabrook and Hall" have been specifically designed for submerged breakwaters and account for the effects of seepage, it is can be reasonably assumed that they provide a better measure of accuracy compared to the other two methods. Based on this assumption it is concluded that he error band for the dataset tested lies in the range of [0.006, 0.11]. The discrepancies near the breakwater are mainly due to the incapability of the traditional diffraction theories to predict K_D over a slope. Finally the agreement between empirical and numerical results seems to be better for longer waves, which is also observed in analysis of Vicinanza et al. (2009). Based on this the overall accuracy for the data creates can be classified "good".

5.2.2   Comparison under the hypothesis of negative correlation

Accoriding to the findings in the previous chapter, there is strong evidence that the wave transmission process and diffraction are not completely indipendant. Increasing wave lengths and permeability show a more homogeneous wave field on the lee side of the breakwater. This in turn may be interpreted as a reduction in the contribution of diffraction to the global wave transmission coefficient. The latter in statistiacal terms suggests a negative correlation of the K_t and K_D. Therefore an analysis based on the assumption that the two processes are correlated will to be seems a reasonable task.

In order to include the effects of correlation between the wave transmission and diffraction coefficient, the proposed formula for the calculation of the global wave transmission coefficient $(K_{D,t})$ by Vicinensa et al. (2009) has been modified and reads as:

$$K_{D,t} = \sqrt{K_D^2 + K_t^2 + 2R\,K_D\,K_t}$$

Eq. 5.1

where R represents the correlation between the two processes.

As was the case in the previous analysis the Penny and Price solution for the calculation of the diffraction coefficient has been implemented using the McCormick and Kraemer (2002) approximation. In order to avoid repetition only two wave transmission formulae have been selected for this analysis. Namely the "Goda and Ahrens" and "Seabrook and Hall", as from all the existing formulae these two seem to describe better the structures analyzed, because both are calibrated for submerged permeable structures.

The strength of the linear association between two variables is quantified by the correlation coefficient (R). A negative correlation indicates a negative association between the variables which in terms of wave transmission means that when more energy is allowed to pass over and through the breakwater (high contribution to $K_{D,t}$) then less energy is transported through diffraction (low contribution) and vice versa. The correlation between K_D and K_t for the test data was calculated and found to have a value of -0.35 for the case where the "Goda and Ahrens" formulation was used, and -0.30 for the "Seabrook and Hall" method.

By the introduction of these correlation factors in the method of Vicinanza a much stronger agreement is observed between the ANN model results and the prediction method (see figures 5.10 and 5.11). The correlation factor between the global transmission coefficient calculated by MIKE 21 and the prediction method shows the agreement between the two datasets is stronger compared to the hypothesis of zero correlation. Additionally the data performance can be evaluated by the introduction of confidence lines. In the cases presented below it can be observed that almost all of the data falls within the 10% confidence limits and therefore the scatter has been decreased significantly.
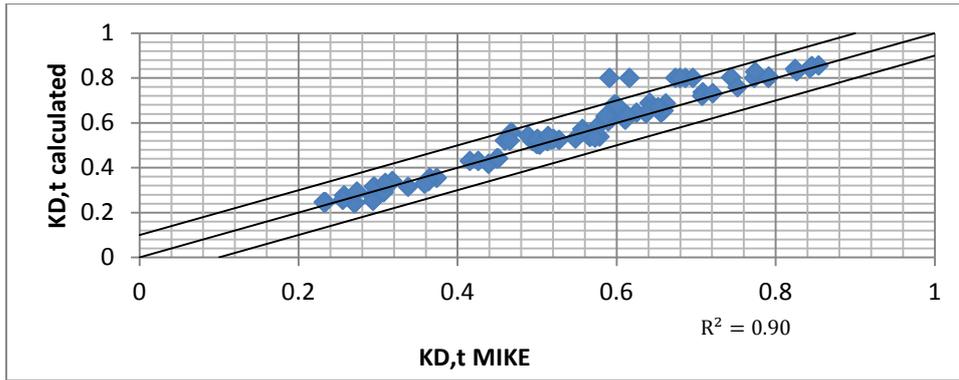
Figure 5.10: $K_{D,t}$ using the "Goda and Ahrens" formulation Vs $K_{D,t}$ of the prediction method, with 10% confidence interval lines
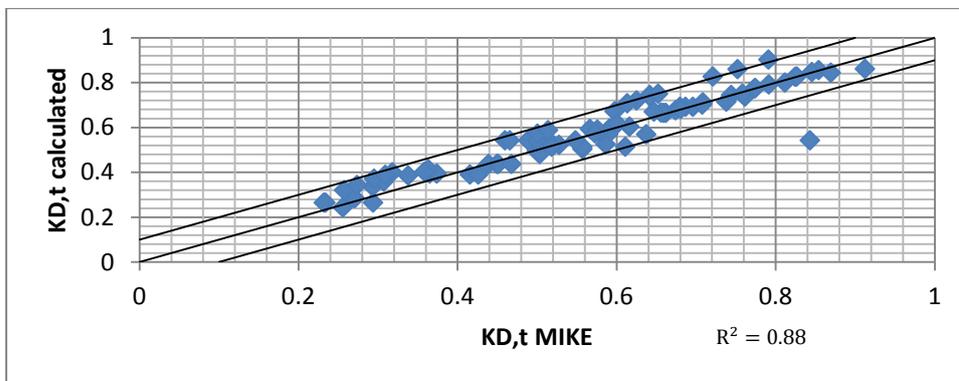
Figure 5.11: $K_{D,t}$ using the "Seabrook and Hall" formulation Vs $K_{D,t}$ of the prediction method, with 10% confidence interval line

Summarizing the results obtained from the data analysis, it can be concluded that MIKE 21 BW has the ability to predict with good accuracy the transmitted wave height for the 2D wave transmission process. Based on the analysis for the 3D case the agreement between the prediction method adopted and the data generated is acceptable. The accuracy of the data increased when the reasonable assumption of negative correlation between K_D and K_t was adopted. It should be also stressed that K_D and K_t each contain a certain amount of uncertainty which increases when added together. Therefore scatter is unavoidable no matter how good the quality of the data is. Concluding it can be stated that MIKE 21 BW produces very good quality data that can be used to train and test an ANN model.

6   ANN modeling, performance and validity

In this chapter the results of the ANN modeling will be presented. This chapter will also give a detail description of the model setup and performance of the ANN model. Also an analysis of the accuracy of the model will be presented.

6.1   Network Data

In chapters 4 and 5 the process of creating the data and assuring their quality was discussed thoroughly. This part of the report will focus on the preparation of the data in order to train the ANN model. The performance of an ANN model not only depends on the quality of data that are used to train it, but also on the several other aspects. These will be discussed in detail in the following sections.

6.1.1   Creating non-dimensional dataset

For the purpose of creating a dataset that could be used in a range of different conditions it was decided the data obtained from the numerical experiment where made dimensionless. This allows input information to be transferable to other applications. It is important for the ANN model to include a sufficient number of input parameters. At the same time it also important to keep the number of inputs small, a large number of input variables may lead the model to unnecessary level of complexity that could possibly introduce "false" connection paths during the training process. In a preliminary basis the correlation of different dimensionless parameters with the wave transmission coefficient were checked in order to determine which parameters contained the largest amount of information. In this study this problem of determining the most important input parameters was treated in the following way. The starting point of the variable selection was the formulations given by Ahmadian (2013) for 3D wave transmission for impermeable breakwaters.

$$K_{t_{3D}} = f\left\{\frac{H_i}{L_0}, \frac{h_s}{H_i}, \frac{H_i}{h}, \frac{h_s}{h}, \vartheta, \frac{r}{L_0}\right\}$$ Eq. 6.1

An initial form of the architecture of the ANN model was then run using different combinations of dimensionless parameters until the set off variables with the least error and correlation was found. During this phase it was concluded that it is important to include a term that represents the effects of seepage in the process. Finally the set of input variables used for the ANN analysis was determined as:

$$K_{t_{3D}} = f\left\{\xi, \frac{h_s}{H_i}, \frac{H_i}{h}, \frac{L_0}{h}, \frac{B}{H_i}, \frac{L_0}{\sqrt{BDn_{50}}}n, \vartheta, \frac{r}{L_0}\right\}$$ Eq. 6.2

In addition to the distribution plots presented in chapter 4 a statistical analysis of the parameters is presented below in order to illustrate the range of input parameters for which the model will be valid.

	Min	Max	Standard Deviation	Mean
ξ	0.99	7.89	1.48	2.55
$\dfrac{h_s}{H_i}$	0.21	4.00	1.10	0.85
$\dfrac{H_i}{h}$	0.05	0.95	0.28	0.50
$\dfrac{L_0}{h}$	4.41	14.89	3.18	9.90
$\dfrac{B}{H_i}$	0.02	0.06	0.02	0.04
$\dfrac{L_0}{\sqrt{BD_{n_{50}}}}n$	1.44	10.53	2.01	4.75
ϑ	-3.10	3.10	1.18	1.27
$\dfrac{r}{L_0}$	0.01	1.90	0.32	0.44

Table 6.1: **Statistical analysis of input parameters**

6.1.2 Training and testing datasets

For the purpose of training properly the ANN model it is important to divide the data obtained from the experiments into two sub sets; namely the training and testing datasets. The first set of data in used to train the model whereas the second is used to supervise the learning process. It is important that the data used for testing not to be included into the training. This will assure that the performance of the model is verified and will also check if a generalization problem occurs. The generalization problem refers to the situation at which the neural network is too powerful for the problem examined. It then does not "recognize" the underlying trend in the data, but learns the data by heart (including the noise in the data). This results in poor generalization and too good a fit to the training data. In order to further improve the generalization capability of the model the training subset is then divided into subcategories; the Estimation subset which is used for updating the weights and biases and the Validation subset which in turn supervises the error over the training process. In order to avoid over fitting (i.e. poor generalization) the bias and weights are saved when the error reaches its minimum value.

The datasets described above where created by randomly selecting experiments from the pool of data files. The composition of each dataset is as follows. From the 1080 experiments 85% comprised the training dataset and the rest (15%) was used to test it. Also 15% of the training dataset was dedicated for the validation of the training process and the rest for the estimation. The following table summarizes the composition of the datasets. It should be mentioned that in order to evaluate the wave height distribution behind the breakwater 9

measurements behind the breakwater where used per experiment resulting in a total number 9720 input arrays.

	Training dataset		Testing dataset	Total size of dataset
	Estimation	Validation		
Number of Experiment	780 (72%)	138 (13%)	162 (15%)	1080
Number of input arrays	7020 (72%)	1242 (13%)	1458 (15%)	9720

Table 6.2: Dataset composition for ANN modeling

6.1.3 Data Normalization

As mentioned in chapter 3 Neural Networks work via transfer functions which transfer information from one unit to another. In order to improve the performance of the model it is desirable to limit as much as possible the range of the input variables that the model handles. This is accomplished by normalizing the input arrays (i.e. preprocessing). This procedure minimizes the range of inputs and forces the model to output results in the same normalized range. Consequently a de-normalization procedure is required at the end of the network (i.e. postprocessing). In this model this problem is tackled with the introduction of a linear scaling algorithm, which reads transforms all variables to the domain of (0, 1) and reads as:

$$x_{norm} = \frac{x - \min(x)}{\max(x) - \min(x)}$$

Eq. 6.3

6.2 ANN model Architecture

The proposed Neural Network makes use of the RBF network architecture, which is the most popular type of network used for function approximation. As described in chapter 3, RBF's are feedforward networks that maps sets of input data onto a set of appropriate outputs. An MLP consists of multiple layers of nodes in a directed graph, with each layer fully connected to the next one. Except for the input nodes, each node is a neuron (or processing element) with a nonlinear activation function. RBF utilizes a supervised learning technique called backpropagation for training the network (Rosenblatt, 1961). In the following sections detailed descriptions of the individual components of the architecture will be presented.

6.2.1 Number of Hidden layers

For the purpose of this study only one hidden layer was selected to approximate the nonlinear function corresponding to the data patterns. It is also possible to include more layers in order to increase the performance of the model but this would increase dramatically the computation time. The increased predictive capability is small compared to

additional computation time and therefore the addition of more hidden layers is not justified. According to Hornic (1989) one hidden layer is adequate to properly describe the underlying function with sufficient detail.

Regarding the input layers are defined by the input parameters that where defined in the previous section. Namely the number of input parameters should match the number the number of input layers.

Finally the output layer is defined by the nature of the problem as well. The architecture of the model could be defined in order to have more than one output layers. This will introduce a non-necessary complexity to the structure of the program. This problem could be solved by the introduction of two input variables that can describe the spatial position of the wave transmission coefficient and therefore allow the model to calculate the specific output one by one. The latter method was selected in this study and therefore one output layer was implemented in the design.

6.2.2   Transfer function

Transfer functions (hereafter TF) are mathematical representations, in terms of spatial or temporal frequency, of the relation between the input and output. In ANN's TF's provide the connection between the units of the network and at the same they limit the range of the output in a certain range. Therefore the output and the accuracy of the model strongly depend on the TF implemented.

In RBFs each hidden unit has its own transfer function. The most common TF in these kinds of Neural Networks is the Gaussian function which shape is defined by a shape parameter (spread). It is of great importance to determine a correct shape factor for the network since, a larger spread, results in a smoother function approximation, which means that many neurons are required to fit a fast-changing function. A small spread means that many neurons are required to fit a smooth function, and the network might not generalize well. For this reason it is important to choose a spread constant larger than the distance between adjacent input vectors, that will give a good generalization, but smaller than the distance across the whole input space. Therefore the need arises that an optimum spread should be determined. In order to establish the optimum shape factor several different shape factors were applied to the elementary model that was created and then the corresponding error was calculated. The input and training data were the same in all scenarios; also the number of neurons was kept constant at 500. Table 6.3 demonstrates the best results were obtained for the last.

Spread	RMSE	R^2
0.8	0.06	0.93
0.9	0.06	0.95
1	0.04	0.98
1.1	0.05	0.96
1.2	0.7	0.90

Table 6.3: Accuracy analysis RBF with different spread factors

Based on the above findings in this MSc thesis a Gaussian TF with a spread of 1 will be applied in the hidden and the output layers.

6.2.3 Training method

The RBF model works in the following way:

The hidden layer originally has zero units (neurons). Pairs of data (training and testing data) insert the network and then the error is computed. Then a new unit with a weight corresponding to the input vector with maximum error is added to the hidden layer. Then the weight factors are adjusted to minimize the error. This procedure continues until the minimum error (specified by the user) is met or when a maximum number of iteration and therefore units have been reached.

Elaborating on the above, input data is passed to the hidden units that compute the Euclidian distance from the centre-point of neuron. Then the RBF function is applied to the distance determined previously. The values obtained from the RBF function (i.e. Gaussian basis function) are then multiplied by a weight factor and then passed over to the output layer where all the weighted values are summed together. The final step involves the addition of a bias. The calculation of the output is then calculated by:

$$y_q(x) = b_q + \sum_{i=1}^{N} w_{qi} \varphi_i(x)$$
Eq. 6.4

Where:

b_q, is the bias

w_{qi}, is the weight factor

$\varphi_i(x) = e^{-(\frac{\|x-\mu_i\|^2}{2\sigma_i^2})}$, is the Gaussian basis function and μ_i is the basis centre σ_i is the width.

It is essential to have a method that will provide an accurate and meaningful measure of the models performance. The error is not only responsible of number of iteration but has an also

determines the value of the new weight factor, as will be explained in the next paragraph. For this study the Sum of the Square Error (SSE) was selected.

$$SSE = \sum_{i=1}^{N}(y_i - \hat{y_i})^2 \qquad \text{Eq. 6.5}$$

Where y_i, is the target value and $\hat{y_i}$ is the ANN model output.

After the SSE has been computed an error function using the Gradient Descent algorithm is used to locate the local minimum of the functions and to reduce the error. The error is reduced by adjusting the weights, centers and widths of the partials using the following expressions:

$$\Delta w_{qi} = -\eta_w \frac{\partial S}{\partial w_{qi}} \qquad \text{Eq. 6.6}$$

$$\Delta \mu_{qi} = -\eta_\mu \frac{\partial S}{\partial \mu_{qi}} \qquad \text{Eq. 6.7}$$

$$\Delta \sigma_{qi} = -\eta_\sigma \frac{\partial S}{\partial \sigma_{qi}} \qquad \text{Eq. 6.8}$$

Summarizing the RBF model used for this research has a total of 9 units in 1 hidden layer. It makes use of the Gaussian function in order to transfer the information from one layer to another and finally uses Gradient Descent algorithm to adjust the weight of the neural network.

6.3   Performance of the ANN Model

After the architecture and the datasets have been finalized the next step is to evaluate the performance of the model. In this section the results of the ANN model will be compared to the data obtained from the MIKE 21 BW simulations. The ability of the model to predict the wave transmission coefficient will be discussed by evaluating several statistical parameters. For this reason analysis of the final model along with a sensitivity analysis, were one dimensionless input parameter at a time is excluded will be presented. The results will be presented in term of Quantile-Quantile plots, error distribution histograms and statistical parameters. In order to describe with accuracy each scenario 5 different statistical parameters where used, these are:

Root Mean Square Error (RMSE)

The Root mean square error is a measure of the differences between values predicted by a model or an estimator and the values actually observed. In the context of model analysis it gives a good estimate of the overall accuracy of the prediction model relative to test data. A small RMSE means that the model is more accurate. In general a RMSE smaller than 0.05 means that the modal has a good predictive capability. The equation for calculating RMSE is:

$$RMSE = \sqrt{\frac{\sum_{i=1}^{N} \frac{(x_{c_i} - x_{m_i})}{x_{m_i}}}{N}}$$

Eq. 6.9

Squared Multiple Correlation Coefficient (R^2)

R^2, gives an indication of the overall trend the model follows. A high correlation coefficient means that the predictions of the model have the tendency to follow the same trend of the data that are used to compare it with. The higher the value of R^2 the better performance the model has. For the purpose of this study a satisfactory correlation coefficient should have a value close to 0.98. This will mean that the model has the same capability as the ANNs created by Panizzo et al. (2004) , van Oosten and Peixó (2005) and Ahmadian (2013). The formula used for calculating the correlation coefficient reads as:

$$R^2 = \frac{\left[\sum_{i=1}^{N}(x_{m_i} - \overline{x_m})(x_{c_i} - \overline{x_c})\right]^2}{\sum_{i=1}^{N}[(x_{m_i} - \overline{x_m})^2 (x_{c_i} - \overline{x_c})^2]}$$

Eq. 6.10

Distortion (β)

The distortion is very helpful tool that allows to measure the accuracy of the individual pairs of calculated and measured variables. As can be seen from the equation below, a β close to 1 means the model has a good accuracy. As β becomes greater or smaller than 1 it means that the model has the tendency to over or under predict respectively.

$$\beta = \frac{1}{N} \sum_{i=1}^{N} \frac{x_{c_i}}{x_{m_i}}$$

Eq. 6.11

Brier Skill Score (BSS)

The BSS is a non-dimensional measure of the accuracy of the prediction relative to the accuracy of a base line prediction. It can be used to classify the prediction method objectively as there are tables that categorize models depending on the BSS. A model is said to have an "excellent" predictive capacity when the BSS is between 1 and 0.8 and to have a "bad" when the BSS is between 0 and 0.2. The equation for calculating the Brier Skill Score is presented below:

$$BSS = 1 - \frac{\sum_{i=1}^{N}(x_{c_i} - x_{m_i})^2}{\sum_{i=1}^{N}(x_b - x_{m_i})^2}$$

Eq. 6.12

Where x_b is the baseline prediction which for this study was selected as the average wave transmission coefficient; in this way more extreme categories of predictions are assigned a higher skill score and therefore a measure of the accuracy of extreme events is also obtained.

Willmott Index (d)

The Willmott Index is one more score based measure of the accuracy of prediction models. The philosophy behind it is the same as the BSS. Based on Willmott's research, it was determined that the average-error or deviation measures that are based on absolute values of differences, like the Mean Absolute Error (MAE) and Mean Absolute Deviation (MAD) are, in general, preferable to those based on squared differences, like the Root Mean Squared Error (RMSE) (Willmott and Matsuura 2005, 2006; Willmott *et al.*, 2009). Therefore a different equation is proposed which is less sensitive to the shape of the error-frequency distribution and, as a consequence, to errors concentrated in outliers. The equation reads:

$$d = 1 - \frac{\sum_{i=1}^{N}\left|x_{c_i}-x_{m_i}\right|}{\sum_{i=1}^{N}\left[\left|x_{m_i}-\overline{x_m}\right|\left|x_{c_i}-\overline{x_m}\right|\right]}$$
Eq. 6.12

6.3.1   Overall Performance of Model

The next figures demonstrate the final performance of the model when compared to test data.
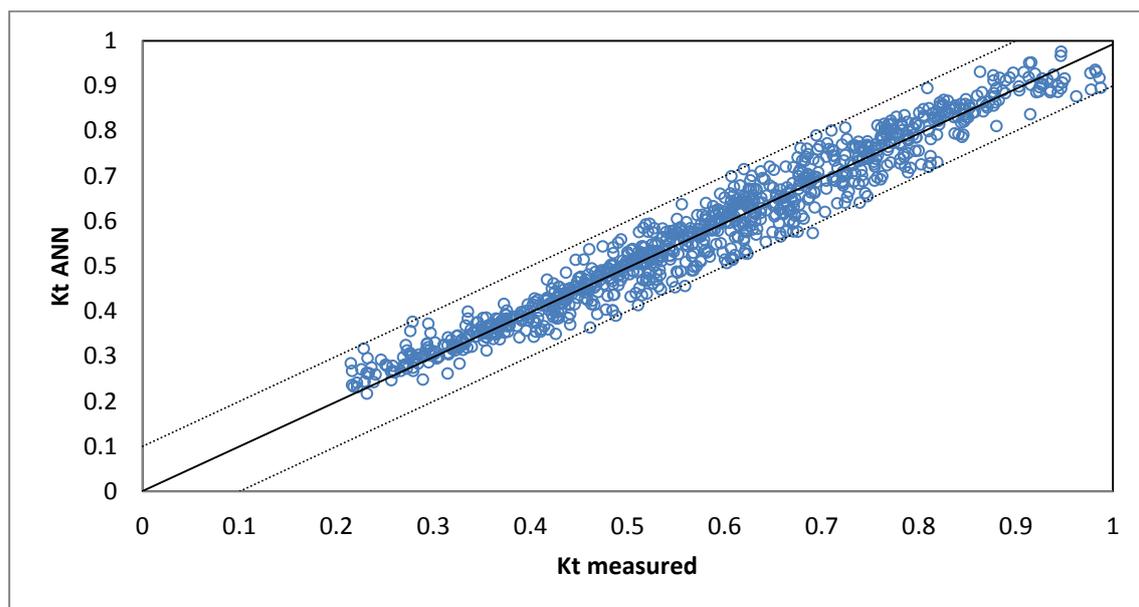
Figure 6.1: Kt ANN versus Kt measured in MIKE21BW modeling, with 90% confidence lines

As can be observed the agreement between predicted values of K_t and the corresponding values obtained during the MIKE 21 BW simulations is very good. Almost all of the data falls within the 90% confidence lines indicating that the model is accurate throughout the entire domain with the exception of a few cases. In order to examine the behavior of the error more closely the classes of the error have also been plotted.
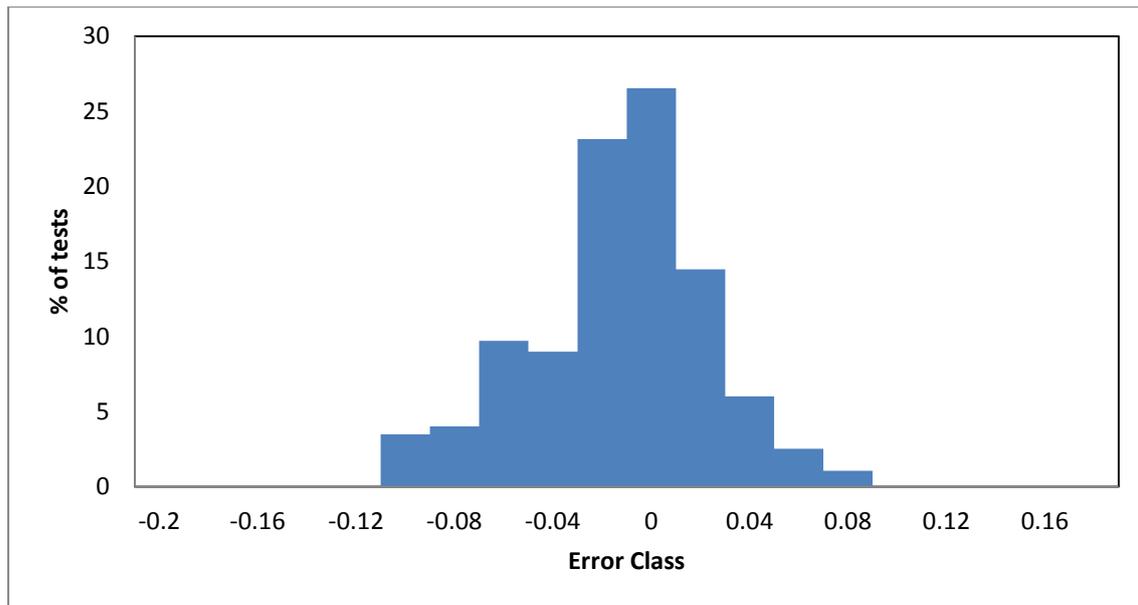
The figure above shows percent of experiments falling within a certain range of error. The behavior of the error follows an almost normal distribution which is slightly skewed towards the positive error values indicating that it has a small tendency to over-predict the wave transmission coefficient. Also the histogram above shows that the spread of error is small as all errors are smaller than 10% and over 90 % of the error is smaller than 0.05. This is an indicator of the very good predicting performance of the model.

The performance of the model was also assessed by calculating several statistical parameters. As the table below reveals the model has an excellent predictive skill based on the brier skill score and Willmott index. In addition the distortion coefficient also shows that the model has a slight tendency to over-predict the wave transmission coefficient. Finally, the RMSE is smaller than 0.05 indicating also a very good accuracy.

Type of Model	RMSE	Correlation (R^2)	Distortion (β)	BSS	Willmott index (d)
Final Model	0.042688	0.984465	1.004628	0.8064	0.756264

Table 6.4: Statistical parameters of final prediction model

It is also of importance to compare the performance of the model to other studies. The next table shows the predictive capacity of several ANN models including the one described in this study.

	Panizzo et al. (2004)	Van Oosten and Peixó (2005)	Ahmadian (2013)	Present Model
Type of Structures treated in model	Mound LCS	Mound LCS	Submerged and impermeable	Submerged and permeable
Type of wave transmission	2D	2D	3D	3D
RMSE	0.04	0.03	0.05	0.04
R^2	0.97	0.99	0.97	0.98

Table 6.5: Comparison of statistical parameters with related studies

Table 6.5 shows that the developed model has a predictive capacity which is better or at least comparable to previous studies, even though the models above do not examine the exact same phenomena.

6.3.2 Sensitivity to Iribarren Number (ξ)

In this paragraph the accuracy of the model when the Iribarren number is excluded is presented.
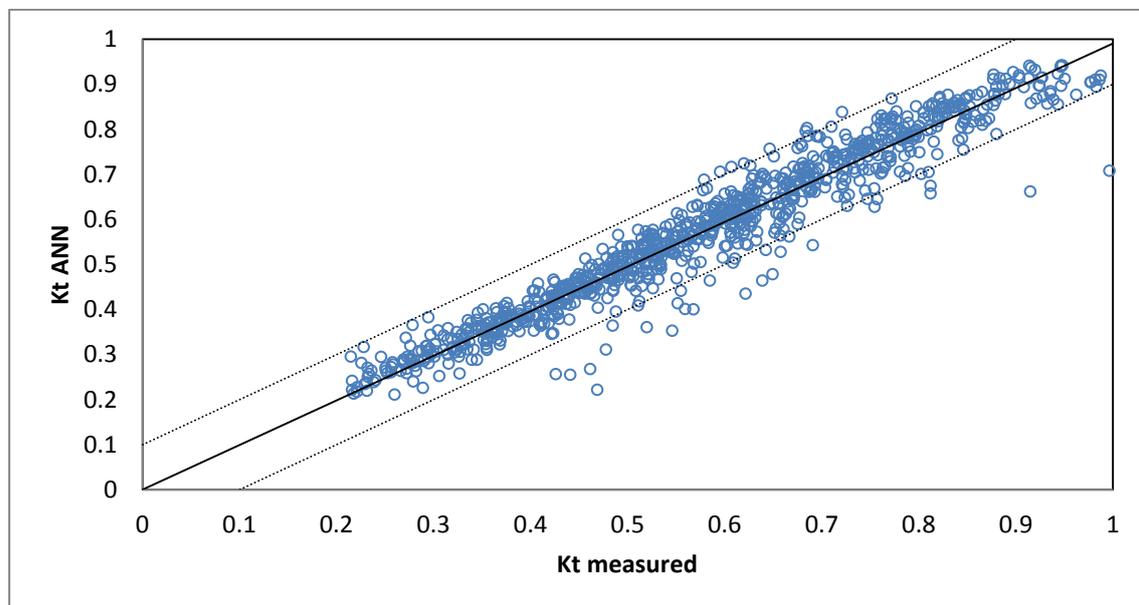

Figure 6.3: Kt ANN versus Kt measured in MIKE21BW modeling, with 90% confidence lines, ksi neglected

Figure 6.3 presents the Q-Q plot of the ANN model when the Iribarren parameter is neglected from the input matrix. As is expected the accuracy of the model decreases

significantly. A significant amount of the predictions values falls outside the 10% confidence limits. Nevertheless, the model does not lose its accuracy for K_t values up to 0.4, after that point a certain degree of under-prediction is observed. The next histogram presents the distribution of error; this will give a sence of the overall accuracy of the model.
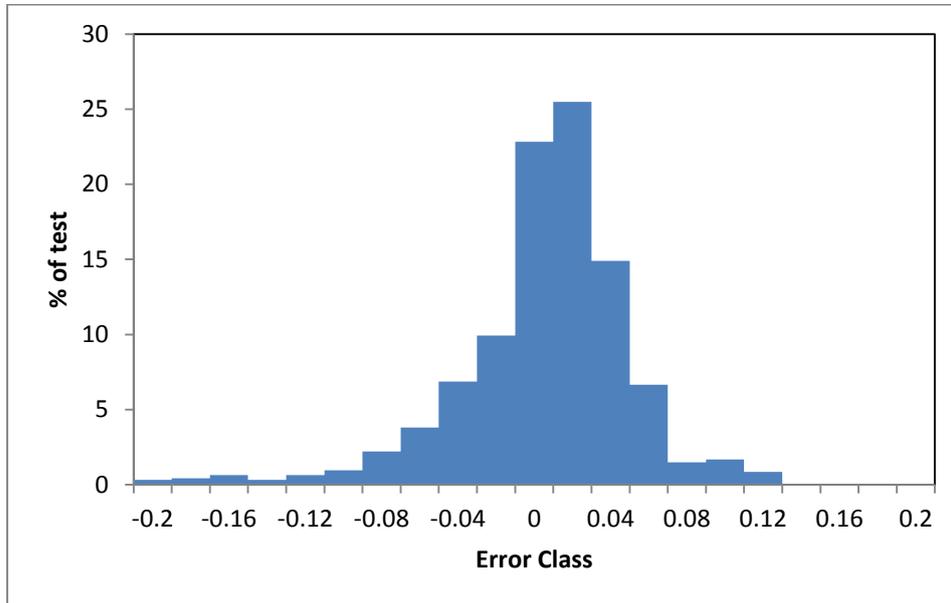

Figure 6.4: Error histogram of complete model, ksi neglected

The error class histogram presented above shows that the data follow an almost lognormal distribution. The left tail of the distribution contains a bigger percentage of the error indicating again the tendency of the model to under-predict the test values. Almost 84 % of the predictions fall within an absolute error of 5%. Finally the table presented bellow shows the evaluation of the model when input parameter ksi is neglected. The most significant finding is that the Brier Skill has fallen to 0.7834 which means that the predictive skill of the model is now "very good", one class lower than the "complete" model. Also a significant increase in the RMSE is also observed, when compared to scenario with all the input parameters.

Type of Model	RMSE	Correlation (R^2)	Distortion (β)	BSS	Willmott index (d)
Final Model	0.082836	0.936177	0.993857	0.7834	0.732456

Table 6.6: Statistical parameters of the ANN model, without ksi

Based on the above it can be concluded that the Iribarren parameter influences significantly the predictive capacity of the model.

### 6.3.3 Sensitivity to submergence ratio hs/Hi
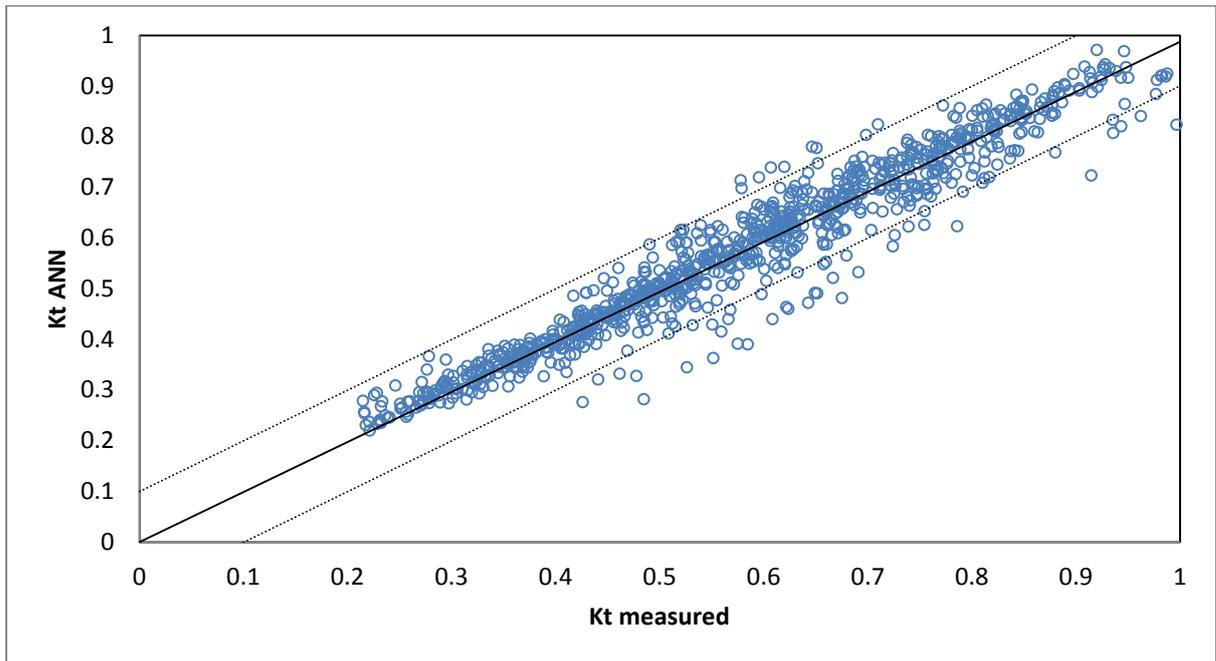
Figure 6.5: Kt ANN versus Kt measured in MIKE21BW modeling, with 90% confidence lines, submergence ratio neglected

The figure above presents the predictive behavior of the model when the submergence ratio is neglected. As can be seen the points lying outside the 10 % confidence lines are increased when compared to the previous scenario (neglected Iribarren number). The model has the tendency to underpredict a few the testing dataset, with the exception of the region with low wave transmission coefficients where the model seems to have much better predictive capacity. Looking into the distribution of the error (figure 6.6) more closely it can be observed that the error tends to follow a lognormal distribution, associated with the large underpredictions mentioned above. To the contrary, when examining the right tail of the error class distribution a higher percentage of errors with low values (<0.1). The percentage of the predictions falling within the 90 % confidence limits is now reduced to 80%, indicating that the discussed factor is of higher relevance.
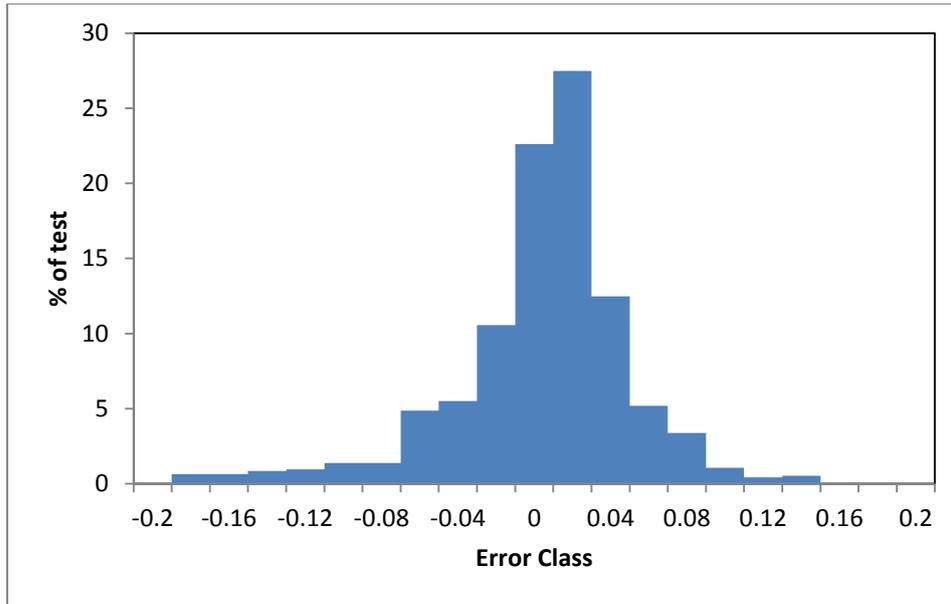
Figure 6.6: Error histogram of complete model, submergence ratio neglected

The table below shows that the submergence ratio has an even greater influence on the accuracy of the model than ξ. The correlation decreases further and the Brier along with Willmott index have an even smaller value indicating, which translates into a worst model performance.

Type of Model	RMSE	Correlation (R^2)	Distortion (β)	BSS	Willmott index (d)
Final Model	0.092024	0.926177	0.994405	0.7801	0.731427

Table 6.7: Statistical parameters of the ANN model, excluding the submergence ratio

Concluding it can be stated that the submergence ratio is an important parameter that describes the wave transmission phenomenon, which also agrees with the literature.

6.3.4 Sensitivity to Hi/h
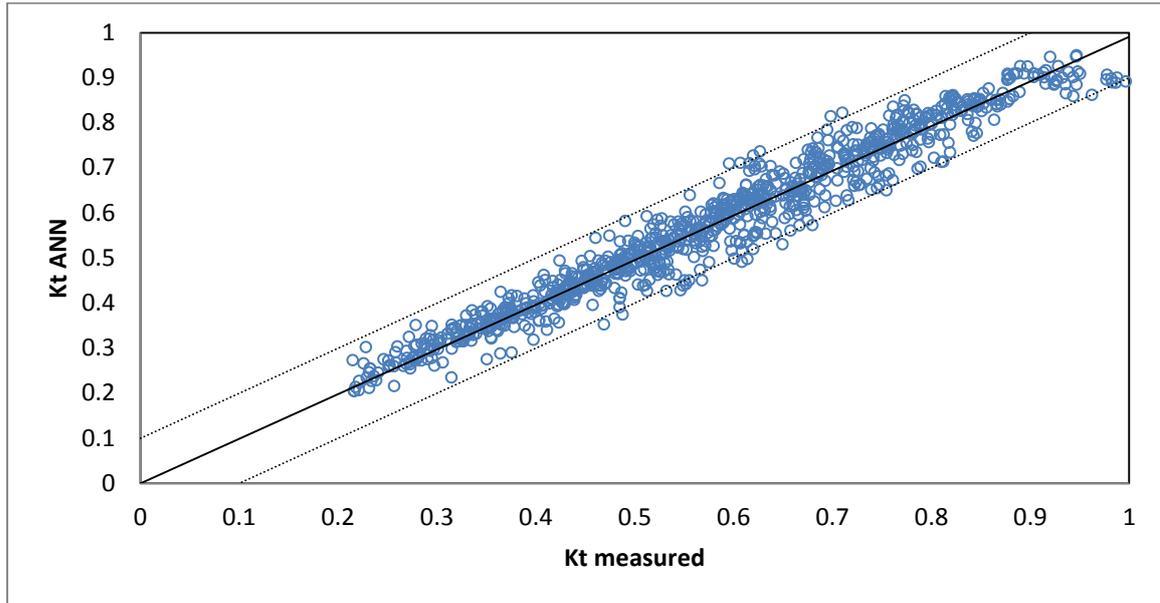
Figure 6.7: Kt ANN versus Kt measured in MIKE21BW modeling, with 90% confidence lines, Hi/h neglected

The Q-Q plot of the scenario where the ratio of the wave height relative to the depth in front of the breakwater reveals its influence is of minor importance compared to the previously examined scenarios. As can be seen in figure 6.7 almost all of the predictions fall within the 10 % confidence intervals. No major discrepancies are observed, based on the error class histogram it can be concluded that in the absence of this input parameters the model tends to slightly overestimate the wave transmission coefficient. This is a result of the slightly skewed normal distribution that the error follows.
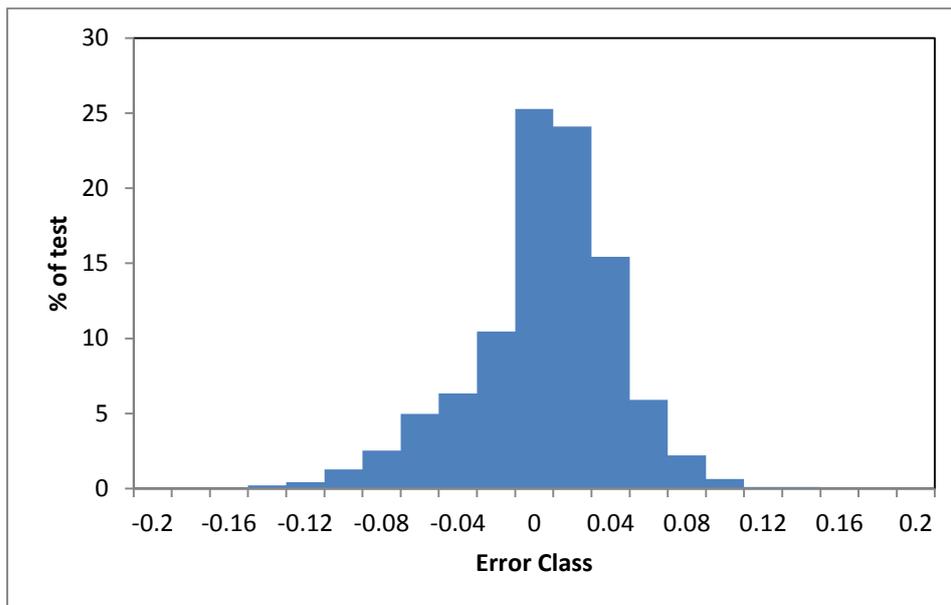
Figure 6.8: Error histogram of complete model, Hi/h neglected

Finally the model statistical parameters presented below show that even though the accuracy of the model has decreased slightly compared to the base scenario (complete model), however the model can still be classified as "excellent", since the BSS value is essentially 0.8.

Type of Model	RMSE	Correlation (R^2)	Distortion (β)	BSS	Willmott index (d)
Final Model	0.054999	0.946138	1.003543	0.7995	0.747522

Table 6.8: Statistical parameters of the ANN model, excluding the submergence ratio

6.3.5 Sensitivity to L0/h

The figures below show the agreement between the predicted wave transmission coefficient and the corresponding measured value. The influence of the wave length relative to the depth in front of the breakwater is big as can be seen in figure 6.9. There is considerable scatter and many predictions fall outside the 10 % confidence interval. There is an obvious tendency of the model to underestimate K_t in some cases.
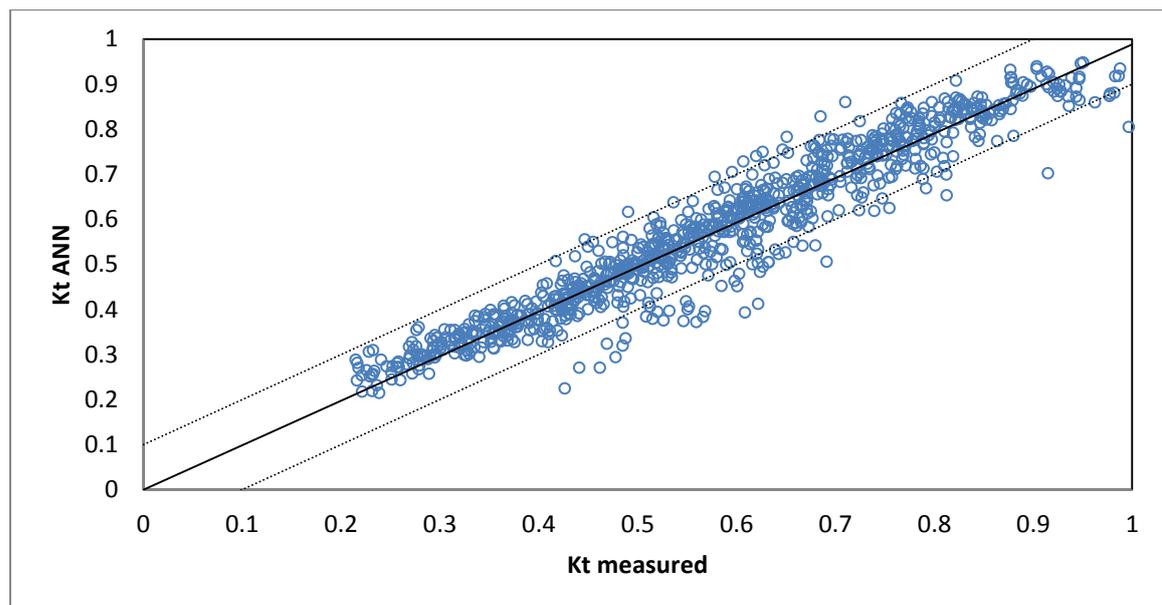

Figure 6.9: Kt ANN versus Kt measured in MIKE21BW modeling, with 90% confidence lines, L0/h neglected

The error histogram shown below demonstrates that the error follows an almost perfect normal distribution, but with a considerable spread. The area of low error (<5%) includes a much smaller percentage compared to the scenarios mentioned above.

Finally table 6.9 shows that the model performs poorly when the effects of the wavelength are not included. The correlation coefficient has relatively small value and the BSS and Willmott index have also decreased indicating a poorer predictive capacity of the model. It also worth mentioning that according to the value of beta the model does not tend to overestimate or underestimate.
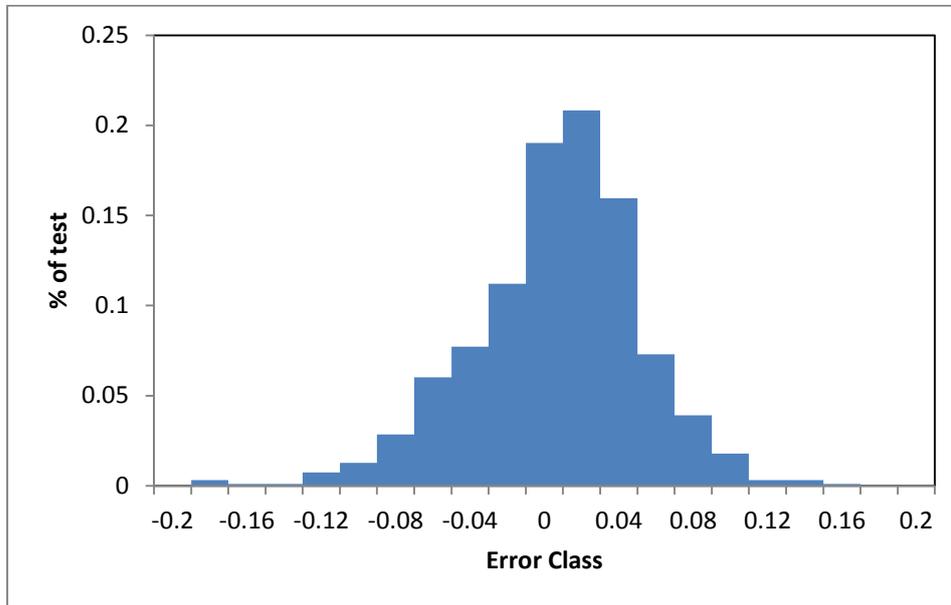
Figure 6.10: Error histogram of complete model, Lo/h neglected

Type of Model	RMSE	Correlation (R^2)	Distortion (β)	BSS	Willmott index (d)
Final Model	0.095313	0.918558	0.99944	0.7795	0.733237

Table 6.9: Statistical parameters of the ANN model, excluding Lo/h ratio

6.3.6 Sensitivity to B/Hi

The figure bellow shows the correlation between the measured and calculated values for the scenario where the ratio of the breakwater width over the wave height is neglected. It can be seen that the model tends to underpredict the wave transmission coefficient in several situations.
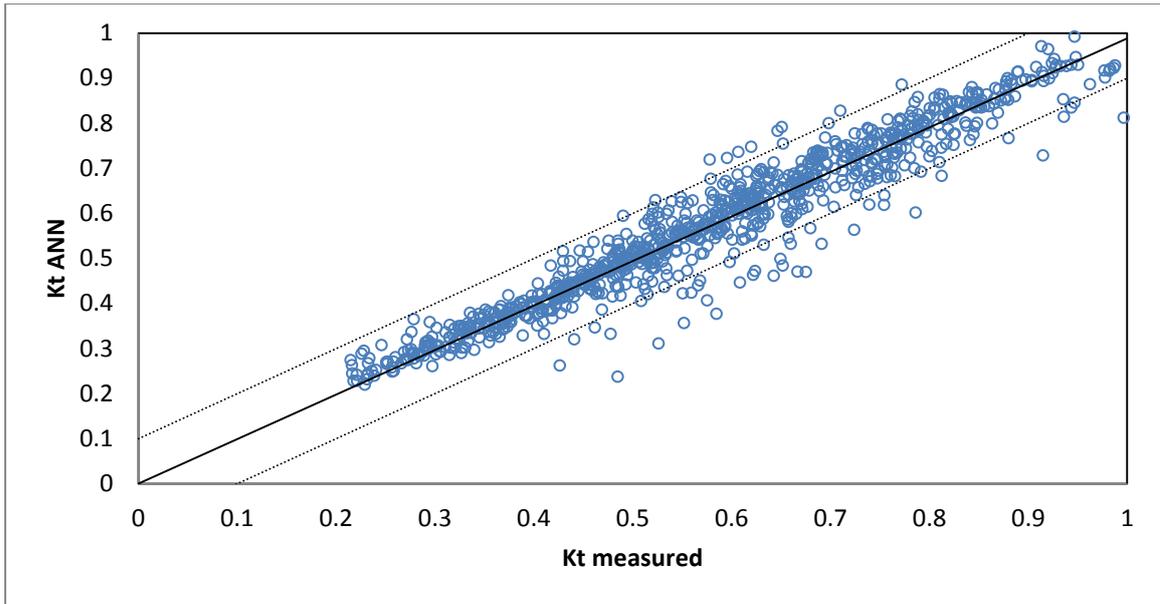
Figure 6.11: Kt ANN versus Kt measured in MIKE21BW modeling, with 90% confidence lines, B/Hi neglected

As was the case for the previous scenarios the histogram of errors follows a slightly skewed normal distribution. In the absence of the relative crest width the model tends to underpredict. There is a tendency of the model to produce a large number of small positive errors (≤ 0.02) and a relatively greater number of large negative errors (≥ 0.06), indicative of the skewness mentioned above.
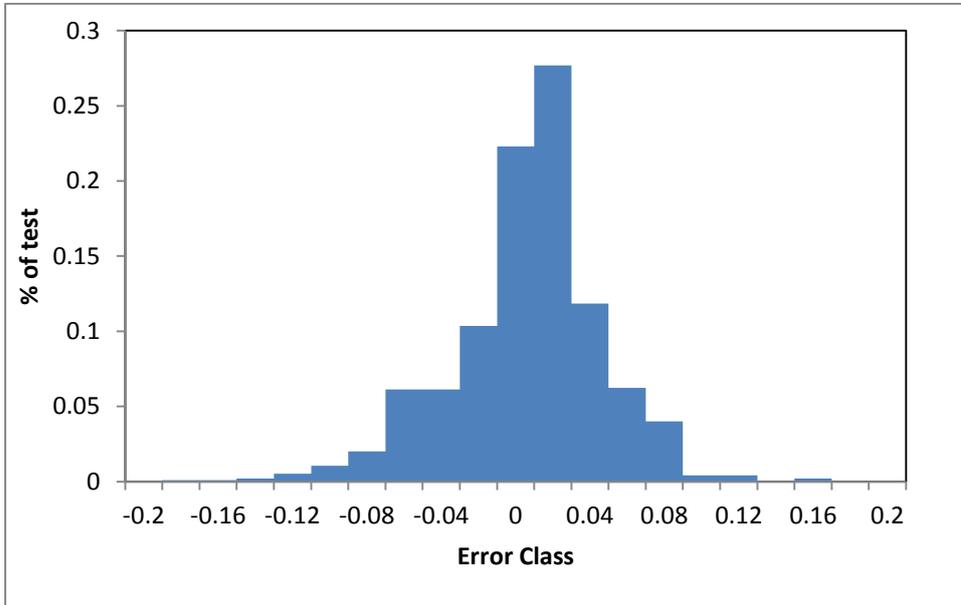
Figure 6.12: Error histogram of complete model, B/Hi neglected

The table below presents the statistical parameters associated with this scenario. It can be concluded that the model where the crest width relative to the wave height is neglected the

accuracy falls. All the parameters in table 6.10 indicate that the model performs worse than the original. Even though the accuracy declines the model still retains a satisfactory level of accuracy.

Type of Model	RMSE	Correlation (R^2)	Distortion (β)	BSS	Willmott index (d)
Final Model	0.057563	0.930512	0.994976	0.7909	0.747411205

Table 6.10: Statistical parameters of the ANN model, excluding B/Hi

6.3.7 Sensitivity to permeability factor

In this section the sensitivity of the permeability factor $\left(\frac{L_0}{\sqrt{B\, D_{n_{50}}}} n \right)$ is examined. The Q-Q plot presented below shows that the correlation between the measured and computed values is very poor. The model has poor performance for the entire range of wave transmission coefficients. Almost half of the predictions fall outside the 90 % confidence lines and most of the results tend to have a positive error.

By examining closely the error histogram of figure 6.14 it can be observed that the error has the tendency to follow a bimodal distribution with two error peaks. This explains the large scatter in the data of figure 9. The larger peak is located near the error value of 0.10 and a smaller peak near -0.08, this is an indicator of the strong overestimating tendency of the model when this parameter is neglected.
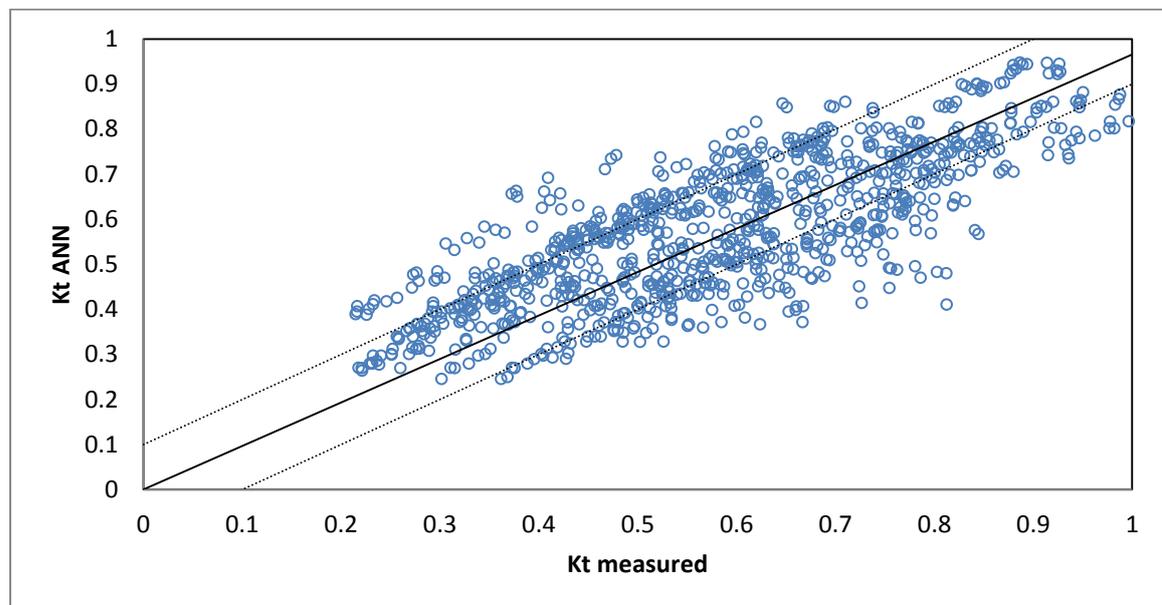

Figure 6.13: Kt ANN versus Kt measured in MIKE21BW modeling, with 90% confidence lines, permeability input parameter neglected
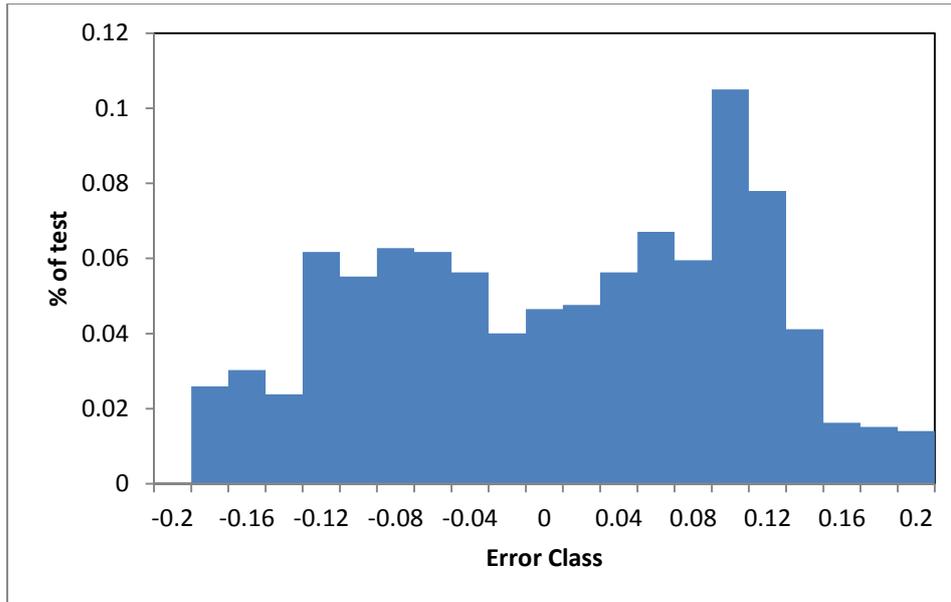
Figure 6.14: Error histogram of complete model, permeability coefficient neglected

The following table verifies the points above in a more qualitative manner. The quality of the model's output is relatively poor as the RMSE is five times greater than the original model. The BSS and d is very low but still in the performance range of "very good". Finally the distortion coefficient shows that the model has the overall tendency to over predict the wave transmission coefficient.

Type of Model	RMSE	Correlation (R^2)	Distortion (β)	BSS	Willmott index (d)
Final Model	0.228869	0.606401	1.028686	0.7617	0.717411205

Table 6.11: Statistical parameters of the ANN model, excluding permeability factor

6.3.8 Sensitivity to theta

Theta is the parameter determining the angle of the estimation point relative to the center of the breakwater head. The next figure demonstrates the importance of this parameter to the overall performance of the model. In the absence of this parameter the model tends to underestimate the wave transmission coefficient, which is a natural consequence as the spatial variation of the wave height and therefore the influence of diffraction cannot be successfully modeled. Nevertheless the most of the points below fall within the 10 % confidence interval.
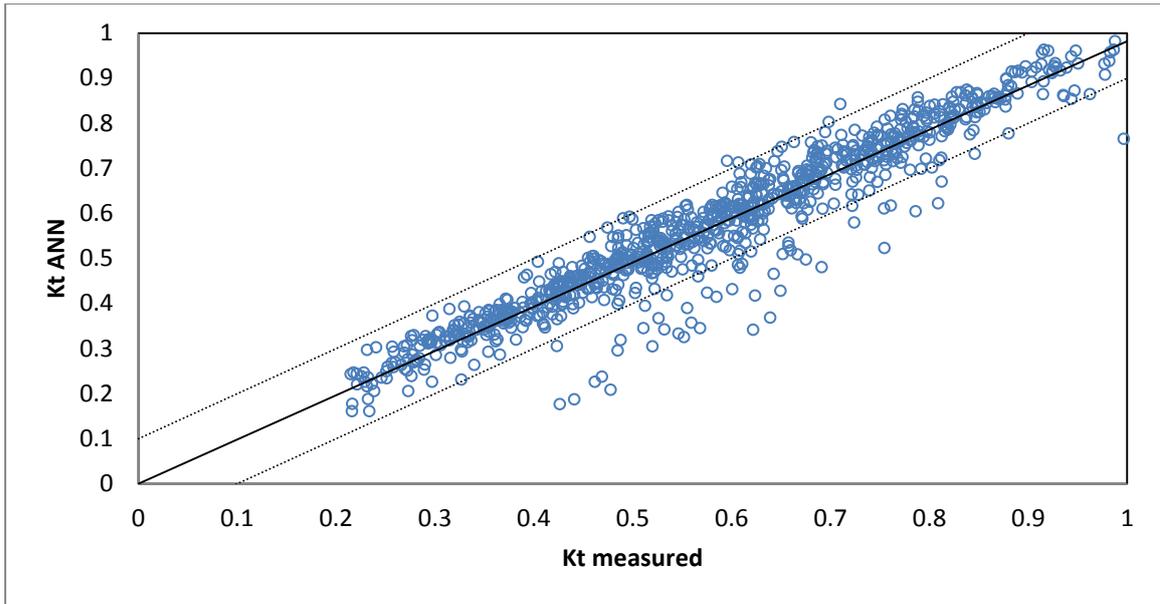
Figure 6.15: Kt ANN versus Kt measured in MIKE21BW modeling, with 90% confidence lines, theta neglected

Figure 6.16 shows the distribution of errors classes. The most impart finding is that it follows an almost normal distribution. The few large negative errors are "compensated" by a large number of small positive errors, for this reason the model does not over or underpredict the wave transmission coefficient.

Based on table 6.12 the model has a relatively poor performance. The RMSE large and the correlation factor is almost 10 % smaller than the originals model's. Also based on Willmott's and Brier indices the performance drops to a lower performance class. It can therefore be concluded that the influence of this parameter is of significance for the purpose 3D wave transmission.
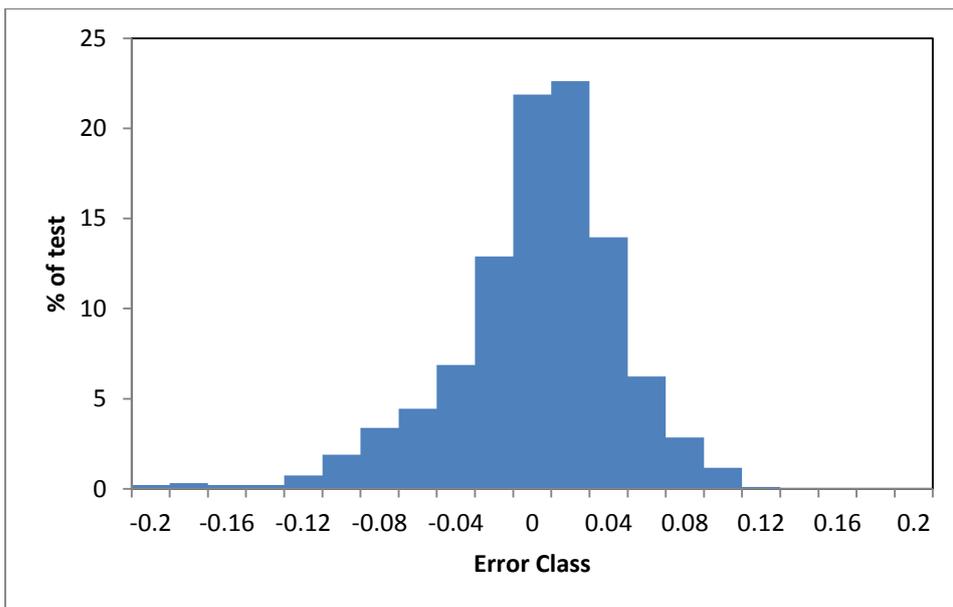
Figure 6.16: Error histogram of complete model, permeability coefficient neglected

Type of Model	RMSE	Correlation (R^2)	Distortion (β)	BSS	Willmott index (d)
Final Model	0.101036	0.902666	0.984757	0.7871	0.740341

Table 6.12: Statistical parameters of the ANN model, excluding theta

6.3.9 Sensitivity to r/L0

This is the second dimensionless parameter responsible for determining the spatial variation of the wave transmission coefficient. As can be seen from the figure below (Figure 6.17) by omitting this input parameter the quality of the model worsens. Also significant scatter is observed for K_t smaller than 0.9, for higher values of K_t it seems that the dimensionless distance from the breakwater head is of minor importance as these predictions retain their accuracy.

Figure 6.18 shows that the error classes follow a normal distribution indicating that the mean prediction values of the model coincide with mean values of the test database. The wide distribution of the error results from the large number of predictions with high error, which practically means that the model in the absence of this parameter tends to produce a larger error.

The above are also confirmed by the statistical parameters listed in table 6.13. The correlation between the predicted and measured values is the lowest after the one found in chapter 6.3.7 indicating the importance of this factor to the overall performance of the model. Finally the BSS, d is also smaller when compared to the other scenarios indicating again the significance of this factor.
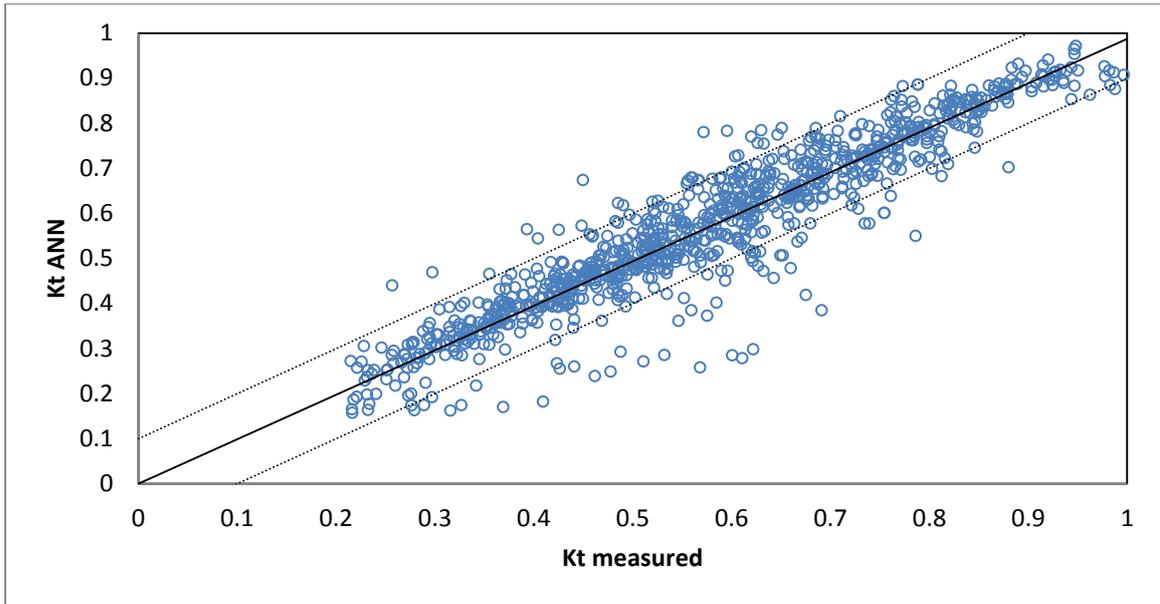
Figure 6.17: Kt ANN versus Kt measured in MIKE21BW modeling, with 90% confidence lines, r/Lo neglected
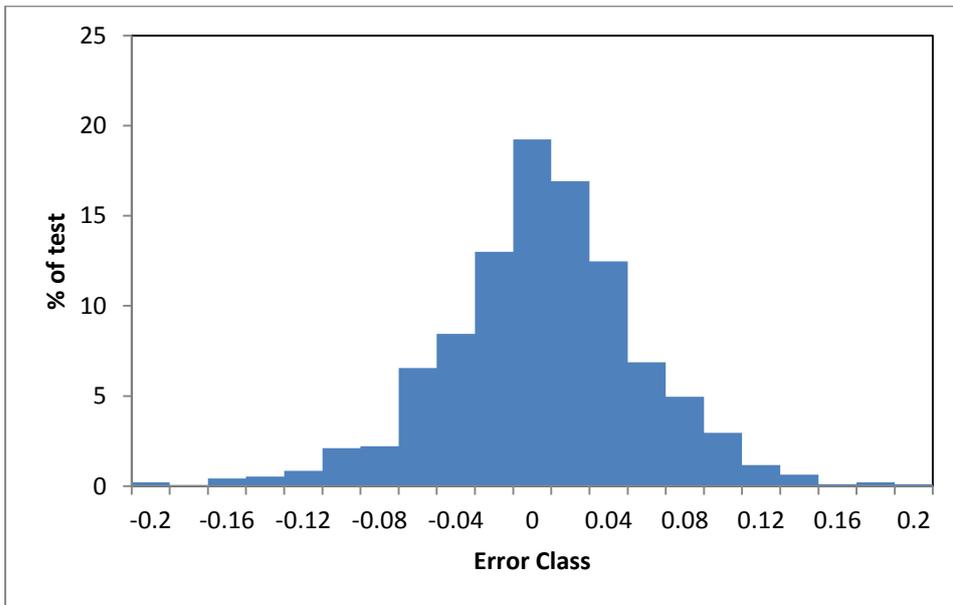
Figure 6.18: Error histogram of complete model, r/Lo neglected

Type of Model	RMSE	Correlation (R^2)	Distortion (β)	BSS	Willmott index (d)
Final Model	0.12585	0.87982	0.9999	0.7781	0.73634

Table 6.13: Statistical parameters of the ANN model, excluding r/Lo

6.3.10 Summary of Sensitivity Analysis

After the performance of the final ANN model was presented a sensitivity analysis of the influence of the input parameters was performed, where one by one each input parameters was neglected. The results of this analysis show:

- The most influential structural input parameter is the permeability factor, which also includes information about the forcing (i.e. wave length).

- From the two parameters designed for determining the spatial distribution of the wave height the most effective parameter is the relative distance to the wave length (r/Lo).

- The ratio of Hi/h is the least influential of all the parameters.

- The incorporation of the parameters describing the spatial distribution of the wave transmission parameter is very important for the performance of the model.

- The model has a small tendency to overpredict K_t.

- The distribution of the error in all the formentioned scenarios is normal or slightly skewed. This is a good indicator of the performance of the model as neither over or under prediction is expected.

6.4 Validity of the ANN model

Based on the previous chapter it has been determined that the model performs the best when all 9 of the input parameters are included in the models architecture. The validation of the model will be performed in two steps. First the model will be validated against a range of different conditions using the prediction method proposed by Vicinanza (2009), and following that the boundaries at which the model is reliable will be presented.

6.4.1 Validation against empirical prediction method

For the purpose of this validation process the global wave transmission formula of Vicinanza will be applied using the 2D wave transmission formula of Goda and Ahrens (2010) and the diffraction theory developed by Penny and Price (1952) using the approximation of McCornmick and Kreamer (2001).

The validity of the ANN model is assessed by plotting the predicted value of the ANN model in the same graph with the prediction of the empirical method of Vicinanza, for three different locations behind the breakwater. It is of great importance to assure the quality of the data. For this reason the variation of the wave transmission coefficient with respect to four most important structural dimensionless parameters will be presented.

6.4.1.1 Validation of model with respect to ksi (ξ)

This section provides an analysis at which the predictions of the ANN model are compared against the empirical method presented earlier. In this figure below the prediction of the ANN (solid line) and empirical formulation (dots) is plotted for varying Iribarren number. The next plots have been produced based on the assumption that the wave period and the breakwater slope are constant at 1s and 45° respectively.

The figure below shows that both predictions follow the same trend. The wave transmission coefficient increases with increasing ksi for the two locations closest to the breakwater head. An interesting finding is that K_t decreases after ξ>6 for the location deepest into the shadow zone. This may be a result of the negligible contribution of diffraction at that point in combination with the increased wave reflection associated with high Iribarren numbers, which reduces the amount of energy passing through and over the breakwater. The absolute error between the two methods is smaller than 10% in all cases which indicated a good agreement. Also it is noticeable that the ANN follows the same trend as the empirical formulation even in the third location which deviates from the response of the two first locations; this is a good indicator of the performance of the model.
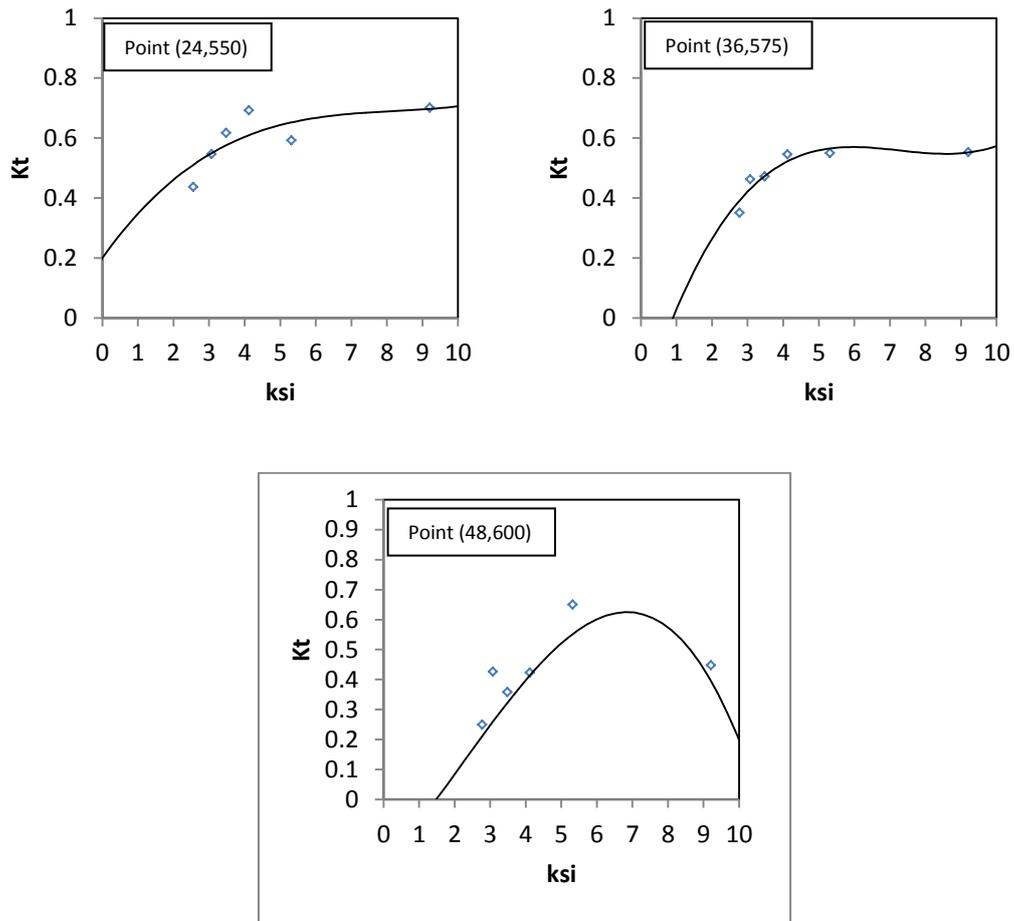
Figure 6.19: Spatial wave transmission of wave transmission coefficient Vs ksi at different locations: Predicted values using Vicinanza (dots), predicted values by ANN (solid line)

6.4.1.2   *Validation of model with respect to relative submergence ratio*

As in the previous paragraph the spatial variation of the wave transmission coefficient in three different locations is presented. The variation of K_t with respect to the relative submergence ratio $\left(\frac{h_s}{H_i}\right)$ is illustrated in the figure below. In the first two locations graphs indicate an upward trend as the relative submergence ration increases. Examining the location furthest into the shadow zone it is observed that K_t decreases after $\frac{h_s}{H_i} = 3$.

It is noticeable that the ANN model follows the general trend indicated by the dots (empirical method) which means that the ANN model can simulate successfully the overall trend with respect to $\frac{h_s}{H_i}$. In addition the absolute error in all location is always smaller than 0.1 indicating that the model has a good predictive capacity. It should be noted that the quality of the predictions are poorer than in the previous paragraph, despite this the ANN is still reliable.
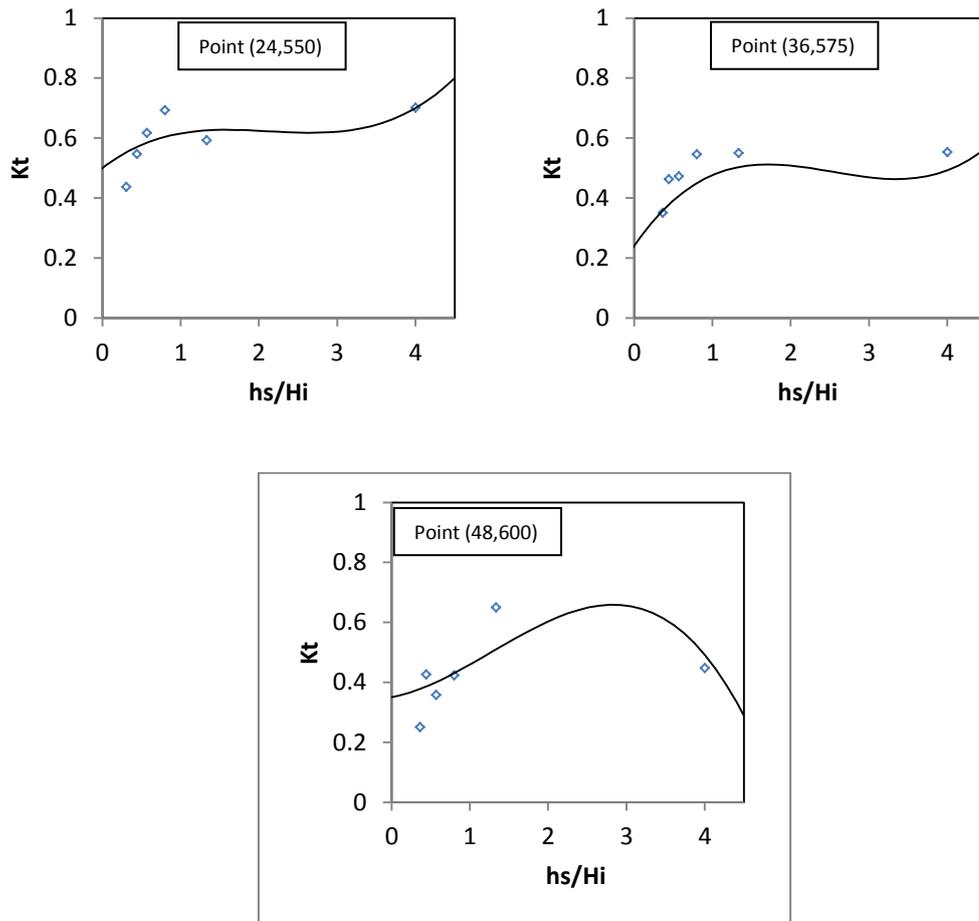
Figure 6.20: Spatial wave transmission of wave transmission coefficient Vs relative submergence depth at different locations: Predicted values using Vicinanza (dots), predicted values by ANN (solid line)

6.4.1.3 Validation of model with respect to $\frac{L_0}{h}$

The same analysis as in the last two paragraphs is presented but in this case the dimensionless parameter examined is the ratio of the wave length to the depth in front of the structure. Based on the both the methods presented in the graphs below the wave transmission coefficient follows a weak sinusoidal trend for varying $\frac{L_0}{h}$. The maximum K_t decreases slightly as the point under consideration shifts deeper into the shadow zone, as the effects of diffraction become less important.

For location (24,550) the offset of the ANN trend line with respect to the empirical method is significant especially for large wave lengths. In the other two locations an apparent lag of the ANN trend line with respect to the empirical predictions can be observed. With the exception of the extreme values in the first location all the predictions of the ANN model have an absolute error smaller than equal to 10 %. Based on the above the model has a very good predictive capability and is its results agree to a satisfactory degree with the empirical formulation of Vicinanza et al. (2008).
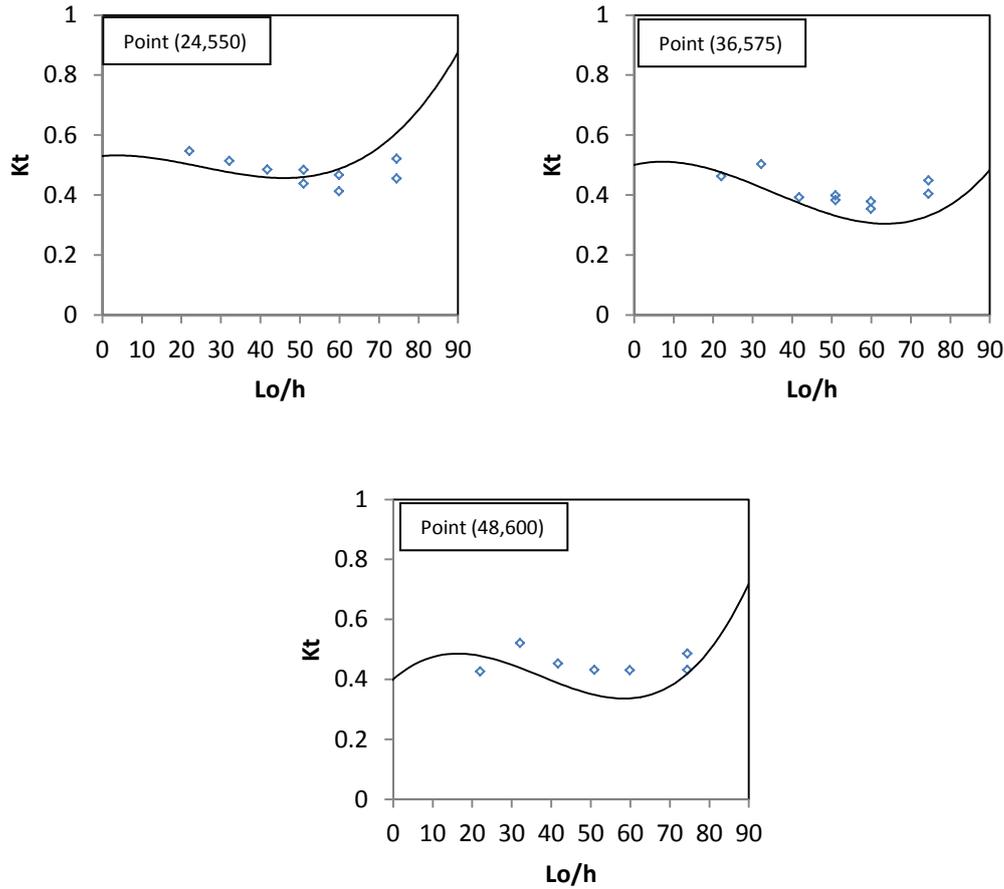
Figure 6.21: Spatial wave transmission of wave transmission coefficient Vs $\frac{L_0}{h}$ at different locations: Predicted values using Vicinanza (dots), predicted values by ANN (solid line)

6.4.1.4 Validation of model with respect to permeability factor $\left(\frac{L_0}{\sqrt{B \, D_{n_{50}}}} n \right)$

The final parameter examined in this section is the permeability factor $\left(\frac{L_0}{\sqrt{B \, D_{n_{50}}}} n \right)$.

According to the ANN sensitivity analysis and the information obtained from the DELOS database (see appendix C) the correlation between this parameter and the wave transmission coefficient is very strong. The ability of the ANN model to produce accurate predictions of K_t with respect to this factor is therefore essential in order to assure that the quality of the model's predictions is satisfactory. Figure 6.22 presents the variation of the wave transmission coefficient with respect to examined parameter for 3 different locations behind the breakwater. The figures include the predictions of the ANN mode and the empirical method. Based on the two first figures it can be observed that K_t decreases for an increasing permeability factor, and reaches a minimum of 0.4. To the contrary the wave transmission coefficient seems to be independent of $\frac{L_0}{\sqrt{B \, D_{n_{50}}}} n$ at the location deepest into the shadow zone, which seems reasonable as the effects of diffraction at that location are of minor importance there. With respect to the accuracy of the model, the scatter between the ANN and the empirical prediction is very small. All points fall within the 10 % error band and

both models follow the same trends. The above are very good indicators of the quality of the model and therefore it can be deducted that the ANN shows a sufficient degree of accuracy.
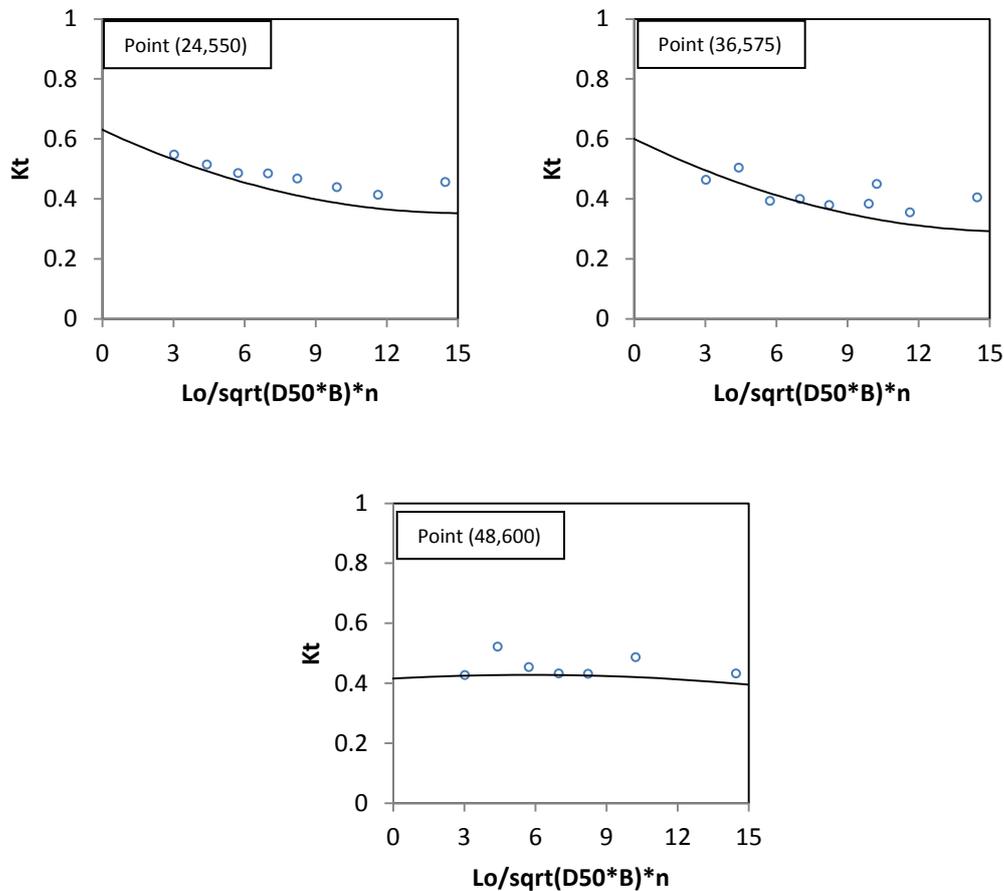
Figure 6.22: Spatial wave transmission of wave transmission coefficient Vs porosity factor at different locations: Predicted values using Vicinanza (dots), predicted values by ANN (solid line)

6.4.1.5   *Summary and Conclusion of the Validation Process*

Based on the finding of the analysis above it can be concluded that over the overall performance of the model compares very well with empirical formulation of Vicinanza et al. (2009). The final ANN model predicts with sufficient accuracy (absolute error ≤ 0.1) the wave transmission coefficient in the entire area behind the breakwater. The model is able to follow the trends of the most influential non- dimensional parameters with sufficient accuracy. In addition to the above figure 6.23 shows the Q-Q plots of the predicted ANN and empirical model for a three different cross-sections behind the breakwater. As table 6.14 illustrates the final model has a good predictive capacity. It performs very well in the regions furthest from the breakwater and its reliability decreases for points closer to the breakwater.

Dataset/Location	550	575	600	Total
Correlation	0.66	0.85	0.94	0.82

Table 6.14: Correlation between the ANN and empirical model predictions
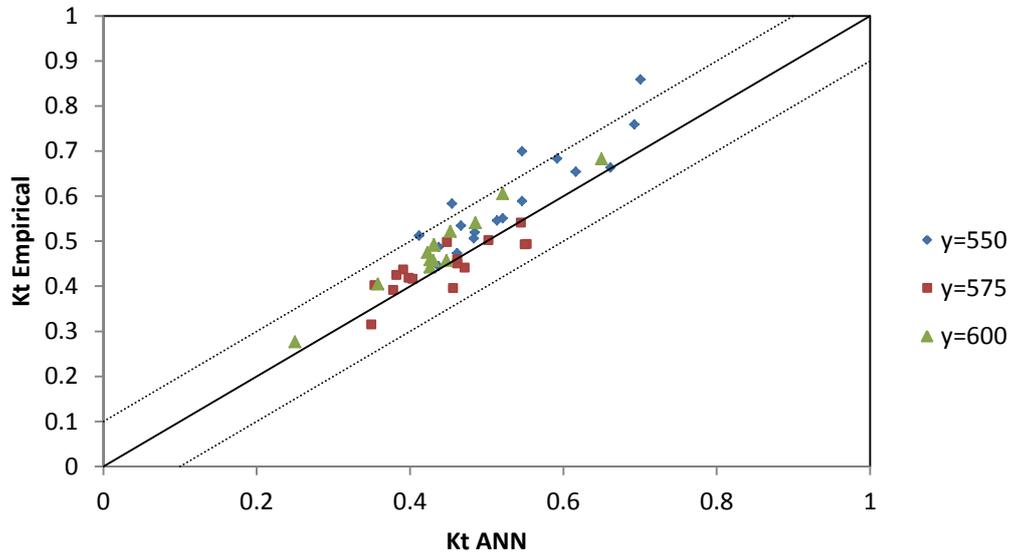
Figure 6.23: Correlation between the ANN and empirical model prediction, for three different cross sections behind the breakwater

Keeping in mind that the method used for comparison accumulates both the error of the 2D wave transmission coefficient and that of the diffraction coefficient it can be concluded that the model is good for predicting the wave climate behind breakwater. The comparisons show that the

6.4.2   Boundaries of the ANN model

In this section the boundaries of the model are determined on the basis of two notions:

- Physical boundaries, the boundaries of each dimensionless parameter depend on the individual physical boundaries of the parameters comprising them.

- High accuracy bands, this are the boundaries at which the model performs accurately. These bands are determined on the basis of a sensitivity analysis. The sensitivity figures presented in the following paragraphs show the 95 % confidence interval along with the mean value of the ANN prediction.

The final validity boundaries of the input parameters will be defined as a subset of the above two ranges. This section will discuss the process followed in order to determine the validity range for each input parameter.

6.4.2.1   *Iribarren Parameter*

The Iribarren number describes the steepness of the wave relative to slope of the structure. It is well known that the maximum wave steepness a have could have is 0.07, the minimum wave steepness could be 0. **B**ased on hypothesis that the slope of the structure is 45° the minimum and maximum ξ that can be obtained is 1.8 and ∞ theoretically.

The figure below shows the results of the sensitivity analysis. According to this the model retains a high level of confidence between ξ ∈ [2, 6] therefore this should be the input range of this parameter in the ANN model
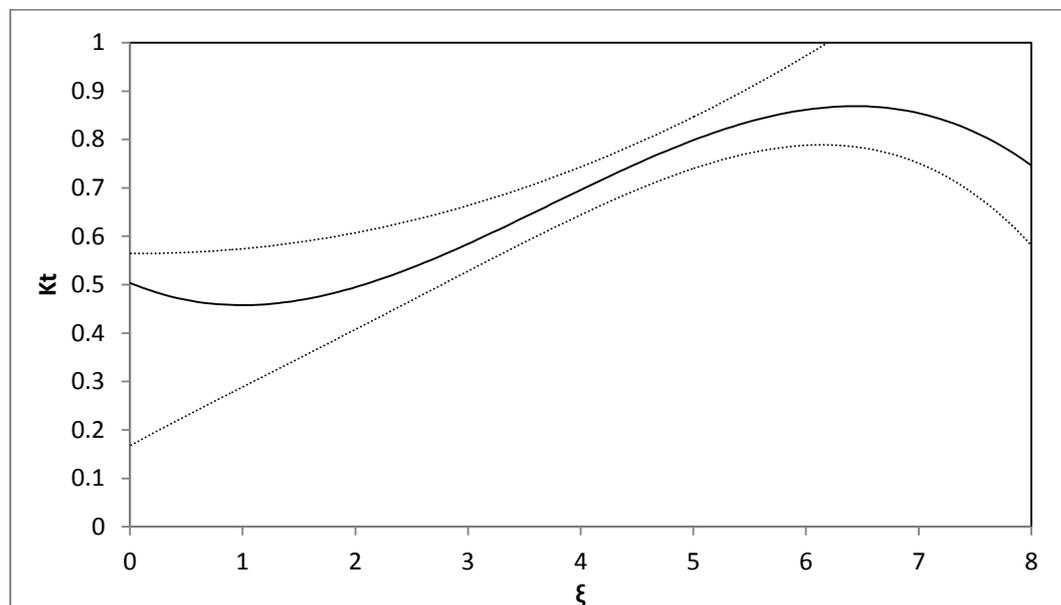

Figure 6.24: Sensitivity analysis of ξ: dotted lines (2.5 and 97.5 % quantile), solid line (ANN mean prediction)

6.4.2.2   *Relative Submergence Depth*

The ratio of $\frac{h_s}{H_i}$ has no physical boundary as can be understood. The only limitation that could
be imposed is the limitation of the incoming wave height due to the depth foreshore of the
structure. One more limitation that is imposed on this ratio is that is should always be
greater than zero, a submergence depth of zero will result in a loss of the information
contained within it. With respect to the accuracy limits determined by the sensitivity
analysis, figure 6.25 shows that model yields reliable results in the range of values between
[1, 3]. Therefore all inputs of $\frac{h_s}{H_i}$ should fall within the limits of [1, 3].
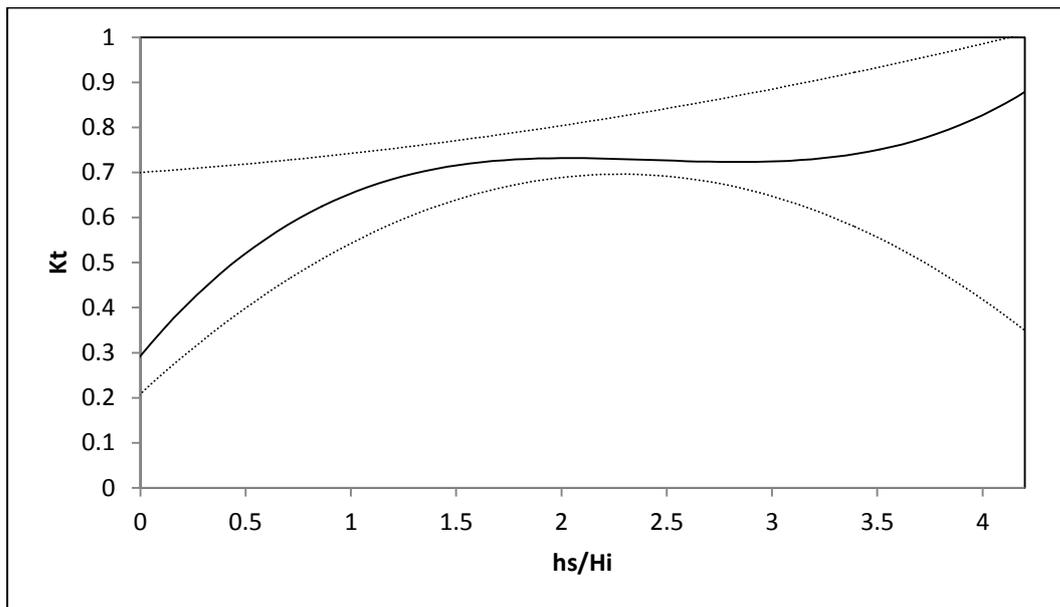
Figure 6.25: Sensitivity analysis of submergence ratio: dotted lines (2.5 and 97.5 % quantile), solid line (ANN
mean prediction)

6.4.2.3   *6.4.2.3 Incoming wave height over foreshore depth*

With respect to the physical boundaries of the $\frac{H_i}{h}$ the lower bound should be greater than 0
and the upper limit should be smaller than 0.8 (Longuet-Higgins and Stewart, 1964). In
addition to this the sensitivity analysis conducted for this parameter (see figure 6.26)
showed that in the ANN model K_t decreases with an increasing $\frac{H_i}{h}$ which is reasonable since
the wave come closer to the breaking limit. The same analysis revealed that the range of
high reliability for this parameter is [0.2, 0.75]. By combining the two findings it is proposed
that the model should be used within the range of [0.2, 0.75]
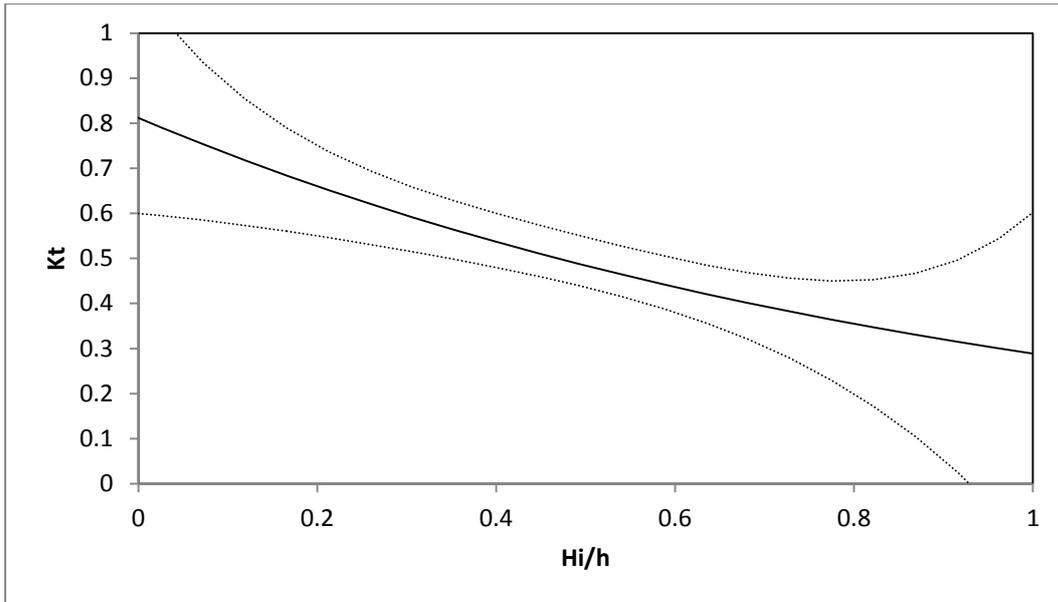
Figure 6.26: Sensitivity analysis of incoming wave height over foreshore depth: dotted lines (2.5 and 97.5 % quantile), solid line (ANN mean prediction)

6.4.2.4   *6.4.2.4 Incoming wave length over foreshore depth*

This parameter has no physical boundaries; both the wave length and submergence ratio can take any positive value. The figure below shows that the wave transmission coefficient grows with increasing $\frac{L_0}{h}$. This is an expected outcome as longer waves force more energy to pass through the breakwater. The sensitivity analysis yields the discussed parameter has a large condfidence band extending from 2.5 to 13.5. From the above it is concluded that input range for this parameter should be [1.5, 13.5].
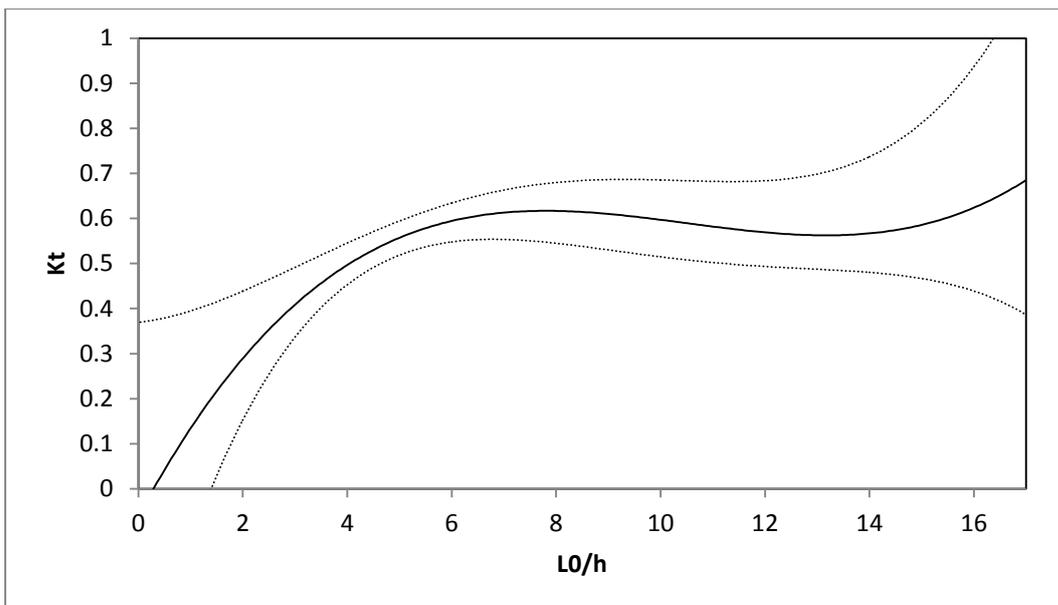

Figure 6.27: Sensitivity analysis of incoming wave height over foreshore depth: dotted lines (2.5 and 97.5 % quantile), solid line (ANN mean prediction)

6.4.2.5   6.4.2.5 Incoming wave height over breakwater width

This ratio again does not have any physical boundaries. The only limitation that is implied is that it should be greater than zero, as was the case in paragraph 6.4.2.3 a ratio of zero value would lose all the information associated with the parameter and would be useless for ANN training and testing. It should be mentioned that very small values of $\frac{B}{H_i}$ are possible, these variables are associated with very small crest widths of deforming breakwaters. In addition to the above the sensitivity analysis reveals that the wave transmission coefficient decreases for an increasing relative breakwater width, which agrees with the literature. The range of 95 % confidence lies between $0.075 \leq \frac{B}{H_i} \leq 0.375$. From the previous finding it is concluded that the optimum results for the model would be obtained for inputs in the range of [0.075, 0.375].
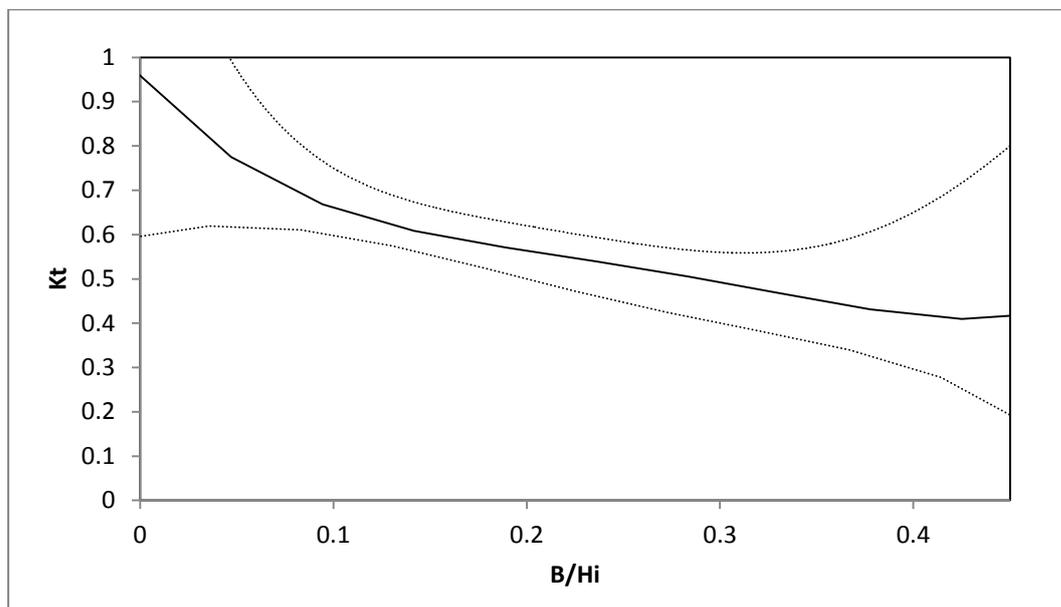
Figure 6.28: Sensitivity analysis of relative breakwater width: dotted lines (2.5 and 97.5 % quantile), solid line (ANN mean prediction)

6.4.2.6   Permeability factor

The permeability factor is defined as $\frac{L_0}{\sqrt{D_{n_{50}} B}} n$. It represents the influence of the wave permeability on the wave transmission process by incorporating the all the variables influencing seepage. The only limitations applied to the physical boundaries are that the porosity (n), nominal stone diameter and crest width should never be zero. A porosity and stone diameter of zero correspond to impermeable structures which are outside the scope of the study and are not covered in the model; also the parameters comprising the denominator of this ratio should be greater than zero in order to avoid the factor going to infinity. Figure 19 reveals that for increasing permeability factor K_t increases, which is reasonable as the less distance the wave travels through the breakwater the less energy is dissipated and therefore more energy is passed over to the lee side of the breakwater. Based on the figure below the model performs well for permeability factors between [6, 35] which is also the final boundary conditions of this model with respect to this parameter.
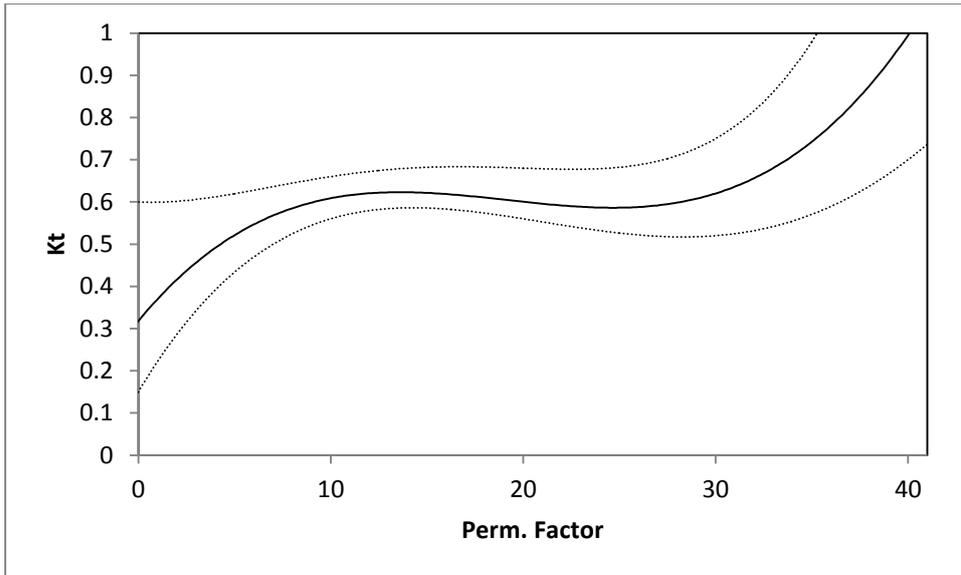
Figure 6.29: Sensitivity analysis of permeability factor: dotted lines (2.5 and 97.5 % quantile), solid line (ANN mean prediction)

6.4.2.7 *Angle between breakwater and prediction point*

The polar angel can take any value from 0° to 360°. For the purpose of this report focus has been given only to the shadow zone behind the breakwater because it the only area where both diffraction and wave transmission exist. The sensitivity analysis presented below shows that the wave transmission coefficient tends to increase as the polar angle increases, this is a reasonable trend since by increasing the angle the point shifts toward the breakwater head where the influence of diffraction is the greatest. From the figure presented below the model has good level of confidence for θ that fall in the interval of [44, 84], this is the final boundary condition of this input parameter.
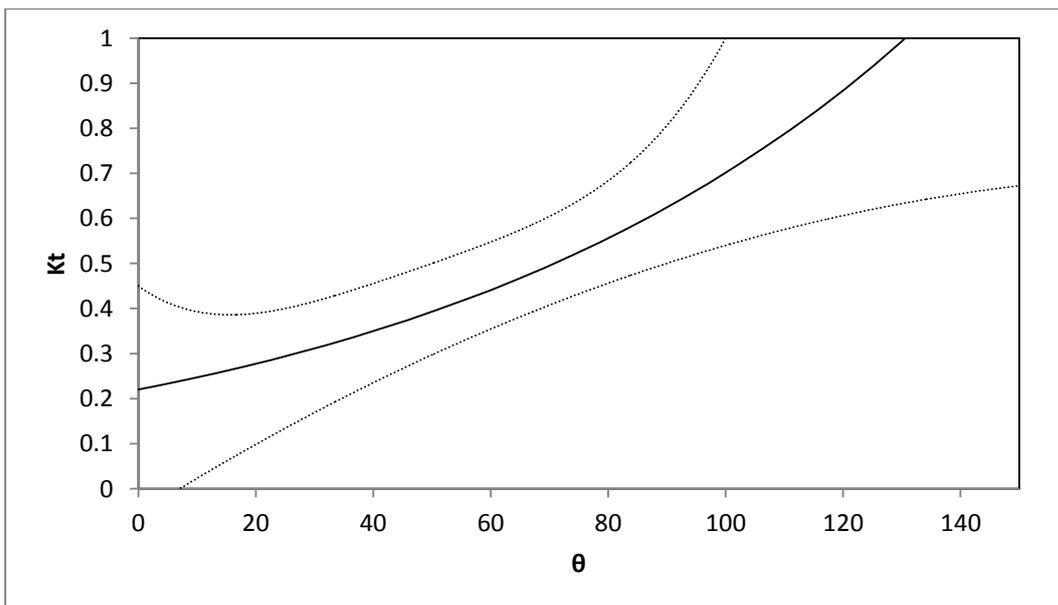
Figure 6.30: Sensitivity analysis of polar coordinate angle: dotted lines (2.5 and 97.5 % quantile), solid line (ANN mean prediction)

113

6.4.2.8   *Relative polar distance*

The relative polar distance is defined as $\frac{r}{L_0}$ gives the absolute distance of the considered point from the breakwater head relative to the incoming wave length. The mean trend line of the ANN mode is constant up until $\frac{r}{L_0} = 0.8$ and then decreases as the ratio increases further. This pattern is logical, as the smaller the ration the closer the point is to the breakwater where higher wave heights are expected. In addition to the above the figure 6.31 shows that the input value of the specific variable should be in the range of [0, 1.1] in order to have reliable outputs.
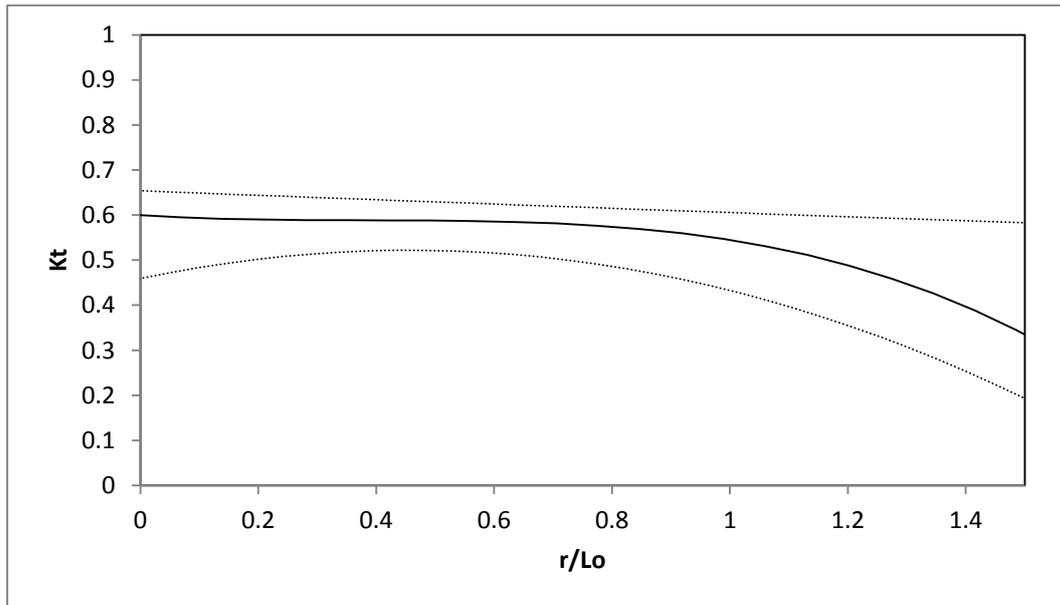

Figure 6.31: Sensitivity analysis of relative polar distance: dotted lines (2.5 and 97.5 % quantile), solid line (ANN mean prediction)

6.4.2.9   Summary of confidence limit analysis

Based on the findings presented in this section the ANN model that has been developed in this study shows very good results. In addition the mean trend of the ANN model has the tendency to follow the same pattern as simple wave-structure dynamics imply which is an encouraging fact. The sensitivity analysis shows that the model can produce more accurate results for a wide range of input parameters. Concluding the ANN can be characterized as a robust and accurate predicting tool for the spatial predictions of the wave transmission coefficient. The summary of the results obtained in the section are presented below:

Input Parameter	Confidence Boundaries
Iribarren Number (ξ)	[2, 6]
Relative Submergence Ratio $\left(\dfrac{h_s}{H_i}\right)$	[1, 3]
Relative Foreshore depth $\left(\dfrac{H_i}{h}\right)$	[0.2, 0.75]
Incoming Wave Length to Foreshore Depth $\left(\dfrac{L_0}{h}\right)$	[1.5, 13.5]
Crest Width over Incoming Wave Height $\left(\dfrac{B}{H_i}\right)$	[0.075, 0.375]
Permeability Factor $\left(\dfrac{L_0}{\sqrt{D_{n_{50}}B}}n\right)$	[6, 35]
Polar Angle (θ)	[44,84]
Relative Polar Distance $\left(\dfrac{r}{L_0}\right)$	(0, 1.1]

Table 6.15: Summary of Confidence Intervals for ANN model

7   Conclusions

In this paper the wave field variation behind submerged porous breakwaters has been investigated. Results via numerical modeling were obtained and analyzed in order to:

i.   Examine the effects of permeability on the wave transmission process behind submerged breakwaters
ii. To create an extensive database used to train an ANN model

The data obtained from the wave model MIKE21 BW were validated against an empirical formulation proposed by Vicinanza et al (2009). In addition to this during the process of validating the data an attempt was also made to extend the applicability of the empirical model to submerged breakwater situations by introducing a correlation factor. Finally an ANN model was trained using the data obtained from the numerical experiments. The new ANN model is capable of predicting the 3D wave transmission coefficient behind the breakwater, with a high level of accuracy.

The main conclusion and findings of the study are presented below:

1. The parameters effecting the greatest the wave field behind the breakwater were determined and are presented in order of descending influence:
    a. Incoming wave height (Hi).
    b. Mean wave period (T).
    c. Nominal stone diameter of breakwater core (Dn_{50}).
    d. Average porosity of the breakwater core (n).
2. The non-dimensional parameters that best describes the wave field are:
    a. $\frac{L_0}{\sqrt{B*Dn_{50}}} n$
    b. $\frac{h_S}{H_i}$
    c. $\frac{B}{H_i}$
    d. $\frac{B}{L_0}$
    e. ξ
3. The amount of energy dissipation observed grows proportionally for increasing incoming wave heights. A higher rate of energy dissipation is observed when the incoming wave height is at least 2 times the submergence depth of the breakwater (i.e. $\frac{h_S}{H_i}$ <0.5). The increase in the effectiveness of wave dissipation is governed by two physical phenomena:
    a. Wave breaking.
    b. Seepage through the breakwater.
4. MIKE 21 BW gives a reasonable prediction of the wave field around the breakwater, when compared to the prediction method proposed by Vicinanza (2009). Four different empirical formulae for wave transmission in combination with the diffraction theory proposed by McIver (2005) show that MIKE 21 BW predictions fall within the 90% confidence band for most cases. Three possible sources of error were identified, namely:

a. All diffraction theories are developed for non-sloping beds on the lee side of the breakwater. In this report a sloping beach on the lee side of the breakwater was introduced, this results in a slight underestimation of K_d.

b. The influence of wave breaking is a phenomenon that cannot be accurately incorporated in simple empirical wave transmission formulae. This could explain the increased error for high values of H_i.

c. Although MIKE 21 BW has been proved to predict successfully the phenomena of diffraction, seepage and overtopping individually it has never been tested against the combined effect of the three above processes. It is therefore also possible that a certain amount of error has been introduced by the specific wave model.

5. The addition of a correlation factor in the theory of Vicinanza increases the agreement between the numerical data of MIKE21 BW and the empirical model.

6. The modified A.N.N. algorithm is able to predict data patterns as accurately as the original model developed for the prediction of non-permeable breakwaters. Also the model has the same and better predictive skill as previous ANN models developed for predicting 2D wave transmission coefficients.

7. The sensitivity analysis for the A.N.N. model reveals that the non-dimensional parameters influencing the most the process are :

a. The relative distance $\frac{r}{L_0}$ indicating a strong influence of diffraction.

b. Parameter $\frac{L_0}{\sqrt{B*Dn_{50}}} n$ representative of the sensitivity of the wave field to permeability effects.

c. The surf similarity parameter ξ which indicates that the amount of energy passing through the breakwater along with the energy reflected back is of great importance to the process.

8. Wave diffraction plays a significant role in the wave transmission process. It was found that the influence of the diffraction to the overall process increases as:

a. Wave transmission through and over the breakwater decreases.

b. θ decreases and approaches zero (i.e. as the measuring point shifts deeper into the shadow zone).

9. ANN models do not have the capacity to extrapolate very accurately. In order to assure that the model works within the interpolation region the user should use the proposed design tool only within the boundaries defined in section 6.4.2.9. This will limit big uncertainties in the predictions.

10. Due to the dimensions of the flume that was used during the experiments a certain amount of error should be expected due to the partial wave reflection from the side walls. Also due to the conflict between the two scaling methods (Froude and Weber number) seepage was not scaled properly in this study. Therefore a curtain amount of error was introduced from the above two reasons. One should bear this in mind when using the method described in this study for real scaled situations.

8 Recommendations

This chapter will present further recommendations that will allow the ANN model to progress and develop and help understand better the wave transmission process for submerged porous breakwaters. The recommendations therefore may be separated in two categories:

- Recommendation related to wave seepage through porous and submerged breakwaters.
- Recommendation related to the prediction model.

The next two sections will elaborate on the subjects further.

8.1 Wave transmission process

Based on the finding of the numerical simulations the author recommends that further studies related to the topic of 3D wave transmission through porous and submerged breakwaters. Namely:

i. Based on the findings of the presented in chapter 5 there is strong evidence that the diffraction pattern depends strongly on the amount of energy allowed to pass over and through the breakwater. For this reason it is recommended by the author that further physical experiments should be conducted in order to examine how wave transmission is influenced by permeability. Experiment with varying porosity (stone grading) and stone diameter should be conducted for this reason.

ii. Based on the numerical data obtained from MIKE 21 BW is shown that the prediction theory of Vicinanza et al. (2009) has the potential to extend its applicability and accuracy for submerged permeable breakwaters by introducing a correlation factor as presented in chapter 5.1.2. In order to validate this hypothesis further physical experiments examining the 3D nature of wave transmission are required, this data can then be used to validate the prediction equation of chapter 5.1.2.

iii. It is also worth investigating the possibility of creating a diffraction coefficient for submerged breakwaters. As was the case in the previous recommendations this will require a large number of physical experiments. This will then allow calculating the global wave transmission coefficient accurately using the original formula proposed by Vicinanza et al (2009).

iv. It will be interesting to examine the dynamics of deforming reef type breakwaters. These types of structure are the most common type of submerged structures and are preferred due to their low cost.

8.2 ANN modeling

i. The ANN model developed in this thesis was programmed using Matlab 9 the model retrieved data from Microsoft Office Excel© spreadsheets and used them to train and test the prediction model. The ANN model could also be programed in Visual Basic 6.0 (VBA) in order to create a standalone version of the model that could be used more easily. VBA is the programing language used in Microsoft Office Excel. The advantages of this are the following:

- Almost all PC's have the Microsoft Office installed, which will make it easier and cheaper to use.
- The program could be download very easily and installed on any PC that has the Microsoft Office©.
- VBA could be linked to Microsoft Access©, which is an easy to use database management system from Microsoft that combines the relational Microsoft Jet Database Engine with a graphical user interface. This makes data handling much more easily to the user especially if one is not familiar or does not has Matlab installed on their PC.
- Microsoft Office Excel© provides a user friendlier interface than Matlab©. Since this tool is designed for preliminary design purposes it is of great importance the model to be fast and easy to use.

ii. The input file should be created with caution. It is important not to include any dimensionless parameter with a value of zero. For this reason it is recommended that all inputs to be in accordance with the boundary conditions presented in chapter 6.

iii. In addition it is recommended that the same simulations as the ones performed in this study to be conducted in real life physical experiments. A dataset comprised of data obtained from actual experiments would increase the quality of the data and the overall reliability of the ANN model as it would include the natural variability that could never be captured by any numerical model, such as MIKE21 BW.

iv. Related to the dataset used to train the ANN model, it is recommended to enhance the dataset with additional experiments with a variety of different structural and wave parameters. This would increase the range of validity of the model as well as the overall accuracy of the model.

References

Adams, C.B., Sonu, C.J. (1986). Wave transmission across submerged near surface breakwaters. Proceedings of the International conference Coastal Engineering 1729-1738.

Ahrens, J. P. (1987). Characteristics of Reef Breakwaters (No. CERC-TR-87-17). COASTAL ENGINEERING RESEARCH CENTER VICKSBURG MS.

Allsop, N. W. H. (1983). Low-crest breakwaters, studies in random waves. In Coastal Structures' 83 (pp. 94-107). ASCE.

Bazartseren, B., Hildebrandt, G., & Holz, K. P. (2003). Short-term water level prediction using neural networks and neuro-fuzzy approach. *Neurocomputing*, *55*(3), 439-450.

Beji, S., & Battjes, J. A. (1994). Numerical simulation of nonlinear wave propagation over a bar. *Coastal Engineering*, *23*(1), 1-16.

Bleck, M. and Oumeraci, H. (2002) Wave Damping and Spectral Evolution at Artificial Reefs. Ocean Wave Measurement and Analysis (2001): pp. 1062-1072.

Bowen, A.J. (1969). Rip currents: 1. Theoretical investigation. Journal of Geophysical Research 74, 5467-5478.

Briganti, R., Van der Meer, J. W., Buccino, M., & Calabrese, M. (2003, August). Wave transmission behind low crested structures. In Proc. 3rd Coastal Structures Conference.

Bruce, T., van der Meer, J.W., Franco, L., Pearson, J. (2006). A comparison of overtopping performance of different rubble mound breakwater armour. Proceedings of the International Conference-Coastal Engineering 1034_1043.

Buccino, M., Calabrese, M. (2007). Conceptual approach for prediction of wave transmission at low-crested breakwaters. Journal of Waterway, Port, Coastal, and Ocean Engineering 133 (3), 213-224.

Burcharth, H.F., Hawkins, S.J., Zanuttigh, B., Lamberti, A. (2007). Environmental design guidelines for low crested coastal structures. Elsevier.

Cáceres, I., Sánchez-Arcilla, A., Zanuttigh, B., Lamberti, A., Franco, L. (2005). Wave overtopping and induced currents at emergent low crested structures. Coastal Engineering 52, 931-947.

Calabrese, M., Vicinanza, D., & Buccino, M. (2002). Large-scale experiments on the behaviour of low crested and submerged breakwaters in presence of broken waves. In COASTAL ENGINEERING CONFERENCE (Vol. 2, pp. 1900-1912). ASCE AMERICAN SOCIETY OF CIVIL ENGINEERS.

Calabrese, M., Vicinanza, D., Buccino, M. (2008). 2D wave set up behind submerged breakwaters. Ocean Engineering 35, 1015-1028.

Charalambous, C., Jun. (1992). Conjugate gradient algorithm for efficient training of artificial neural networks. Circuits, Devices and Systems, IEE Proceedings G

139 (3), 301-310.

d'Angremond, K., Van Der Meer, J. W., & De Jong, R. J. (1996). Wave transmission at low-crested structures. Coastal Engineering Proceedings, 1(25).

Dalrymple, R.A., Knio, O., Cox, D.T., Gomez-Gesteira, M., Zou, S., 2001. Using a Lagrangian particle method for deck overtopping. In: Proceedings of the Waves ASCE 2001, pp. 1082–1091.

Dean, R.G., Chen, R., Browder, A.E. (1997). Full scale monitoring study of a submerged breakwater, Palm Beach, Florida, USA. Coastal Engineering 29, 291-315.

Goda, Y. (1967). The fourth order approximation to the pressure of standing waves. Coastal Engineering in Japan, 10(1).

Goda, Y., Yoshimura, T., Ito, M. (1971). Reflection and diffraction of water waves by an insular breakwater. Report of the Harbour Research Institute, Japan 10, 4-52.

Goda, Y., Takaiama, T., Suzuki, Y. (1978). Diffraction diagrams for directional random waves. Proceedings of the International Conference Coastal Engineering, 628-650.

Goda, Y., Ahrens, J.P. (2008). New formulation for wave transmission over and through low crested structures. Proceedings of the International Conference Coastal Engineering 3530-3541.

Hagan, M. T., Demuth, H. B., Beale, M. H. (1996). Neural network design. PWS Pub.

Hanson, H., Kraus, N.C. (1991). Numerical simulation of shoreline change at Lorain, Ohio. Journal of Waterway, Port, Coastal and Ocean Engineering, Vol. 117. No. 1, 1-18.

Hotta, S. (1978). Wave height distribution around permeable breakwaters. Proceedings of the International Conference Coastal Engineering 695-714.

Karayiannis, N.B. Reformulated radial basis neural networks trained by gradient descent. IEEE Trans. Neural Netw.1999, 3, 2230-2235.

Kobayashi, N. and Wurjanto, A. (1989). Wave Transmission over Submerged Breakwaters. *J. Waterway, Port, Coastal, Ocean Eng.*, 115(5), 662–680.

Kramer, M., Zanuttigh, B., van der Meer, J.W., Vidal, C., Gironella, F.X. (2005). Laboratory experiments on low-crested breakwaters. Coastal Engineering 52 (10-11), 867-885.

Lin, P. and Liu, P. (1999). "Internal Wave-Maker for Navier-Stokes Equations Models." *J. Waterway, Port, Coastal, Ocean Eng.*, 125(4), 207–215.

Losada, I. J., Silva, R., & Losada, M. A. (1995). 3-D non-breaking regular wave interaction with submerged breakwaters. *Coastal Engineering*, *28*(1), 229-248.

Lynett, P., Liu, P., Losada, I., and Vidal, C. (2000). "Solitary Wave Interaction with Porous Breakwaters." *J. Waterway, Port, Coastal, Ocean Eng.*, 126(6), 314–322.

Madsen, O.S. (1971). On the generation of long waves. Journal of Geophysical Research 76 (36), 8672-8683.

Madsen, P. A., Murray, R., & Sørensen, O. R. (1991). A new form of the Boussinesq equations with improved linear dispersion characteristics. *Coastal Engineering*, *15*(4), 371-388.

Madsen, P. A., & Sørensen, O. R. (1992). A new form of the Boussinesq equations with improved linear dispersion characteristics. Part 2. A slowly-varying bathymetry. *Coastal Engineering*, *18*(3), 183-204.

Madsen, P. A., Sørensen, O. R., & Schäffer, H. A. (1997). Surf zone dynamics simulated by a Boussinesq type model. Part I. Model description and cross-shore motion of regular waves. *Coastal Engineering*, *32*(4), 255-287.

Massel, S., & Butowski, P. (1980). WIND WAVES TRANSMISSION THROUGH POROUS BREAKWATER. *Coastal Engineering Proceedings, 1*(17).

McCormick, D., Kraemer, R.B. (2002). Polynomial approximations for Fresnel integrals in diffraction analysis. Coastal Engineering 44, 261-266.

McIver, P. (2005). Diffraction of water waves by a segmented permeable breakwater. Journal of Waterway, Port, Coastal, and Ocean Engineering 131 (2), 69-76.

Owen, M.W. (1980). Design of seawalls allowing for wave overtopping. Rep. EX 924b. Hydraulics Research Station, Wallingford, England.

Panizzo, A., Briganti, R. (2007). Analysis of wave transmission behind low-crested breakwaters using neural networks. Coastal Engineering 54 (9), 643-656.

Péchon, P., Rivero, F., Johnson, H., Chesher, T., O'Connor, B., Tanguy, J. M., ... & Hamm, L. (1997). Intercomparison of wave-driven current models. Coastal engineering, 31(1), 199-215.

Penny, W.G., Price, A.T. (1952). The diffraction theory of sea waves and the shelter afforded by breakwaters. Philosophical Transactions of the Royal Society of London. A 244, 236-253.

Rojanakamthorn, S., Isobe, M., & Watanabe, A. (2011). MODELING OF WAVE TRANSFORMATION ON SUBMERGED BREAKWATER. *Coastal Engineering Proceedings, 1*(22).

Sanchez-Archilla, A., Rivero, F., Gironella, X., Verges, D., & Tome, M. (1999). Vertical circulation induced by a submerged breakwater. Coastal Engineering Proceedings, 1(26).

Sanchez-Archilla, A., Rivero, F., Gironella, X., Verges, D., & Tome, M. (2001). VERTICAL CIRCULATION INDUCED BY A SUBMERGED BREAKWATER. *Coastal Engineering Proceedings, 1*(26). doi:10.9753/icce.v26

Seabrook, S.R., Hall, K.R. (1998). Wave transmission at submerged rubble mound breakwaters. Proceedings of the International Conference Coastal Engineering 2000-2013.

Sharif Ahmadian, A., and Simons, R. (2012) Dec 15. 3-D WAVE FIELD AROUND SUBMERGED BREAKWATER. Coastal Engineering Proceedings. [Online] 1:33

Shore Protection Manual, 1984. 4th ed., 2 vol., U.S. Army Engineer Waterways Experiment Station. U.S. Government Printing Office, Washington, DC.

So/rensen, O. and So/rensen, L. (2001) Boussinesq Type Modelling Using Unstructured Finite Element Technique. Coastal Engineering 2000: pp. 190-202.

TAW/van derMeer, J.W. (2002). Technical Report on wave run-up and wave overtopping at dikes. Report of the Technical Advisory Committee on Flood Defence, NL.

van der Meer, J.W. (1992). Conceptual design of rubble mound breakwaters. Proc. of the Short Course on Design and Reliability of Coastal Strucures, pp. 447-509.

van der Meer, J. W., & Daemen, I. F. (1994). Stability and wave transmission at low-crested rubble-mound structures. Journal of waterway, port, coastal, and ocean engineering, 120(1), 1-19.

van der Meer, J.W., Briganti, R., Zanuttigh, B., Wang, B. (2005). Wave transmission and reflection at low crested structures: design formulae, oblique wave attack and spectral change. Coastal Engineering 52 (10-11), 915-929.

van Gent, M. R. (1994). The modelling of wave action on and in coastal structures. *Coastal Engineering*, *22*(3), 311-339.

Van Oosten, R.P. and Peixó Marco, J. (2005) Wave transmission at various types of low-crested structures**,** M.Sc.-thesis, Delft University of Technology, Faculty of Civil Engineering, Delft, The Netherlands

Vicinanza, D., Cáceres, I., Buccino, M., Gironella, X., & Calabrese, M. (2009). Wave disturbance behind low-crested structures: Diffraction and overtopping effects. Coastal engineering, 56(11), 1173-1185.

Wamsley, T.V., Ahrens, J.P. (2003). Computation of wave transmission coefficients at detached breakwaters for shoreline response modelling. Proceedings of Coastal Structures 2003, 147-159.

Yu, B.; He, X. Training Radial Basis Function Networks with Differential Evolution. In Proceedings of IEEE International Conference on Granular Computing, Atlanta, GA, USA, 2006; 369-372.

Zanuttigh, B., Lamberti, A. (2006). Experimental and numerical simulations
of wave and current flows around low-crested rubble mound structures. Journal of
Waterway, Port, Coastal and Ocean Engineering 132 (1), 10-26.

Zanuttigh, B., Martinelli, L., Lamberti, A. (2008). Wave overtopping and piling-up
at permeable low crested structures. Coastal Engineering 55, 484_498
232